UNIVERSITÀ DEGLI STUDI DI PADOVA

DIPARTIMENTO DI INGEGNERIA INDUSTRIALE

CORSO DI LAUREA MAGISTRALE IN INGEGNERIA DELL'ENERGIA ELETTRICA

Tesi di Laurea Magistrale in
Ingegneria dell' Energia Elettrica

PERFORMANCE ENHANCEMENT OF THE NIO1 EXPERIMENT

Relatore: Prof. Piergiorgio Sonato

Correlatore:
Ing. Mauro Recchia
Ing. Tommaso Patton

Laureando: Sebastiano Mancin

ANNO ACCADEMICO 2016-2017

Performance Enhancement of the NIO1 Experiment

Sebastiano Mancin

Thanks to my father for supporting me in everything I did, I do and I'm gonna do;
Thanks to the love of my life for being by my side everywhere and at any time;
Thanks to my relatives for being here and loving me;
Thanks to all the friends of mine for walking with me through the path of life;
Thanks to You that despite everything are in the heart of who knows You, and in mine forever.
Thanks to all of you that make this possible.
This work is dedicated to all that count for me, to all that helped me somehow and to You who will live forever in our memories, thoughts and dreams.

Sebastiano Mancin

Padova, Settembre 2017

Abstract

Negative Ion Optimisation step 1 (NIO1) is an experiment built in Padua, at the Consorzio RFX, in the framework of energy from nuclear fusion reaction with the aim to study the neutral beam heating. NIO1 main parts are the source and the acceleration stages for negatively charged particles. So far NIO1 is not able to reach its nominal voltages of operation because of some limitations in the electric system. Even though the power supply system (PSs) on NIO1 is already at its final configuration, the electric protection system and some diagnostics are still under development. This thesis focuses on both these aspects: the design of a proper electric protection system which allows the NIO1 PSs to securely reach its maximum potential and a wide-bandwidth voltage measurement system which permits to do measurements about the plasma breakdowns that can occur in the NIO1 source chamber. The protection system already installed in NIO1 does not allow to exceed a precise voltage values since it is not sized for this and because initially NIO1 must have been operated at a limited regime. A voltage measurement system for cheap fast measure is instead not yet present in NIO1. The protection circuit is firstly described in this thesis. First of all the component that must work as overvoltage suppressor has been identified in the Silicon Diode for Alternating Current (SIDAC); then a proper test bench has been assembled in order to test the designed circuit and to understand if it can be suitable for the installation in NIO1. The result about the circuit will also lead to the choice of the other components part of the protection circuit. The second improvement for NIO1 is a measurement system which allows to characterise the plasma breakdown events occurring between the accelerator grids. A suitable cheap data acquiring board has been identified in the Red Pitaya which needs a particular input voltage. In order to obtain this particular input voltage a proper wide bandwidth high voltage divider has been designed, simulated and tested. The

result is a 10kV voltage divider with a division ratio equal to 1:1000 which allows to have a suitable input voltage value for the Red Pitaya; a 15MHz bandwidth has been obtained and this permits to measure fast events such as the plasma breakdowns between the grids in the plasma chamber.

Sommario

Negative Ion Optimisation step 1 (NIO1) è un esperimento costruito a Padova, presso il Consorzio RFX, in un ambito di ricerca circa la produzione di energia da fusione termonucleare con lo scopo di studiare il riscaldamento tramite raggio di particelle neutre. Le parti principali di NIO1 sono la sorgente di plasma e lo stage di accelerazione delle particelle negative. Attualmente NIO1 non può raggiungere le prestazioni nominali a causa di alcune limitazioni del sistema elettrico. Nonostante il sistema di elimentazione (PSs) installato sia già quello definitivo, il sistema di protezione ed alcune diagnostiche sono ancora in via di sviluppo. Questa tesi è focalizza su entrambi questi aspetti: il design di un opportuno sistema di protezione che permetta al sistema di alimentazione di NIO1 di raggiungere in sicurezza le prestazioni nominali e lo sviluppo di un sistema di misura di tensione a banda larga completo che permetta di effettuare alcune misure circa le scariche che avvengono nel plasma. Il sistema di protezione attualmente presente in NIO1 non gli permette di superare determinati valori di tensione sia perchè non è dimensionato per tali valori sia per il fatto che inizialmente NIO1 aveva la necessità di operare in regime limitato. Una misura di tensione che sia economica e veloce non è ancora presente in NIO1. Inizialmente viene descritto il sistema di protezione. Innanzitutto i componenti che devono operare come sopressori di sovratensioni vengono identificati nei Diodi al Silicone per Corrente Alternata (SIDAC); successivamente viene assemblato un opportuno banco di prova al fine di testare il circuito soppressore di sovratensione e per capire se può essere adatto all'installazione in NIO1. I risultati di questi test porteranno inoltre alla scelta degli altri componenti facenti parte del circuito di protezione. Il secondo miglioramento da apportare a NIO1 è un sistema di acquisizione dati che permetta di caratterizzare le scariche che avvengono nel plasma tra le gliglie dell'acceleratore. Un sistema di acquisizione economico è stato identifi-

cato nella Red Pitaya la quale però richiede una tensione di input abbastanza limitata. Al fine di ottenere questa tensione di ingresso un partitore di alta tensione avente con una buona larghezza di banda è stato progettato, simulato e testato. Ne è risultato un partitore utilizzabile per 10kV, avente un rapporto di partizione 1:1000 che permette di avere una tensione di ingresso accettabile per le Red Pitaya; è stata ottenuta una banda di 15MHz la quale permette di effettuare misure veloci della scariche tra le gliglie presenti nella camera del plasma.

Contents

List of Figures

Chapter 1

Introduction

1.1 Introduction

Nowadays, one of the most important problem that we all are called to solve, is the availability and the sustainability of our energetic sources. At today's date we are struggle against pollution of air, water and soil; this pollution is completely imputable to anthropic causes.
One of the most contributing sector to pollution is the production of energy; since, in the field of energy, a sector could be considered sustainable if and only if it is sustainable by three different point of view: environmentally, socially and economically. Unfortunately, until now, none of the sources of power utilised by humans can win the title of "*sustainable*".
For the reasons above one of the most demanding challenge for the future years is the research of one or more sources of power which can be considered completely sustainable. It seems that thermonuclear fusion can fit perfectly into this scenario of sustainability for more than one reason. First of all no waste (referring e.g. to the nuclear waste produced by nuclear power plants or to chemical products) are produced by this technology; secondly the reactants needed by the fusion reaction are extremely available on the earth surface or, however, easily producible. Last, but not least, this technology is intrinsically safe. Thanks to this three features the requirements of sustainability have been satisfied.
This introduction has two objectives: to explain the main physical principle of operation of the thermonuclear fusion and to show why a particular type of "*additional heating systems*" called "*neutral beam injection*" is not only nec-

essary but also sufficient to achieve the goal of a stable and controlled nuclear fusion reaction.
This will lead us directly to the description of the NIO1 experiment since the latter is a source and accelerator of negative ions; and, as will be explained soon in this chapter, source (or production) and acceleration of negative ions are two out of four stages of a NBI[1].
The description of NIO1 and in particular of its electrical system will make us consider one of the most important electrical problem that the team has to face with during the operation of NIO1. The solution of this problem is one of the main issue of this master thesis. The latter has the objective to find a way to protect the power system of NIO1 from breakdown that can occur during the operation; the study of this aspect will bring us through some important subjects such as: the ability of insulating material to withstand high voltage, the comprehension of the tricks to increase the bearable voltage of an insulating material, the research of the best possible component to suppress the overvoltage in the case of breakdown in order to protect the sensible part of the circuit, the design of a perfect layout which has to be the best possible compromise between efficiency and space requirement, the design of the test bench in order to test the protection circuit before the installation it in NIO1 experiment and at the end the test itself to prove the proper functioning of the designed circuit. The first part of this master thesis is going to talk about this first issue, just presented, and will be organised in sections which will follow the order of the list above.
The second target of this thesis is the design of a high voltage divider in order to be able to take measurements on high voltage system among which the power supply system of NIO1. This voltage divider has to have very high performances in terms of bearable voltage at the high voltage stage and bandwidth in order to be able to measure impulsive signals with a very short peak time. The design of such a voltage divider bring with itself severe challenges, one among them the perfect compensation of the entire voltage measurement till a very high frequency. Since the study of the voltage divider has been carried out both through numerical simulations and practical experimentations, this second part will be organised into two sub-parts: the first sub-parts will

[1]NBI is an acronym that stands for Neutral Beam Injection. This acronym will be used during the writing of the entire thesis.

handle with the numerical simulation carried out throughout MATLAB code and some circuit simulators; the second sub-parts deal with the practical experimentations. The two way to study the circuit are extremely connected one each other and the study has been carried out in parallel with the two method. This *modus operandi* has allowed us to continuously adjust and tune both the simulations and the experiments, on the basis of the results given by the experiments and by the simulations, to obtain the best we can every time. After the design of the circuit a low voltage prototype has been designed and tested. The last stage is the design and test of the high voltage divider.
Also in this study we have to face with some problem such as: design of a proper case for the voltage divider in order to prevent discharge, the comprehension of the influence of stray parameters on the dynamic behaviour of the circuit, the necessity to be almost completely independent from the stray parameter (compensation) in order to reach the desired bandwidth, the choice of suitable components and so on.
As seen in the introduction both the target of this thesis, the wide bandwidth high voltage divider and the passive protection system for the power supply of NIO1 experiment, are correlated to the occurrence of plasma breakdown. Thus, also the two target of the thesis are correlated to each other: the passive protection system is oriented to the safety of the power supply system; the wide bandwidth high voltage divider points towards the diagnostic of there breakdown occurrences.
As the title of this thesis points out these objectives have the aim to enhance the performance of NIO1 experiment allowing it to reach its maximum potentialities.

1.2 Thermonuclear fusion

During a nuclear fusion reaction two light nuclei collide producing an heavier nucleus. The mass of the resultant nucleus is generally less than the total mass of the reactants and this mass difference, the so called **mass defect**, will transform into energy according to mass-energy Einstein's equivalence. This theorem state that:

$$E = mc^2$$

Even if the mass defect is extremely small ($\sim 10^{-10}$), the constant of proportionality is very high ($\sim 10^{16}$) and therefore the resulting energy is appreciable. The following graph, fig.(1.1) explain what just said, for example: when a fusions reaction between tritium and deuterium occurs, it results in an alpha particle and a neutron. This lithium atom is lighter than the sum of the mass of the reactants and the mass defect will transform into energy. The graph (1.1) displays how much this mass defect is, for single particles, relatively to the species that react.

Since the fusion reaction occurs between the nuclei of the atoms and these

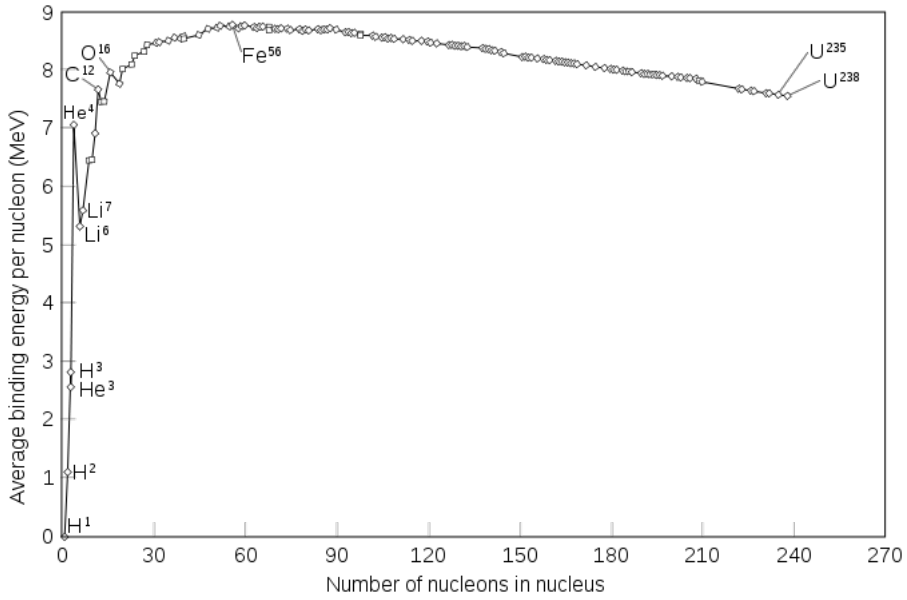

Figure 1.1: This graph represent a benchmark in fusion ad fission physic because it shows the possible exoenergetic reactions that will lead to a probable production of energy. `http://www.ilpost.it/filippozuliani/2012/12/05/fusione-nucleare/`.

ones are positively charged, atoms must have a very high velocity in order to overcome the Coulombian repulsive force between them. This very high kinetic energy can be reachable only with very high temperatures, in the order of tens of millions degrees. When the repulsive electrostatic force is won, *strong force* sets in and makes possible the fusion reaction to happen.

More than one fusion reaction are theoretically possible: deuterium-deuterium, deuterium-Helium3, tritium-deuterium.

Let's now have an insight on these reactions and on the understanding of which of these is the best possible choice.

1.2.1 Deuterium-deuterium nuclear reaction

deuterium is almost inexhaustible on the earth since it is contained in sea water with a concentration of 30 mg/l; it has been estimated that at the today consumption rate of electric energy, supposing that all the energy is produced completely with thermonuclear fusion, the deuterium will last more than the life of the Earth itself.
Unfortunately, between all of the possible fusion reaction, as can be seen in figure (1.2), this one has the smaller cross section; this means that the reaction is more difficult because it takes more to start. The reaction between two nuclei of deuterium can evolve into two ways:

$$\begin{aligned} D + D &\rightarrow He^3 + n + 3.27MeV \\ D + D &\rightarrow T + p + 4.03MeV \end{aligned} \tag{1.1}$$

These reactions are characterised by an energy density of about 70 TJ/Kg-D and 100TJ/kg-D respectively.
Considering an actual fusion reaction the production of neutrons could represent a problem because of the activation of metallic materials which surround the plasma. The activation results in more than one problem: an activated material become radioactive and hence has to be treated in a particular way [2]; an activated material could lose some of his particular characteristics (mechanical, electrical and so on) and become unsuitable for the application that it is meant for.

1.2.2 Deuterium-Helium3 nuclear reaction

The deuterium-helium$_3$ reaction has two advantage: it exerts a very high energy density quantifiable in about 350 Tj per kilograms of fuel; it doesn't produce any neutron avoiding the problem described above of the activation of the material surrounding the plasma. Unfortunately this reaction is characterised by a low cross section and, furthermore, helium3 is practically not present on Earth.
Even if the reaction has not been considered for practical applications, it is:

$$D + He^3 \rightarrow He^4 + p + 18MeV \tag{1.2}$$

[2]Disposal of nuclear waste is a wide and difficult argument.

1.2.3 Deuterium-tritium nuclear reaction

This last one reaction is the most convenient with respect to those examined until now because of the high cross section reachable at relatively low temperature, as shown in figure (1.2). The only disadvantage seems to be the practically null presence of tritium at the natural state in nature, but fortunately tritium is easily producible by means of the reaction between tithium and neutrons. Two reactions between these two elements are possible according to the velocity/temperature of neutrons:

$$\begin{aligned} Li^6 + n_{slow} &\rightarrow \alpha + T + 4.8MeV \\ Li^7 + n_{fast} &\rightarrow \alpha + T + n - 2.5MeV \end{aligned} \tag{1.3}$$

Regarding lithium, for it is the same as said before about deuterium: it is almost inexhaustible on the Earth surface.
Once tritium has been created, the fusion reaction is:

$$D + T \rightarrow \alpha + n + 17.6MeV \tag{1.4}$$

The latter reaction produce 340 TJ per kilograms of the mixture of the reactants.

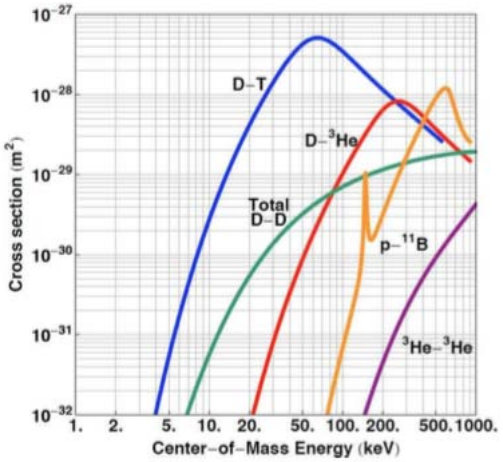

Figure 1.2: Different cross sections for different fusion reactions. The figure shows that the most convenient fusion reaction is that between deuterium and tritium since it has the highest cross section at the lowest temperature. physics.stackexchange.com/questions/318390/why-do-fusion-cross-sections-drop-after-a-certain-temperature

1.3 Additional Heating System

1.3.1 Fusion Reaction Power Balance

Considering just for example the fusion reaction between tritium and deuterium (since as it has been seen it is the one with the most favourable activation energy and so the one considered for the commercial application at the date of today) the thermonuclear power is proportional to the: density of reactants, energy release by the reaction and reaction rate $\langle \sigma v \rangle$. Since the maximum power can be achieved when the two reactants have the same density n, the fusion power can be express as:

$$p_{th} = \frac{1}{4} n^2 \langle \sigma v \rangle E \tag{1.5}$$

The energy produced by the fusion reaction is divided between the energy acquired by neutrons and that acquired by the alpha particles, in particular: one fifth is acquire by alpha particles and four fifth by neutrons. Since only the energy owned by alpha particles is suitable for the purpose of plasma heating, the power that has to be taken into account is one fifth of that calculated above:

$$p_{alpha} = \frac{1}{20} n^2 \langle \sigma v \rangle E \tag{1.6}$$

For the purpose to derive the ignition condition (the condition for which a self-sustaining plasma has been obtained) and the Lawson criterion, besides the nuclear power, the losses have to be taken into account too. The losses of power can be categorised into two: conductive losses and radiative losses.
The thermal conductive losses take into account the decrease of plasma temperature due to physical phenomena of conduction and convection which may lead to contact between plasma and first wall. These losses can be derived starting from the energy contained in the plasma inside the vessel. The total amount of energy for a quasi-neutral plasma[3] is:

$$W = 3\overline{nkT}V \tag{1.7}$$

W can be expressed as a power loss by means of **confinement time** τ_E, and this result in:

$$p_{cond} = \frac{W}{\tau_E} = \frac{3\overline{nkT}V}{\tau_E} \tag{1.8}$$

[3]A quasi-neutral plasma is a plasma in which the density of negatively charged particles

The radiative losses comprise: Bremsstrahlung radiation, cyclotron radiation, line radiation and recombination radiation. Since the Bremsstrahlung radiation leads to a loss far greater than the other, only this one can be considered. The radiation loss can now be written as:

$$p_{rad} = bn^2\sqrt{T} \tag{1.9}$$

Considering a zero dimensional model in which $P_{in} = P_{out}$, and the efficiency η, it's possible to write as follow:

$$P_{out} = P_{in} \quad \Rightarrow \quad P_{th} + \eta(P_{th} + P_{cond} + P_{rad}) = P_{th} + P_{cond} + P_{rad}$$

$$\Rightarrow \quad \eta P_{th} = (1-\eta)(P_{cond} + P_{rad})$$

From which, by means of few mathematical steps, is possible to derive the Lawson criterion:

$$n\tau_e = \frac{3kt}{\frac{\eta}{1-\eta}\frac{1}{4}n^2 \langle\sigma v\rangle E - b\sqrt{T}} \tag{1.10}$$

From here it is possible to derive the so called **ignition condition** for which the reaction is self-sustained[4]. In this case only the alpha power has to be taken into account in the calculation, and the result is:

$$n\tau_e = \frac{3kt}{\frac{\eta}{1-\eta}\frac{1}{4}n^2 \langle\sigma v\rangle E - b\sqrt{T}} \tag{1.11}$$

The ratio between temperature and reaction rate is minimised by the plasma temperature of 15 keV; in the range of temperature between 10 and 20 keV the reaction rate is well known, and considering the energy associated to alpha particles equal to 3.5 MeV, the ignition condition becomes:

$$nT\tau_E > 3 \times 10^{21}[m^{-3}keVs] \tag{1.12}$$

The achieving of the breakeven temperature is a process articulated into two stages: during the first of these two stages a combination of different plasma heating technologies heat the plasma until about 5 to 7 keV; during the second stage the alpha power becomes dominant and takes the plasma to the right temperature of about 15 keV. During the first stage the alpha power is almost

and positively charged particles are almost the same; so that, by a macroscopic point of view the plasma con be considered electrically neutral.

[4]A reaction is self-sustained when it can continue by itself since it produces the energy

negligible and so the heating technologies must compensate the losses (conductive and radiative). The goal is to understand the best possible way, in terms of inexpensiveness and efficiency, to achieve the first step and take the plasma until about 7 keV.
The simplest technology usable for this purpose is the **ohmic heating** which exploits the transformer-like operation by means of an inductive coupling: toroidal currents are induced in the plasma, as if the latter were the secondary of a transformer, thanks to the current flowing in the primary coils powered by the external source of energy. However the plasma resistivity is inversely proportional to the plasma temperature, according to the formula:

$$\eta = \frac{1}{T^{\frac{3}{2}}}$$

As a consequence of this law, as the temperature get higher the resistivity grow less than proportional with it and the heating efficiency decrease. The analyses carried out until now seem to confirm that the maximum temperature reachable with the sole usage of ohmic heating technologies is about 3 keV (see Kruskal-Shafranov criterion). Since this temperature is not sufficient to reach the ignition condition, it is required to find additional heating system. More than one system has been analysed, and all of these have been integrated in ITER in order to find out which one is better (in terms of efficiency, cost, simplicity and versatility): Ion Cyclotron Resonance Heating (ICRH), Electron Cyclotron Resonance Heating (ECRH) and Neutral Beam Injection Heating (NBI or NBH). Both the first two system exploit the cyclotron resonance, respectively the one relative to ions and the one relative to electrons, and permit a direct transfer of energy from the electromagnetic wave, which is emitted from an antennae facing the plasma, to the plasma itself; unfortunately, although very efficient, both of these two systems bring with itself severe technological challenges. Regarding ECRH the steady state required power at very high frequency (electron's cyclotron frequency is in the order of hundreds of MHz and the exact value depends from the intensity of the static magnetic field in the plasma) isn't attainable yet. Concerning ICRH in order to have a good efficiency in the energy transferring the antennae should be very close to plasma and this can lead to plasma arch and plasma breakdown. The rest of the chapter gives an insight in Neutral Beam Injection system;

required too; there's no need to provide energy anymore.

this focus is an obliged step toward the comprehension of the usefulness of NIO1 experiment and it is able to demonstrate some of the NIO1's peculiar characteristics, i.e. the reason why negative ions are used.

1.3.2 Neutral Beam Heating - NBH

The basic idea of neutral beam heating consists of a beam of high energy neutral particles injected into the plasma; high energy means that the energy of the particles which compose the beam must be very high relatively to the energy owned by background plasma particles, for example: since, as seen before, the optimal temperature of the plasma should be about 15 keV, the energy related to the beam should be at about 1 MeV.
Since beam's particles are neutral (they don't have electric charge), they are not affected by magnetic fields and can go straight following their original trajectory; when the neutral particles are inside the plasma they are ionised by impact with background plasma particles. Once they have been ionised they feel the effect of magnetic field and so they remains confined. The particles just ionised are high energetic yet, so by hitting with the original plasma particles kinetic energy is transferred leading to a plasma heating. Obviously, the energy owned by the beam has to be optimised since if it was too high the beam would pierce the plasma without depositing energy and if it was too low it wouldn't reach the bulk of the plasma and the efficiency of the process would be very low.
As said before, the energy of the beam sould be about 1 MeV and this poses some severe technological challenges. In order to overcome this issue seems that the usage of primary negative particles[5] permit to reach the required energy; the reason for this is that for positive ions the efficiency of the entire[6] process decrease as the energy get higher, vice versa working with negative primary particles lead to a constant, or at most weakly increasing, efficiency of the entire process (see the following to section 1.3.2.1 and 1.3.2.3). On the other hand, the technology required in order to produce a neutral beam starting with negative ions is more complicated and so more expensive by energetic point

[5]Primary is a reference to the fact that these particles are those created in the vacuum chamber at the beginning of the process. Before these there were no charged particle at all. They are also known as native particles.

[6]These data about efficiency refere to (22).

of view (since it requires more external power to be supply) and consequently from the economic points of view too.

1.3.2.1 How a neutral beam is created

As can be seen in fig.1.3 a neutral beam source is articulated in 4 stages: production and acceleration of negative ions, neutralisation and a filter which serves to avoid ionic residues from the neutral beam. In the first stage low temperature negative ions are produced through low temperature discharge during which electrons attach themselves to neutral molecules. Even though it is more difficult to create negative ions instead of positive ones, the first one bring with them an advantage: electrons are attached very weakly to the molecules and therefore their removal during the neutralisation stage is more easy and require less energy; this is already an advantage of the usage of negative particles instead of positive particles. Between the first and the second stage there is a perforated surface, known as textitoptic, which allows the transit of the particles in a much more focused manner. The second stage provides the acceleration of the ions previously produced until the required energy, in this case of about 1 MeV. This acceleration is obtained by means of an high potential difference. The second stage has as output a beam of well confined negative charged particle with a uniform energy.
The third stage is the neutralisation stage, practically it is a pipe filled with a proper density of neutral particles, typically of the same species of the primary particles, in which negative ions are neutralised thanks to the inelastic impact with neutrals: the impact remove the extra electrons. Also in this stage the usage of negative particles lead to ad increase of efficiency, in fact with positive particles the neutralisation efficiency decrease as the energy of the beam get higher while in the case of negative ions the efficiency remains constant.
The last stage is the magnetic deflector which has the role to remove the eventual ionic residues (ions escape to ionisation) and makes possible to have only neutral particle to get into the plasma. Magnetic deflector produces a magnetic field which deflects charged particles toward the beam dumper.

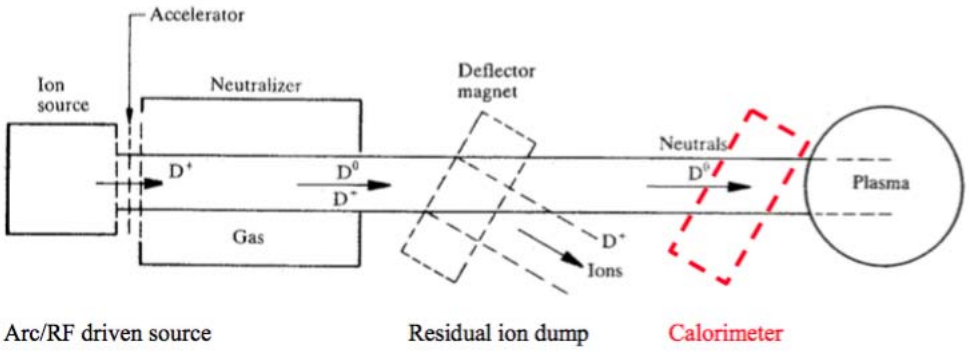

Figure 1.3: Beamline[22]

At this point the beam is ready to penetrate inside the plasma ad cedes its energy. Penetration's modes are two: perpendicular and tangential:

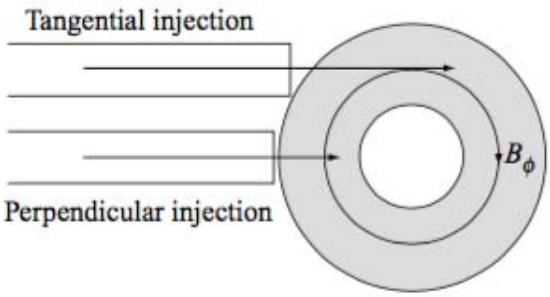

Figure 1.4: Two different modes of injection of the neutral beam into the plasma[22].

1.3.2.2 Beam energy optimisation

One of the most important problem to solve for the NBH to work properly is the optimisation of energy in order to make the beam penetrates the plasma in the proper way and deposits its energy where it is need: in the bulk of the plasma. Ionisation mechanisms of neutral beam, once it has penetrated the plasma and has reached the bulk, are three: **charge exchange**, **ionisation by ions** and **ionisation by electrons**. Immediately, it can be stated that the effect of ionisation by electrons is negligible with respect to the other two ionisation mechanisms (see (22)). In the following the mechanisms are described.

Charge exchange Supposing the collision between two deuterium atoms, charge exchange process is explainable as:

$$D_b + D_p^+ \rightarrow D_b^+ + D_p \tag{1.13}$$

where the subscript b indicates a particle associated to the beam, which has an high energetic content; and the subscript p indicates a particle associated to the background plasma which has an energy comparable to the plasma temperature. To this process, which occurs thanks to the exchanging of electrons between the ion and the energetic neutral, is associated the charge exchange cross section σ_c.

Ionisation by ions Ionisation by ions occurs when there is a violent impact between a neutral particle and an ion which belongs to the background plasma. Neutral particle splits itself into an ion and a free electron; both of these impact product own an energy comparable with that of the beam. However, because of its greater mass, the ion bring most of the kinetic energy belonging originally to the neutral particle. The process, with an associated cross section σ_i can be summarised as:

$$D_b + D_p^+ \rightarrow D_b^+ + D_p^+ + e^- \tag{1.14}$$

Thanks to the following graph, figure (1.5), it can be seen that for energy less than 90 keV the main ionisation mechanism is the charge exchange, contrariwise for energy greater than 90 keV the main ionisation mechanism is the ionisation by ions.

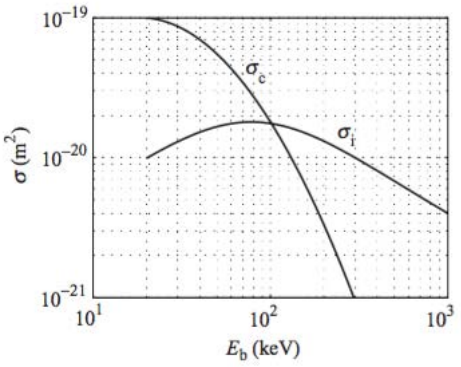

Figure 1.5: Cross section relative to ionisation by ions and charge [8].

Returning to the original problem, i.e. finding the proper beam's energy in order to deposit the energy exactly in the bulk of the plasma, the energy

is related to the **penetration depth** and to the **decay length**. These two indexes are directly proportional to one another since as the beam penetrates its energy diminishes because of the momentum exchange collisions.
Neutral particle's flux $\Gamma_b = n_b v_b$ decay with the distance according to:

$$\frac{\mathrm{d}\Gamma_b}{\mathrm{d}x} = -n_p(\sigma_c + \sigma_i)\Gamma_b \tag{1.15}$$

where n_p is the density of the background plasma.
Since there is a correspondence between the loss of high energy neutral particles Γ_b and the increase of the energy of the charged particle Γ_b^+, the solution to the eq.(1.15) is:

$$\Gamma_b^+(x) = \Gamma_b(0)\left(1 - e^{\frac{-x}{\lambda}}\right) \tag{1.16}$$

where λ is the decay length, and it is equal to:

$$\lambda = \frac{1}{n_p(\sigma_c + \sigma_i)} \tag{1.17}$$

Obviously, since the penetration depth a and the decay length λ are proportional, for the heating to be as focused as possible in the bulk of the plasma should be $\lambda \approx a$.

1.3.2.3 Neutralisation efficiency

During the neutralisation, it has to be considered that two processes occur: the first process is the neutralisation of ions after an impact with a background particle with the associated σ_s cross section; the second process involves the ionisation of high energetic neutral particles after the collision with neutral background particles. Regarding the first process since the binding energy of the electron to the atom is very low, the cross section is greater than that in the case of positive ions; referring instead to the second process, for it the associated cross section is σ_i. Basically σ_s is greater than σ_i.
The entire neutralisation process is mathematically described by the following model[7]:

$$\begin{aligned} \frac{\mathrm{d}\Gamma_b^-}{\mathrm{d}x} &= -n_n\sigma_s\Gamma_b^- \\ \frac{\mathrm{d}\Gamma_b}{\mathrm{d}x} &= -n_n\sigma_i\Gamma_b + n_n\sigma_s\Gamma_b^- \end{aligned} \tag{1.18}$$

The right hand side of the first equation represent the negative variation of the number of negative ions because of the electronic stripping due to the collision

with the background neutrals; such a loss of ions is traduced into an increase of the flux of the neutral particles: in fact the same term appears in the right hand side of the second equation with the opposite sign. The first term of the right hand side of the second equation represent the loss of neutral particles due to the ionisation after the collisions with the background neutrals.
So, if the neutraliser was infinite, as the flux go through it both the flux of negative particle and the flux of neutral particles would decay to zero; that fact means that must exist a specific length for which it can be obtained the maximum possible neutralisation. Eq.(1.18) solved gives:

$$\Gamma_b^- = \Gamma_0 e^{-\frac{x}{\lambda_s}} \Gamma_b = \Gamma_0 \frac{\lambda_i}{\lambda_s - \lambda_i} \left(e^{-\frac{x}{\lambda_i}} - e^{-\frac{x}{\lambda_s}} \right) \tag{1.19}$$

where $\Gamma_0 = \Gamma_b^-(0)$, $\lambda_s = \frac{1}{n_n \sigma_s}$ e $\lambda_i = \frac{1}{n_n \sigma_i}$.
Neutralisation fraction is a function of x given by:

$$f_x(x) = \frac{\Gamma_b(s)}{\Gamma_0} = \frac{\lambda_i}{\lambda_s - \lambda_i} \left(e^{-\frac{x}{\lambda_i}} - e^{-\frac{x}{\lambda_s}} \right) \tag{1.20}$$

The latter function has a maximum in:

$$x_m = \frac{\lambda_i \lambda_s}{\lambda_s - \lambda_i} \ln \frac{\lambda_i}{\lambda_s} = \frac{1}{n_n(\sigma_s - \sigma_i)} \ln \frac{\sigma_s}{\sigma_i} \tag{1.21}$$

This coordinates corresponds to the optimal length for the neutraliser. For a negative particle flux with an associated energy of 1 MeV the neutralisation efficiency remains constant and on the order of 60%; contrariwise for a positive particle flux with an associated energy of 1 MeV the efficiency would decay to 1%. This is the reason why most of the researchers suppose that positive particle won't have any future in this application and have focused their attention to the usage of negative particles.

Part I

Design and Test of the Protection System for NIO1 Experiment Power Supply System

Chapter 2

NIO1 experiment

2.1 Introduction: description of NIO1 experiment

NIO1 (Negative Ion Optimisation step 1) experiment, whose construction had started in 2010 at Consorzio RFX in Padova in collaboration with INFN-LNL and whose complete installation has occurred in 2013-2014, is a radio-frequency Hydrogen negative ion source designed to produce a beam current of 130 mA (subdivided in 9 beamlets, that is 15 mA per beamlet) with 60 keV particle energy, with an electron-to-ion current ratio up to 2. The aim of the experiment is to provide a highly flexible system to test material properties of source components and to benchmark simulation codes for beam optics and plasma behaviour[2].
A scheme of the NIO1 is shown in the figure 2.1:

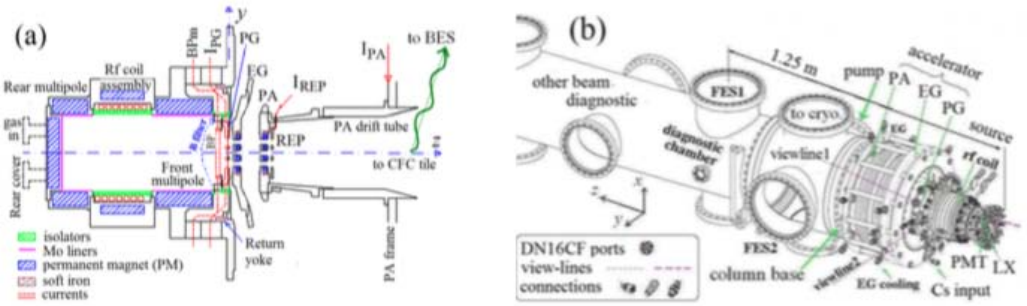

Figure 2.1: Two different images which show an overview of NIO1 experiment and beam line components[11].

NIO1 is composed of three main parts:

- The **source** (shown in figure 2.2)in which the plasma is generated by a radio-frequency magnetic field produced by the RF coils. The source is a cylindrical chamber (210 mm long, 50 mm radius) in which plasma is generated by a water cooled RF coil made up of 7 copper turns made from a pipe with 6 mm external diameter wound around an alumina cylinder of 78 mm height forming the source chamber. The coil is coupled to the source and it can provide a power up to 2.5 kW at the adjustable frequency $2MHz \pm 10\%$. In the source walls magnets are inserted, arranged in a multipole configuration in order to confine the plasma.
  The vacuum in the chamber is maintained with a proper vacuum system composed by two pumps: a volumetric pumps used for reach a low vacuum degree and a turbomolecular pump which allows to reach a high level of vacuum ($\sim 10^{-7}$ mbar).
  Two more component are mounted in the source stage of NIO1:
  - **plasma grid (PG)**: it is the source output, facing the plasma; it is a copper plate, with 9 holes having 7.6 mm diameter arranged in a 3x3 matrix and spaced by 14 mm for a total area of about 400 mm^2, which can provides an ion current density of 300 A/m^2 at nominal ratings. The PG is electrically insulated from the source and thus it can be biased at some volts ($\leq$ 30 V) with respect to the source; more precisely in NIO1 the reference potential is PG, which can be polarised up to -60 kV with respect to ground.
  - **bias plate**: it is located just before the PG and it is composed by two different insulated elements:
    * **magnetic bias plate** that is a sort of rectangular frame which provides the return path for the current of the magnetic filter, the so called PGF, flowing through the PG that acts so as to deflect hot electrons reducing the amount extracted through the PG holes;
    * **electrostatic bias plate** that is a round frame, exposed to the plasma, that can be biased up to 20 V with the aim to attract electrons by modifying the charge profile in the source.
- The **particle accelerator** stage in which negative particles are extracted

from the source and accelerated up to 60 keV thanks to potential difference between the grids. On the contrary with respect to what has been said before NIO1 is not equipped with the last two stages of a neutral beam source. This happens because NIO1 has not been built to operate as a true additional heating system but only for the study and the characterisation of the source and the negative particles beam. The acceleration column basically is made of:

  - **Extraction grid** (EG) which can be biased with respect to PG up to +9 kV (-51 kV from ground reference), in this way negative charges coming from the plasma grid are extracted and partially accelerated, moreover the polarisation voltage is completely tunable form 0 to 9 kV allowing to adjust the beam optics. Like PG it is made of copper and 9 holes in a 3x3 matrix are present in order to let the particles to go through. With the purpose to deflect co-extracted electrons four magnets are embedded inside the grid with magnetic axis along the direction of the beam with alternating polarity; the magnets are arranged in the vertical direction.
  - **Post acceleration grid** (PA) which is built like the others and is at the ground potential.
  - **Repeller grid** (RG) is placed just after the PA and can be biased with positive voltage (up to 150 V) with respect to ground in order to prevent positive ions (e.g. generated by background gas stripping) from going into the accelerator where they would be accelerated upstream up to the source damaging it by sputtering mechanism.

- A complete plasma and beam diagnostic set of **probes**.

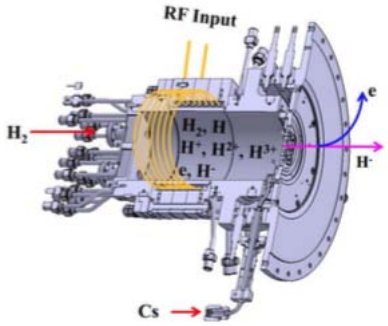

Figure 2.2: Source chamber of NIO1: the chamber in which the negative ions are created starting from neutral native particles thanks to an induced RF discharge[11].

All the grids are water cooled and the extraction grid is insulated from post acceleration grid by two insulating ceramic rings made of alumina; another ring insulates the EG from PG. Finally, the third part is the diagnostic chamber that is a metallic tube (length=1.5 m, inner diameter= 350 mm), connected downstream to the acceleration column, in which several ports are present for different diagnostics to be used to characterise the beam. Moreover inside the diagnostic tube the beam dump is placed; it is a carbon fiber composite tile used for calorimetry purposes.
The picture 2.3 represents an exploded view of the whole NIO1 system in which it is possible to see all the main parts:

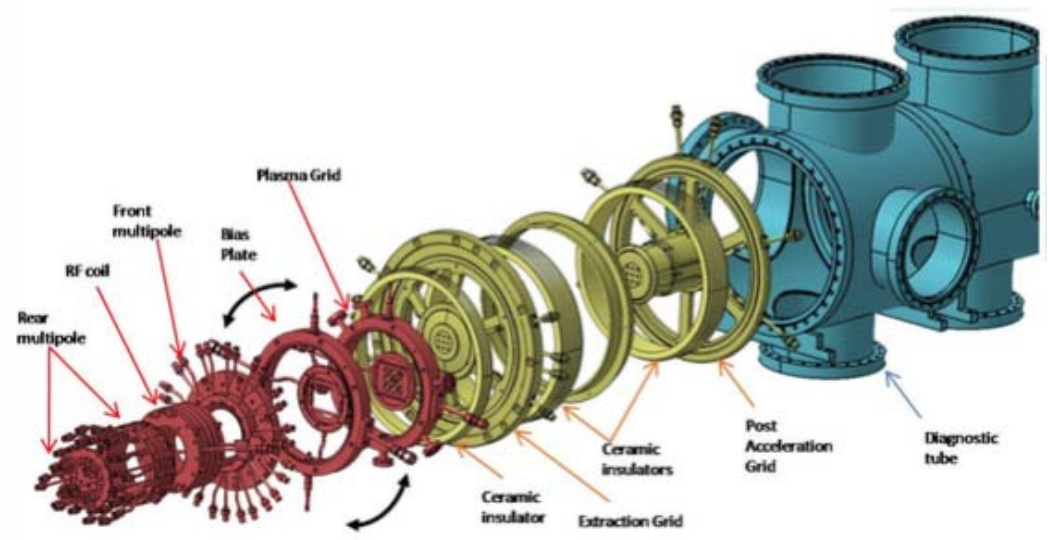

Figure 2.3: Exploded view of NIO1 experiment.

2.2 NIO1 experiment electric circuit

The NIO1 PSs (Power Supply System) is composed of a radio-frequency generator, high current-low voltage power supplies, high voltage-low current power supplies and auxiliary power supplies. The high current PSs are employed with the purpose of limiting extracted fraction of electrons in the ion beam; they include: Source Bias PS (SBPS), Bias Plate PS (BPPS) and Plasma Grid Filter PS (PGFPS). The high voltage PSs for the extraction and acceleration of the beam includes Extraction Grid PS (EGPS) and Acceleration Grid PS (AGPS).
The exit of the accelerator is at ground potential and the ion source works at high potential, polarised by the AGPS (as can be seen in fig. 2.4). Consequently, the power supplies for the ion source and the EGPS are housed on an insulating platform, named High Voltage Deck (HVD) which has the same potential as the AGPS high voltage output. HVD is isolated from ground potential by ceramic insulators. Then the devices on the HVD are fed by an insulator transformer (70 kV and 50 kVA). Along with the PSs, the diagnostic equipments working at the ion source potential are installed in the HVD too. The cables which connect the PSs in the HVD to the beam source are routed through a High Voltage Line.
The following figure, fig. 2.4, gives an insigh on the NIO1's electrical system:

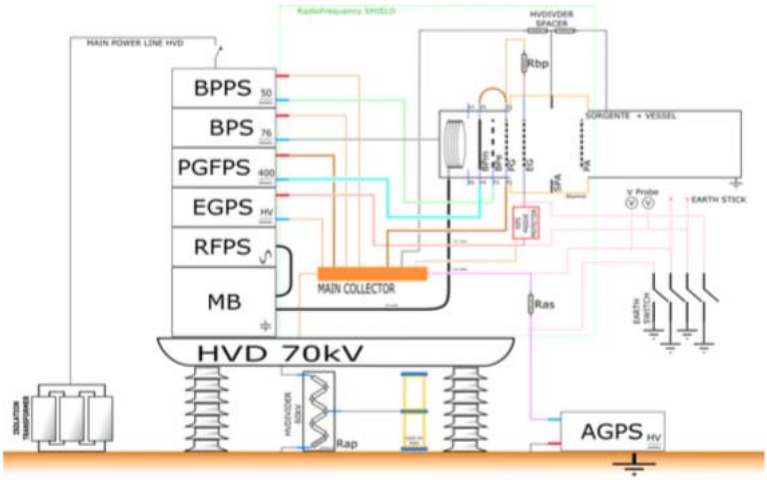

Figure 2.4: NIO1's electrical system overview[3].

In NIO1 the plasma source operates at high potential (up to -60 kV voltage)

and the beam extracted is accelerated and hits the beam dump which is at ground potential. The beam is extracted from the source by a 10 kV HV PS called EGPS connected between the PG and EG; the acceleration of the beam is powered by the AGPS connected between the PG and ground.

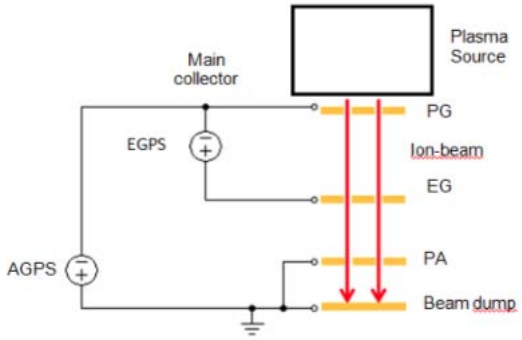

Figure 2.5: NIO1 electrical system overview[3].

Since the HV PS have a High Voltage Multiplier Stage made of high voltage diodes and capacitors, a resistor with suitable value, called bleeder resistor, is connected in parallel to the HV output in order to provide a minimum load and guarantee a fast discharge of the electrostatic energy stored in the capacitors when the output is off. The value of the resistance of the bleeder resistor has to be a compromise with respect to the time needed to discharge the HVPS and the current drained during the normal operation where the output is active. In particular, on NIO1 two bleeder resistors are present one on the AGPS's output with a value of $300M\Omega$ and the other at the output of EGPS with a value of $6 \times 50M\Omega$.
On HVD there is also the radio-frequency PSs (RFPS) which is connected to the Matching Box (MB) which contains adjustable capacitors. A transmission line connects the MB to the RF coil. The MB is intended to permit a good coupling between the RFPS and the plasma in the source.
At the date of today a NIO1 is equipped with a protection system suitable for the range of voltages utilised until now. The bearing structure of this voltage divider is showed in figure 3.1 where the over voltage suppressor is composed by MOV (Metal Oxide Varistor). This protection system doesn't allow to reach the rating voltage of the PSs because it can handle a lower voltage: it is sized for 5kV (EGPS voltage) and 10kV (AGPS voltage). This voltage regime is no longer sufficient for NIO1 operation and thus a new protection system which

allows NIO1 PSs to reach its nominal voltages is required. The following of this chapter is about the design of a new protection system. In particular the chapter focuses on the design of a new voltage suppressor made up with sidac and a test to verify this solution; the aim is to understand if this could be the final solution to the problem.

Chapter 3

New protection system

3.1 Introduction to the new protection system

In NIO1 experiment electric discharges between the extraction grid and the acceleration grid are likely to happen and they must be properly treated in order to avoid, or at least mitigate, detrimental effects on both power supplies and grids due to electrical and thermal stresses.
In particular the HV circuit shows an electrical configuration with AGPS and EGPS in parallel when a EG-PA breakdown occurs (figure 3.1). In this configuration AGPS can drive a voltage increase on the EGPS output stage. In order to mitigate the effect on the EGPS of this particular configuration, a protection circuit is required. The conceptual scheme of the situation above described and the idea for the design of the protection system is reported in the figure 3.1.

The aim of this circuit is to isolate the EGPS in the particular breakdown occurrence described above. The circuit developed is composed of diodes and sidacs. The principle of operation is the following: as the breakdown occurs and the current from AGPS starts to flow into the fault, the path toward the EGPS is blocked by the series diodes D_s since they are counter polarised. The sidacs role is to conduct, since, over a certain voltage, they act as short circuit, the AGPS discharge current to block the PG-EG voltage at a controlled level. The antiparallel diodes D_{ap} diverts the current from flowing in the EGPS in situation in which as a consequence of the oscillation associated to PG-EG breakdown, the potential reverses with respect to the normal operation. The series resistor R_{bs} is introduced to limit the EGPS discharge current in case a

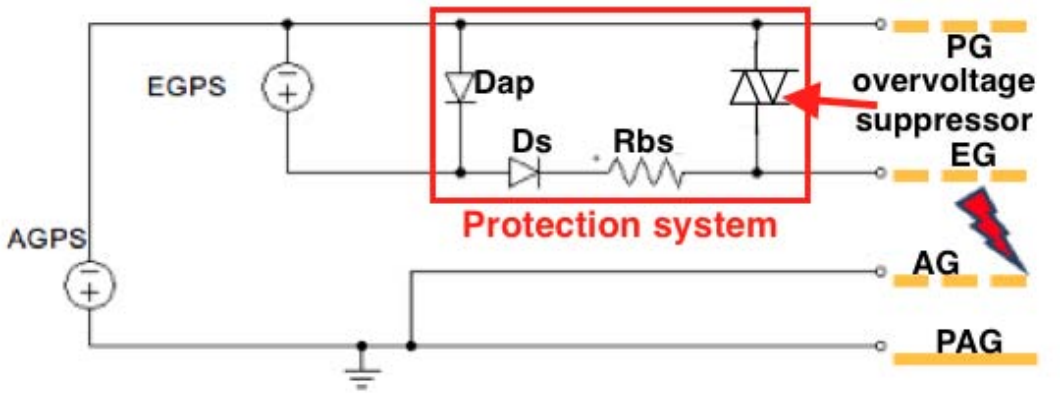

Figure 3.1: Conceptual scheme of breakdown between EG and PA above described and the idea for the design of the protection system[3].

EG-PG breakdown occurs.
The list below summarises the role of the components present in the protection circuit:

- D_{ap}: the anti-parallel diodes handle the EG-PG voltage reversal. In the case of such an occurrence D_{ap} is directly polarised, so they conduct almost as a short circuit, and protect the EGPS thanks to a short circuit in parallel.

- D_s: the series diodes protect the EGPS in the case of PA-EG breakdown; since they result inversely polarised - by the AGPS voltage - they block the flow of the current since they acts almost as an open circuit.

- R_{bs}: it reduces the EG breakdown current. In this way a control of the diode maximum current can be. there is a margin with respect to the current that the diodes can withstand.

- sidacs: when the voltage overcomes a characteristic value the impedance is set nearby to zero and the breakdown current is deviated to ground. The principle of operation and main characteristics of sidacs will be explained later in a dedicated section.

Below some design considerations are presented:

- Series connection of either diodes and sidacs need a high resistance resistor and a capacitor in parallel in order to equalise the voltage drop on

each component. This is explainable with the following reasoning: not all the components are characterised by exactly the same value of internal resistance and parasitic capacitance, this is true both for diodes and sidacs. This lead to a non-homogeneous voltage drop along the series of components. This can be avoided thanks to a high value resistance, sized considering the leakage current of the component, and a capacitance that has to have a value more than 10 times the value of the characteristic parasitic capacitance of the component. The resistance guarantees a good division of the voltage drop in a steady state situation; the capacitor guarantees instead a good sharing of the voltage drop during transient situations. Both the resistance and the capacitance must be placed in parallel with the component.

- Series resistance is a further protection component to mitigate the current flowing in case of fault. Because of this its value has to be a compromise between a proper mitigation of the current, the fact that the value of the breakdown current can't be too low in order to be detected by the protection system and the power dissipation in normal operation.

- Series of anti-parallel diodes has to withstand the total voltage across the EGPS. The series has to be over-dimensioned in order to fulfil: a perfect protection and the assurance that there will not be any fault in the diodes. Because of this the series of diodes is dimensioned for about 13 kV voltage, a value with a reasonable margin with respect to the operating voltage (10 kV).

- The rapid evolution of voltage and current during breakdown, require components with fast intervention time. The choice for the series diodes also considers the high working voltage, the surge current and reverse voltage required. Consequently the selection of the diodes was directed to Fast Recovery High Voltage Diodes. The D_s, which is a series of diodes, has to withstand the EGPS breakdown current of 70 A, the dc current of the EGPS of about 600 mA and a reverse voltage due to the sidac breakover voltage. In the worst case, in which the EGPS out voltage is zero, this reverse voltage would be equal to the sidacs clamping voltage and thus proportional to the number od sidacs put in series. This number must be consequently chosen in an optimal way in line with the

sizing of the protection system.
Furthermore, it is better to assemble a series of diodes that can withstand a higher voltage with respect to the sidacs clamping voltage in order to obtain some margin. It has to be remembered that any eventual fault in any of the components of the protection system will result in a non-functioning of the whole system with consequent possible disruptive consequences.

- with reference to parallel capacitors for the voltage sharing along a series of diodes or sidacs they must be chosen by considering the following items:
  - capacitance has to be more than 10 times the capacitance of the diodes;
  - capacitor must withstand the maximum reverse voltage bearable by diodes;
  - it is better to over-dimension the capacitance just to be sure that there will not be any fault (voltage across the capacitor greater then the rating bearable voltage).

3.2 Sidac

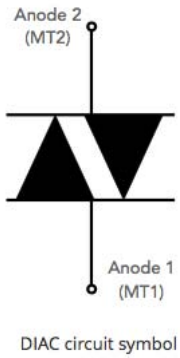

Figure 3.2: Schematisation of a DIAC[32]

DIAC (Diode for Alternating Current) is a bidirectional silicon diode with two terminals: anode 1 and anode 2. Their bidirectional behaviour is referred at the current between the two anodes; the latter can flow from anode 1 to

anode 2 or from anode 2 to anode 1: when DIAC is directly polarised anode 1 is set to a greater potential with respect to that of anode 2 and the polarisation voltage is $V > 0$; when it is inversely polarised anode 1 is at a smaller potential than anode 2 and $V < 0$.
DIAC's resistance can be brought either to a high value (clamping state - OFF mode), or to a very low value (conduction state - ON mode). Therefore DIAC acts as a switch.
If V is the voltage across the two anodes, the commutation OFF-ON occurs at the breakover voltage ($\pm V_{BO}$); instead the commutation ON-OFF occurs when V becomes smaller than the maintenance voltage V_H. Commutation happens for both the polarisation sign of V.
Main parameters of DIAC are:

- **breakover voltage** V_BO;
- **breakover current** I_BO: it is the small reverse current which characterises the quality of the interdiction level of DIAC; smaller is the breakover current higher is the interdiction level of DIAC;
- **maintenance voltage** V_H;
- **symmetry offset**: it is the small difference of potential between $+V_BO$ and $-V_BO$ which is caused by the non-perfect symmetric structure of DIAC.

V-I characteristic of DIAC is shown in figure 3.3:

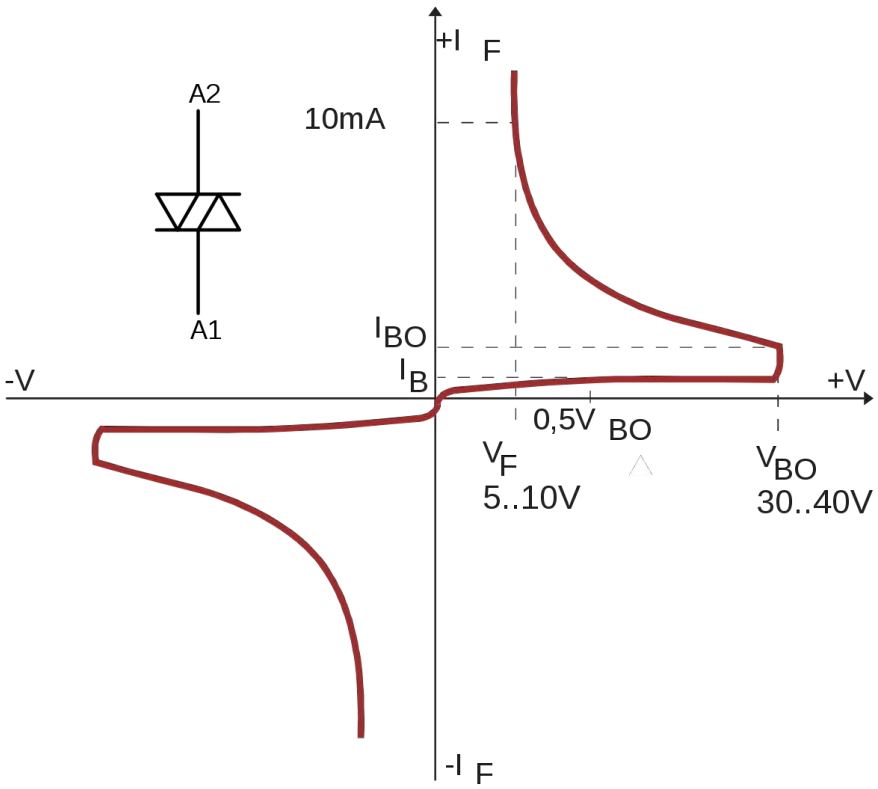

Figure 3.3: V-I characteristic of DIAC[33]

SIDAC (Silicon Diode for Alternating Current) is electrically similar to DIAC, but it has a higher breakover voltage and greater current handling capacity. SIDAC is also known as SYDAC (Silicon thYristors for Alternating Current or simply bidirectional thyristor diode); it is technically specified as a bilateral voltage triggered switch. Thanks to its characteristic it can be directly used for switching.

Conceptually the working operation of a SIDAC is assimilable to that of a spark gap, with the only difference that a SIDAC has a smaller temperature rating. A SIDAC doesn't conduct until the applied voltage exceeds the nominal breakover voltage. Then the SIDAC continues to conduct, it enters the so called *dynamic resistance region*, until the applied current falls below its rated holding current. When this happens the SIDAC returns to its non-conductive state ready to begin a new cycle.

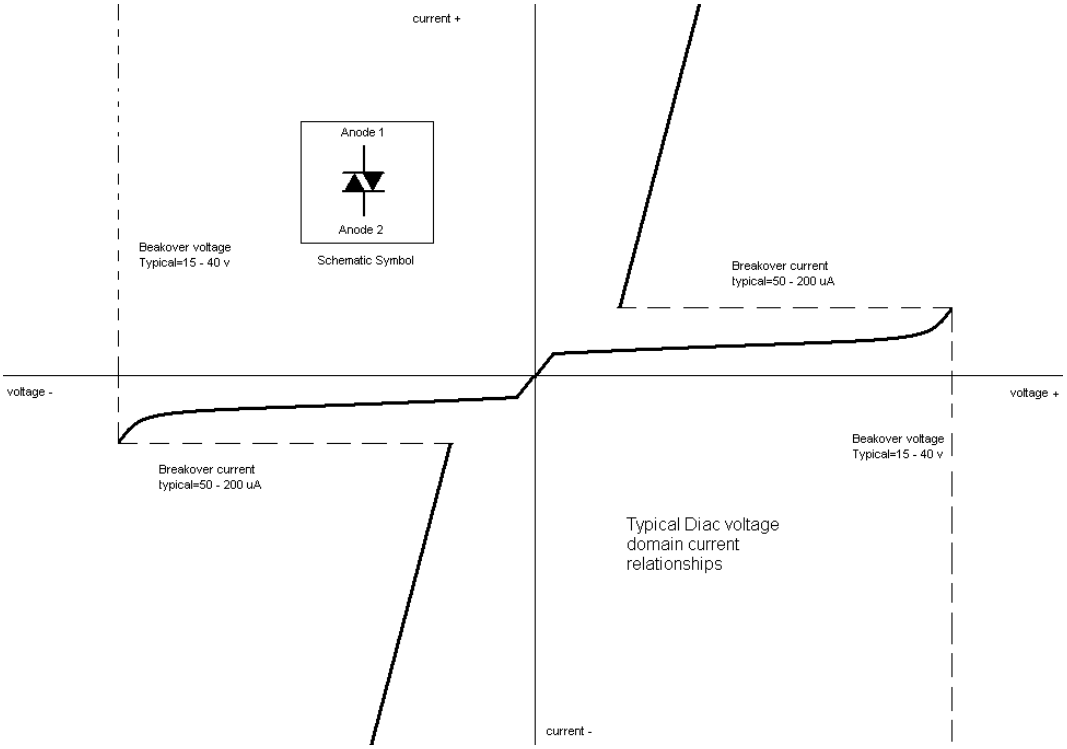

Figure 3.4: V-I characteristic of SIDAC (`https://en.wikipedia.org/wiki/DIAC/media/File:Diacgraph.png`).

After a market survey a proper SIDAC suitable for our purpose has been chosen: SMP100MC-400. Such a component is characterised by the following main parameters (the others may be found in (31)):

- $I_{pp}(8/20\mu s) = 300A$
- $V_{RM} = 360V$
- stray capacitance = 30pF
- leakage current = 2μA

This component has just been tested(1) and seems to accomplish its mission. In (1) this component has been confronted with also MOV (Metal Oxide Varistor) and TVS (Transient Voltage Suppression Diode) but they have some problems, respectively: the voltage to the clamps doesn't remain constant and a too much high cost. In line with the analysis carried out in (1) sidac has been chosen for this application.

3.3 PCB critical issues

A PCB (Printed Circuit Board) is an insulated support for an electric circuit, it gives: mechanical support and allows to electrically connects the electronic components mounted on it. This connection occurs through conductive tracks and pads etched from copper sheets laminated onto a non conductive substrate. This non conductive substrate can be made of FR-4 (Flame Retardant - 4) glass epoxy which is a composite material composed by fibreglass brained in a glass epoxy flame retardant matrix.
The electrical characteristic of such a material is summarised in the table 3.5[34]:

Rigidità dielettrica	KV/mm	CEI	d)15
Resistenza superficiale	MΩ	CEI	c)10^3
Resistività elettrica tra spine	MΩ	CEI	c)10^5
Costante dielettrica 1MHz		CEI	c)7

Figure 3.5: Main physical characteristics of vetronite FR-4.

The main problem that can rise from the usage of PCB circuits in high voltage application is that the distance between tracks could be too small to withstand the intense electric field present due to the high value of voltage. The following section describes this aspect by taking into account the various elements that contribute to both mitigate the effect and promote the latter. First of all, the distance between the tracks, known as spacing, which has to be sufficient to withstand the voltage, is described by two different indexes[28]:

- **Clearance** is the shortest distance in air between two conductive parts. Clearance shall be dimensioned to withstand the required impulse withstand voltage.

- **Creepage** is the shortest distance along the surface of a solid insulating material between two conductive parts. The values of table 3.6 are based upon existing data and are suitable for the majority of applications.
  The basis for the determination of a creepage distance is the long-term r.m.s. value of the voltage existing across it.

The influence of the degrees of pollution in the micro-environment on the dimensioning of creepage distances is taken into account in table 3.6. To keep

in mind is also that in the same equipment, different micro-environment conditions can exist.
A creepage distance cannot be less than the associated clearance so that the shortest creepage distance possible is equal to the required clearance. However, there is no physical relationship, other than this dimensional limitation, between the minimum clearance in air and the minimum acceptable creepage distance.
The table 3.6 is the just cited "Creepage distances to avoid failure due to tracking[35] ".

Creepage distances to avoid failure due to tracking *(table F.4)*

Voltage r.m.s.	Minimum creepage distances								
	Printed wiring material								
	Pollution degree								
	1	2	1	2			3		
	All material groups	All material groups except IIIb	All material groups	Material group I	Material group II	Material group III	Material group I	Material group II	Material group III
V	mm	mm	mm	mm	mm	mm	mm	mm	mm
10	0.025	0.040	0.080	0.400	0.400	0.400	1.000	1.000	1.000
12.5	0.025	0.040	0.090	0.420	0.420	0.420	1.050	1.050	1.050
16	0.025	0.040	0.100	0.450	0.450	0.450	1.100	1.100	1.100
20	0.025	0.040	0.110	0.480	0.480	0.480	1.200	1.200	1.200
25	0.025	0.040	0.125	0.500	0.500	0.500	1.250	1.250	1.250
32	0.025	0.040	0.14	0.53	0.53	0.53	1.30	1.30	1.30
40	0.025	0.040	0.16	0.56	0.80	1.10	1.40	1.60	1.80
50	0.025	0.040	0.18	0.60	0.85	1.20	1.50	1.70	1.90
63	0.040	0.063	0.20	0.63	0.90	1.25	1.60	1.80	2.00
80	0.063	0.100	0.22	0.67	0.95	1.30	1.70	1.90	2.10
100	0.100	0.160	0.25	0.71	1.00	1.40	1.80	2.00	2.20
125	0.160	0.250	0.28	0.75	1.05	1.50	1.90	2.10	2.40
160	0.250	0.400	0.32	0.80	1.10	1.60	2.00	2.20	2.50
200	0.400	0.630	0.42	1.00	1.40	2.00	2.50	2.80	3.20
250	0.560	1.000	0.56	1.25	1.80	2.50	3.20	3.60	4.00
320	0.75	1.60	0.75	1.60	2.20	3.20	4.00	4.50	5.00
400	1.0	2.0	1.0	2.0	2.8	4.0	5.0	5.6	6.3
500	1.3	2.5	1.3	2.5	3.6	5.0	6.3	7.1	8.0
630	1.8	3.2	1.8	3.2	4.5	6.3	8.0	9.0	10.0
800	2.4	4.0	2.4	4.0	5.6	8.0	10.0	11.0	12.5
1000	3.2	5.0	3.2	5.0	7.1	10.0	12.5	14.0	16.0
1250			4.2	6.3	9.0	12.5	16.0	18.0	20.0
1600			5.6	8.0	11.0	16.0	20.0	22.0	25.0
2000			7.5	10.0	14.0	20.0	25.0	28.0	32.0
2500			10.0	12.5	18.0	25.0	32.0	36.0	40.0

Figure 3.6: Creepage distances to avoid failure due to tracking. The table gives the creepage value in function of the insultagin material and the environment pollution degree.

The environment determines the effect of pollution on the insulation.

- Pollution Degree 1: No pollution or only dry, non-conductive pollution

occurs. The pollution has no influence.

- Pollution Degree 2: Only non-conductive pollution occurs except that occasionally a temporary conductivity caused by condensation is to be expected.
- Pollution Degree 3: Conductive pollution occurs or dry non-conductive pollution occurs which becomes conductive due to condensation which is to be expected.
- Pollution Degree 4: Continuous conductivity occurs due to conductive dust, rain or wet conditions.

The dimensions for creepage distance cannot be specified where permanently conductive pollution is present (Pollution degree 4). For temporarily conductive pollution (Pollution degree 3), the surface of the insulation may be designed to avoid a continuous path of conductive pollution, e.g. by means of ribs and grooves. It has to be remembered too, that an anti-moisture coating is always present on the surface of PCB.
CTI (an acronym that stands for Comparative Tracking Index) is an index used to measure the capability of an insulator to withstand superficial discharges. Based on the CTI different isolation groups of electric material are introduced (refferring to EN50124):

Materiale	CTI
Gruppo I	>600
Gruppo II	400 < CTI < 600
Gruppo IIIa	175 < CTI < 400 (FR4 [2])
Gruppo IIIb	100 < CTI < 175

Figure 3.7: Comparative Tracking index[36]; the numbers on the right column are voltage so that a material belonging to group one should be able to withstand a voltage greater than 600V.

Taking into account:

- the table of CTI
- the table of creepage distances to avoid failure due to tracking
- the fact that, in our case, tha maximum voltage across a single SIDAC is 800V

it is possible to conclude that, at least, the track on our PCB must be spaced of 2,4 mm, considering a degree pollution of 1; or 4 mm considering a pollution degree of 2.
The most compelling regulation that has been found is the IPC - 2221[15]; it introduces a simplified formula, which gives the creepage according to the rms value in the case of AC or DC values, in a very overdimensioned manner with respect to that introduced by the table above. The mentioned formula is:

$$\text{creepage (mm)} = 0.6 + V_{peak} \times 0.005 \tag{3.1}$$

It gives, in our case, a creepage of 4,6 mm needed to avoid superficial discharge on PCB. In conclusion it can be said that a compromise between the two found values could be an optimal choice for the creepage spacing in our PCB.
Concerning the clearance and the danger of aerial discharge it has to be considered that:

- the dry air dielectric constant is 30 kV/cm;
- the corona effect takes place whenever the condition $E > 30$ kV/(cm of radius) is satisfied;
- for rounded smooth surface the distance in millimetres between two electric conductors necessary to give rise to a discharge can be calculated as kV/30; for sharp point the same value is kV/85; there is almost a factor of 3 between the two values.

Regardless the discussion above, some precautions can be taken in order to prevent fault situations:

- avoid any sharp parts on the circuit either in the inner layers of PCBs such as pads (which ought to be all but circular), track angles (which have to be avoided), and in the outer parts like weldings (which must be as rounded as possible);

- pad area should not be too small.

There are moreover some methods useful to prevent fault situations in those cases in which the operator can not be quite sure that the fault is impossible at all[10]; for example:

- concerning the welding, it is possible to cover the sensible parts with a thermosetting silicon in order to increase the clearance and the dielectric constant of the path between two parts at different potential;
- on the PCB a cut can be made in order to increase the creepage distance between two parts at different potential;
- to further isolate high voltage areas an inert insulator such as polyester or Teflon can be press inserted in to a pre-routered slot in the board. In addition a suitable glue or retaining clip can be designed. This is shown in the figure 3.8[10].

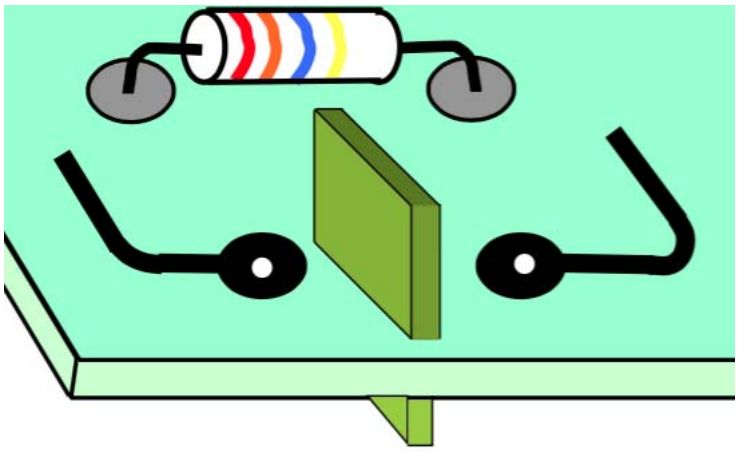

Figure 3.8

3.4 Sidac circuit

3.4.1 Description of the sidac circuit

Finally, after the considerations above, the sidac circuit has been built; twenty-five series connected sidacs distributed in five strings, taking into account the rating of the breakover voltage of the chosen component (SMP100MC-400), have been used in order not to intervene with the maximum nominal voltage of the EGPS (10kV) but only when over voltage occurs. As explained above, parallel resistor and capacitor of proper value are connected in order to equalise the voltage drop on the single component; both the resistor and capacitor are SMD (an acronym that stands for Surface Mounted Devices) and have a value respectively: 10 $M\Omega$ and 360 pF. The project criterion for the capacitor is those explicated before: it has to be at least 10 times bigger than parasitic capacitance of the sidac which is about 30pF[31]. Such a big value serves because the capacitive impedance associated must be much smaller with respect to that of the sidac internal capacitance in order to draw off the current. The sizing of the resistor starts from considering the leakage current of the sidac which, il line with the data sheet is 2 μA[31]. Since the resistor must draw off a current much higher with respect to the leakage current, the ratio between the voltage across the sidac clamps and the inserted resistance has to be higher than the leakage current. With 10 $M\Omega$, the chosen value for the resistance, considering that the voltage across the sidac is theoretically 400V, the resulting current through the is 40μA which is much higher that the leakage current.
The layout shown in figures (a), (b), (c) and (d) has been chosen after some other hypotheses have been considered: S connection in a single plane, zig-zag connection on a single plane. The great advantage of this configuration is that it avoids the fact of having two components with a d.d.p. equals to two times the voltage across a single string of sidacs faced. This layout avoids strong electric field between facing components and so reduces the possibilities of discharges between component. It is furthermore the most compact layout considered.

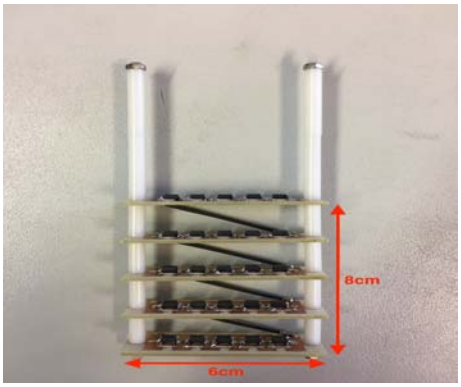

(a) *sidac circuit.*

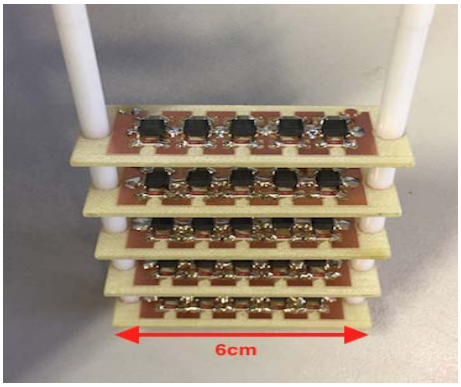

(b) *sidac circuit.*

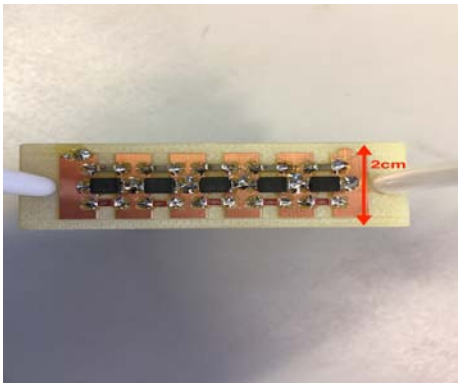

(c) *sidac circuit.*

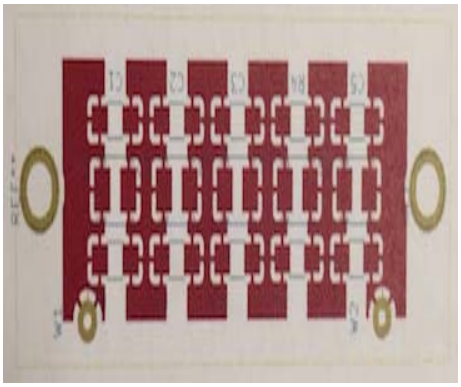

(d) *sidac cad.*

3.4.2 Preparing the test bench

In order to test the sidac circuit the following test bench has been built:

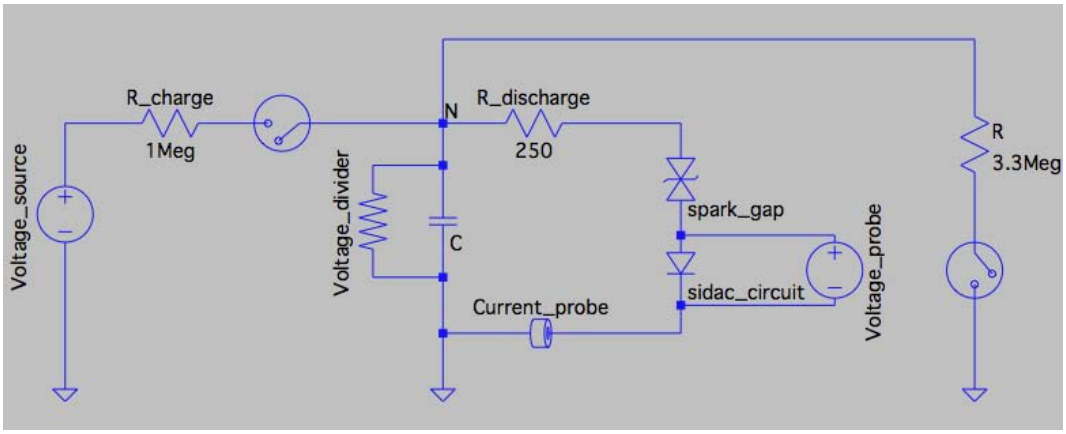

Figure 3.9: Test bench necessary to test the sidacs circuit behaviour.

Practically the test bench is designed in order to understand what happens

when the sidac circuit receives a voltage impulse; in particular: if the circuit is strong enough to withstand high voltage impulse, how the circuit behaves with respect to such a fast discharge, if sidacs work properly as they should do (i.e. they should act as an open circuit until the voltage at their clamps exceeds a specific voltage and then they should act as a short circuit) and to measure the overvoltage on the stack of sidac before they intervene.
The first three components on the left-hand side of the circuit 3.9 are a voltage source a resistance and a switch. The resistance has the scope to control the current supplied by the power supply. The source is connected to the capacitor and the latter is charged so that at its clamps there is the test voltage (up to 70 kV); once the condition of completely charged capacitor is reached the switch S1 is opened. The capacitor discharges through the sidac as the spark gap is triggered[1] through the sidacs circuit. Two measurement tools are present in the circuit: a voltage probe in order to measure the voltage across the sidacs circuit and a current probe in order to measure the current; both these probes are connected to an oscilloscope. In parallel with the discharge capacitor a voltage divider is placed, from which a voltage measure is taken in order to have a live measure of the voltage across the capacitor.
The branch composed by a resistance and a switch (R_s and S2) has the aim to discharge the entire circuit when the tests are finished; this branch has only a safety scope. With the same aim also a earth stick is comprise and it can be connected to the principal node of the circuit (node N), the one where all the branches of the circuit converge.
Now the analysis proceed with the sizing of the components of the circuit above. Let's start from the known data:

3.4.2.1 Test bench sizing

In the following section the ratings of the test bench components are discussed. Known data and requirements are now fistrly presented:
KNOWN DATA:

[1] From wikipedia[(37)]: A spark gap consists of an arrangement of two conducting electrodes separated by a gap usually filled with a gas such as air, designed to allow an electric spark to pass between the conductors. When the potential difference between the conductors exceeds the breakdown voltage of the gas within the gap, a spark forms, ionising the gas and

- Capacitance: $C = 0,3\mu F$;
- Nominal Voltage rating of the capacitor: $V = 100kV$.
- Capacitor energy:

$$\text{energy} = E_{cap} = \frac{1}{2}CV^2 = \frac{1}{2}0.3 \cdot 10^{-6} \cdot (100 \cdot 10^3)^2 = 1500J$$

ASSUMPTIONS:

- Maximum voltage step during the capacitor charging phase to the regime value: $\Delta V_{max} = 1kV$.
- Maximum current: $I_{max} = 1mA$.

CHARGE RESISTANCE: The value of the charge resistance can be calculated as:

$$I_{max} = \frac{\Delta V_{max}}{R_{carica}} \quad \Rightarrow \quad R_{carica} = \frac{\Delta V_{max}}{I_{max}}$$

$$\Rightarrow \quad R_{carica} = \frac{\Delta V_{max}}{I_{max}} = \frac{1kV}{1mA} = 1M\Omega$$

Power rating of the resistor:

$$P_J = R_{carica} I_{max}^2 = 1W$$

Charge time in the case of $V_{max} = 70kV$:

$$Q_{tot} = C \cdot V_{max} = 0,3 \times 10^{-6} \times 70 \times 10^3 = 0.021C$$

$$\Delta t = \frac{Q_{tot}}{I_{max}} = 20sec$$

Time constant of the charge circuit with $I_{max} = 1mA = const$:

$$\tau_c = R_{carica} C = 0,3sec$$

The time constant is useful to understand how long the capacitor takes to charge to the regime voltage when a certain voltage step is applied, in this

drastically reducing its electrical resistance. An electric current then flows until the path of ionised gas is broken or the current reduces below a minimum value called the "holding current". In our case the spark gap is used in the opposite mode: the pressure is decreased until the discharge starts.

case 1kV.
In a RC circuit the current follows an exponential decay described by the law:

$$I(t) = I_{max} e^{-\frac{t}{\tau_c}}$$

Integrating from 0 to infinity the current a finite value is obtained equal to $\tau_c \cdot I_{max}$, indeed:

$$\int_0^\infty I_{max} e^{-\frac{t}{\tau_c}} = I_{max} \int_0^\infty -\frac{1}{\tau_c} e^{-\frac{t}{\tau_c}} dt = I_{max}(-\tau_c) e^{-\frac{t}{\tau_c}} |_0^\infty = -\tau_c I_{max}$$

Supposing that the transient can be considered extinct after $5\tau_c$ is possible to calculate the total charge that the capacitor has to accumulate in order to satisfy the calculation above:

$$Q = 5\tau_c \frac{I_{max}}{5} = 0.0003C$$

This last calculation points out that for each 1 kV step a charge equal to Q goes into the capacitor and with 70 steps it is possible to reach the desired $Q_{tot} = 0.021C$.
DISCHARGE RESISTANCE: Now the discharge resistance will be sized. It is known, from past experimentation, that in the worst case and considering also some margins, the current is about 250A with a time constant equal to $50\mu s$. Supposing that the maximum voltage is 60 kV and knowing the current peak, the discharge resistance can be easily calculated by means of Omh's law:

$$R_{discharge} = R_d = \frac{60kV}{250A} = 240\Omega$$

Considering that resistances value 120Ω, 106Ω e 103Ω and a fourth resistance with a value of 24Ω was available.
With 120Ω and 106Ω resistance, the circuit's time constant would be:

$$\tau = R_d C = 226 \times 0.3\mu = 68\mu s$$

Considering now the same decay law for the current as before, with this circuit parameters values the half current time would be:

$$I_{max} e^{-\frac{t}{\tau}} = \frac{I_{max}}{2} \quad \Rightarrow \quad -\frac{t}{\tau} = 0.5 \quad \Rightarrow \quad t_{1/2} = 47\mu s$$

The current peaks bearable from the sidac as reported in the datasheet[sidacdatasheet] are:

Symbol	Parameter		Value	Units
I_{PP}	Repetitive peak pulse current	10/1000 µs	100	A
		8/20 µs	300	
		10/560 µs	140	
		5/310 µs	150	
		10/160 µs	200	
		1/20 µs	300	
		2/10 µs	500	

Figure 3.10: Current peaks bearable from the sidac as reported in the data sheet[31].

From the table fig.3.10 it can be seen that the value to whom we are interested, i.e. 250A, is comprised between two values (200 and 300 A). For this reason another resistance is added, 24Ω, in order to have 250 Ω. The time constant of the circuit becomes:

$$\tau = R_d C = 250 \times 0.3\mu = 75\mu s$$

and the half current time:

$$t_{1/2} = 52\mu s$$

with a maximum current of 240A.
In this way the peak current is deceased and the half time is stretched. Since from the table 3.10 it can be seen that if the current were halved the corresponding t/2 would increase much more (current and half time are more than proportional) and since it is impossible to decrease the current derived from the experimentations in NIO1, in this way the half time was stretched a bit in order to fit better the component characteristic impulsive behaviour.
PROTECTION RESISTANCE: This resistance serves to discharge the test bench when the experimentations are finished. Supposing a very fast transient with a time constant equal to 5 second:

$$R = \frac{\tau}{C} = \frac{5sec}{C} = 17M\Omega$$

This hypothesis is very cautelative to be sure that the test bench is safe immediately afterwards the end of the experimentation. A $20M\Omega$ resistance has been mounted on the circuit. This means that even if the stored energy is greater it is discharged more slowly and this leads to some improvements, such as: less instantaneous power on the resistors and less parasitic effect. After

a market survey the following resistance has been chosen: OHMITE MOX-4N-131005FE, Through hole resistance, Maxi-Mox, 10 Mohm, 40 kV, Axial conductor, 5 W, ±1%, Maxi-Mox series.

3.4.2.2 Test bench

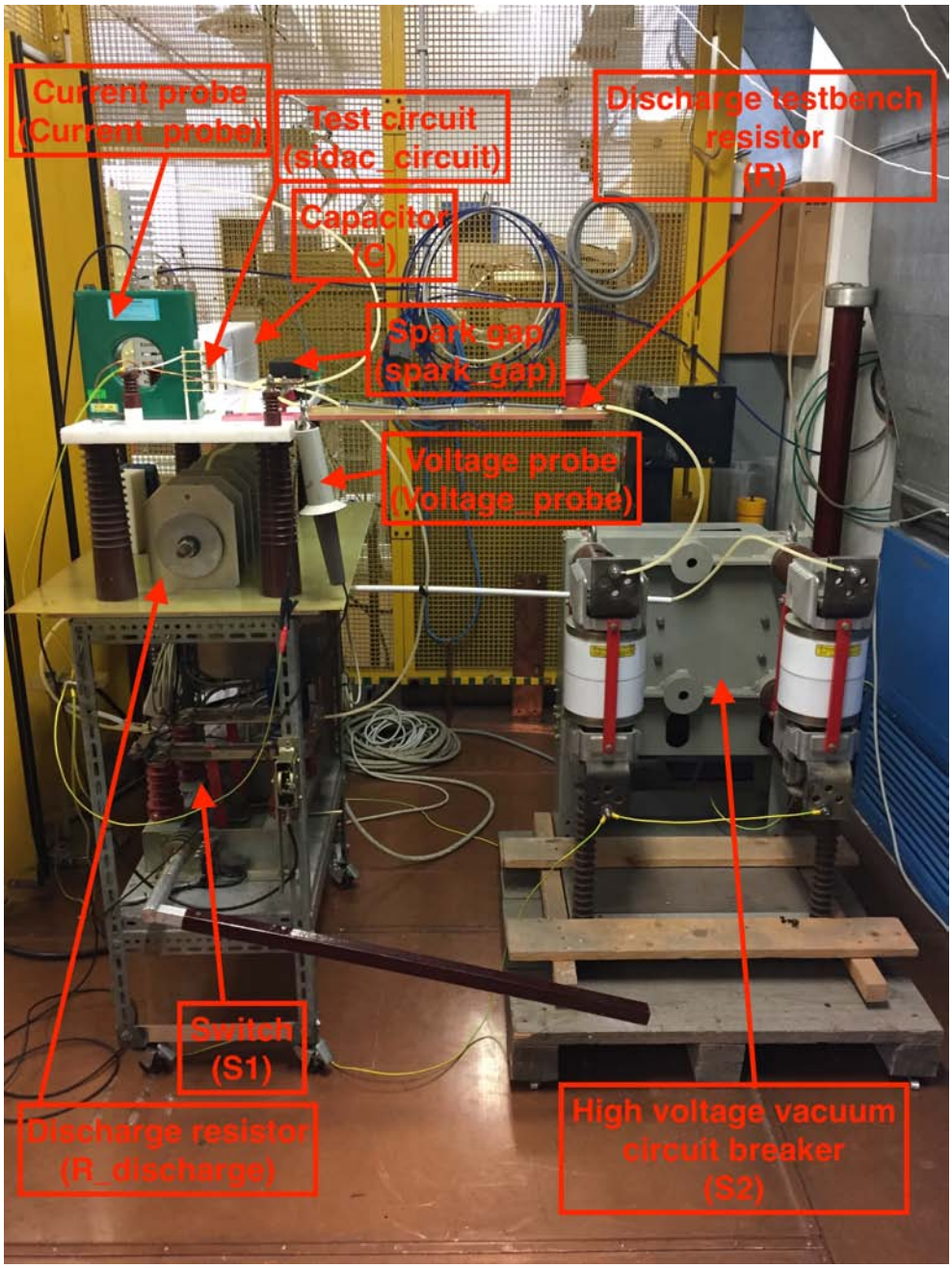

Figure 3.11: Sidac test bench

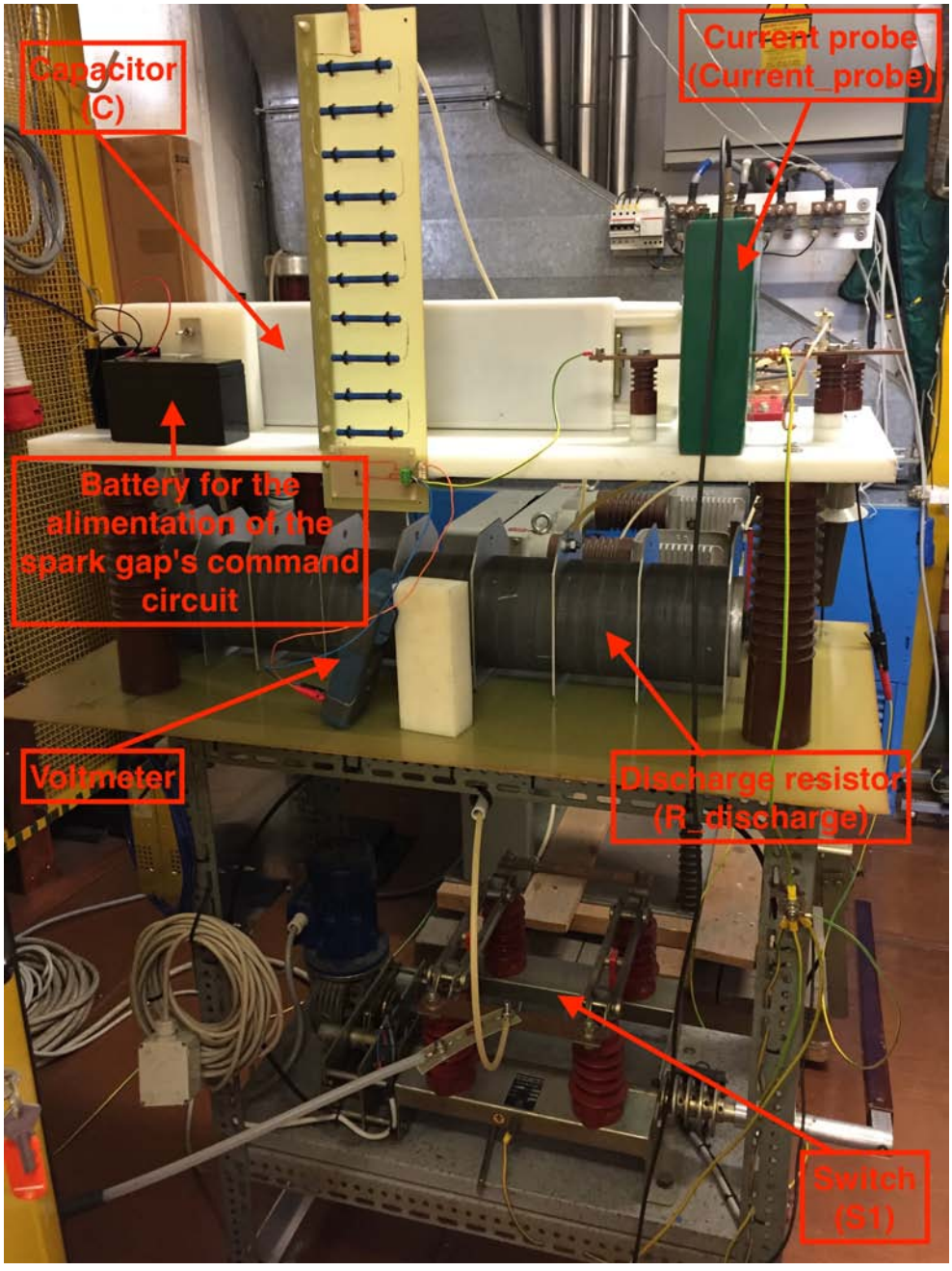

Figure 3.12: Sidac test bench

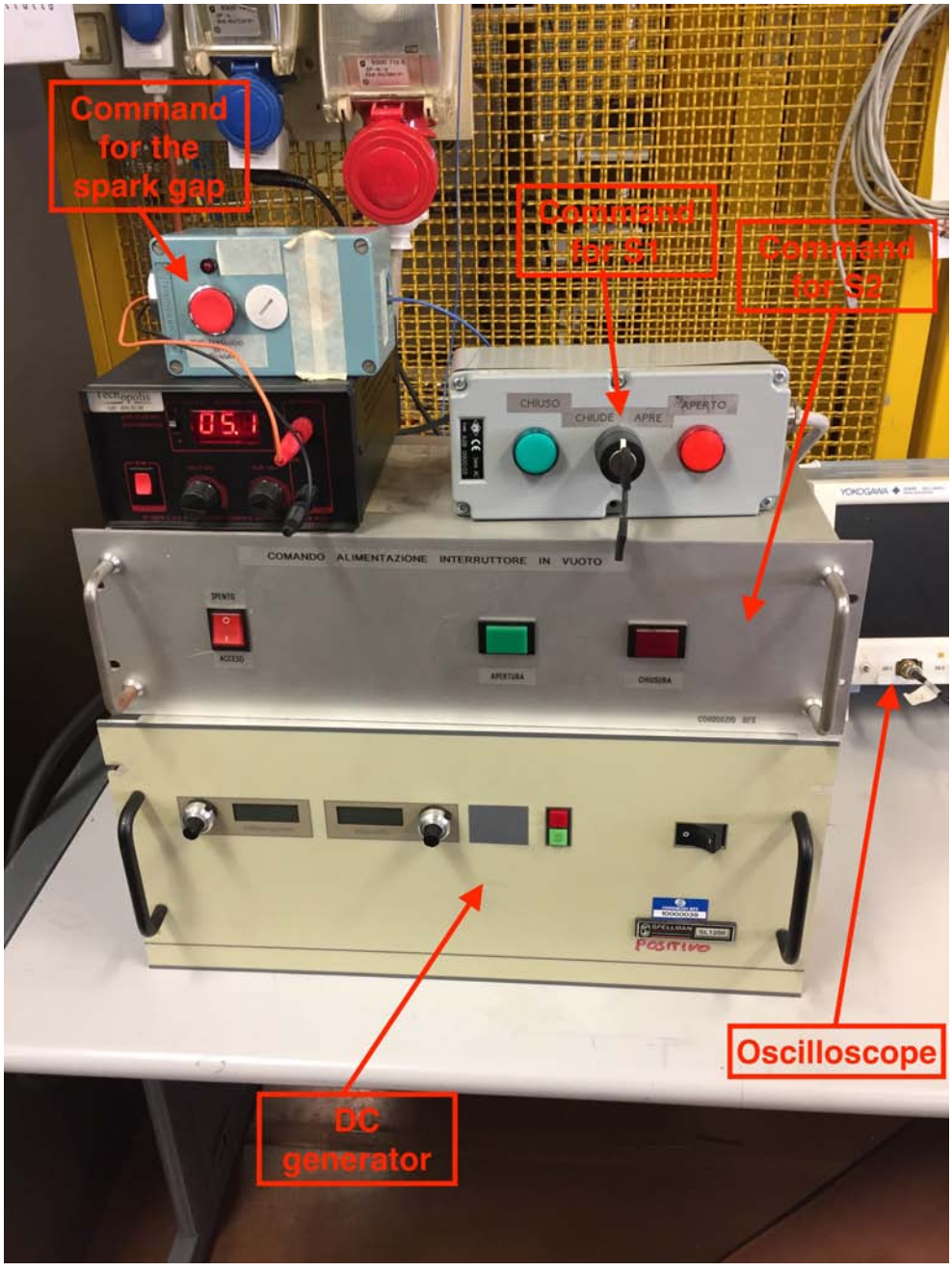

Figure 3.13: Power supply and switches command.

Part II

Design and Test of the Wide Bandwidth High Voltage Divider

Chapter 4

Wide Bandwidth High Voltage Divider

4.1 Introduction

In the second part of this thesis the design and test of the **wide bandwidth high voltage divider** is discussed.
The necessity for NIO1 of such a handmade voltage probe comes from the fact in NIO1 the voltage waveform of the two sources of DC power,one at 60 kV (actually the installed generator is able to provide up to 70kV) and one at 10kV, need to be measured during the operation. Up to now, the measures on NIO1 are carried on by using commercial voltage probe. Voltage probe and its relative acquisition system are generally very expensive especially for high frequency operation. One of the solutions to avoid this problem, and also to increase the possibilities of measurements, is to utilize oscilloscopes and in particular a device known as Red Pitaya, which is much less expensive than oscilloscopes. Red Pitaya is an open source control and measurement device based on Linux OS. It can be linked with computers or tablets via USB or Wi-Fi using an additional component mounted on it. It is very small, having the dimensions 107 x 60 x 21 mm. It has: a dual core processor ARM Cortex A9+ FPGA, DDR3 RAM 512 MB, 2 analog inputs, 2 analog output, Ethernet connection, micro SD slot, 16 digital I/O. Red Pitaya can operate as oscilloscope, function generator, spectrum analiser and PID controller [1].

[1]This brief description is directly taken from Red Pitaya official web site.

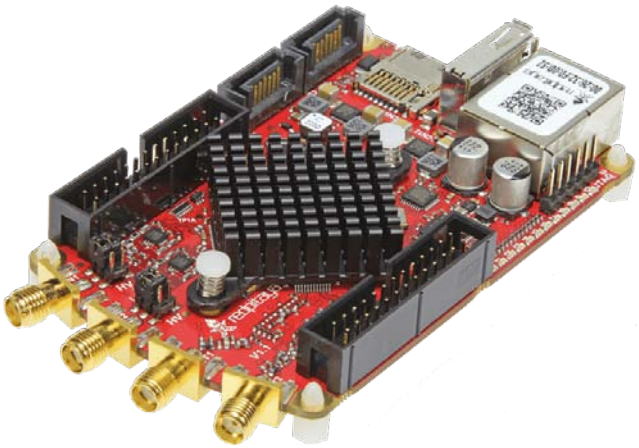

Figure 4.1: Overview of the Red Pitaya.

Red Pitaya is powered with 5V and 2A. Since it has to be used with 10 or 60 kV, the levels of voltage present in NIO1, a proper voltage divider is required. To comply with the Red Pitaya input voltage limit it can be assumed that the divider has to provide a ratio 1/1000 between the output voltage and the input voltage.
Instead, the reason for the wide bandwidth requirement for voltage divider lies in the fact that in NIO1 plasma breakdown events con occur and these are very fast. Very fast occurrences are associated to a wide frequency spectrum and so the voltage divider has to be capable of detect also the very high frequency (see 4.3). In order to achieve such a wide bandwidth it is necessary to use what is known as **compensated voltage divider**. The peculiarity of a **compensated voltage divider** is the theoretical independence of its functioning from the frequency.
One of the main purposes of this second part of the thesis, beyond the construction and the test of the voltage divider itself, is the study of how the divider can be properly compensated for the desired bandwidth.

4.1.1 Installation layout

With regard to the final installation layout three possibilities can be considered. In the first connection case the probe is installed far from the measurement point (in which the divider itself is present) by means of a RG58 coaxial cable; the principal problem of this configuration is the fact that, since

divider and measurements tool (this could be the Red Pitaya or an oscilloscope) are far from each other, there must be a long connection between them. The connection through a coaxial cable introduces inductive and capacitive components that make the compensation more challenging. In the second case probe and divider are placed in the same point, with the shortest connection possible between them and consequently the smallest inductive component; in this case the compensation would probably be easier than before but, on the other hand, the arrangement of the entire system results more difficult. In the last installation case both the divider and the data acquisition system are installed near the measurement point.
The figure 4.2 highlights the possible installation area of the voltage probe.

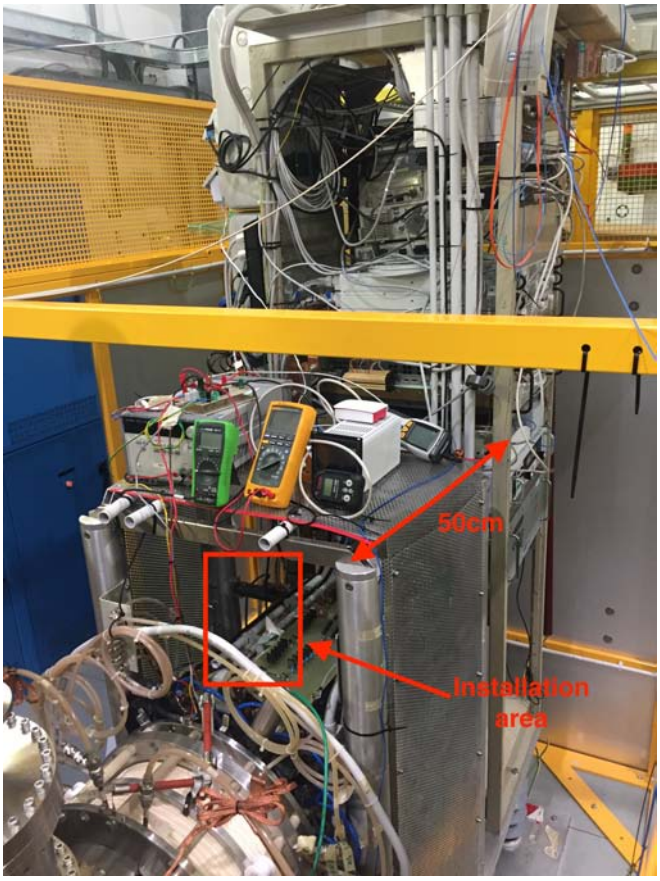

Figure 4.2: Installation layout of the final voltage probe in NIO1 experiment.

4.1.2 Compensation modes

Also regarding the compensation two ways are viable: active and passive compensation. Obviously passive compensation is easier by the point of view of

the circuit since it doesn't require active components; active components, such as operational amplifiers, need a power supply which complicates the circuit and increase the space usage of the system. Nevertheless an active compensation, made by using, e.g., a buffer input stage made with operational amplifier immediately afterwards the voltage divider, could be taken into account by the point of view of the pure performances. An operation amplifier with a differential configuration in such a position, would permit the decoupling of the line starting at the low voltage clamps of the divider and ending in the probe making possible to better and easier compensate the system. A 50 Ω load would then be necessary between the connection line and the probe in order to adapt the probe to the line since the line has a characteristic impedance of 50 ohms.

The main problem to face with during the sizing of the voltage divider is the presence of the stray capacitance which could assume a relevant value considering the desired frequency (some tens of MHz). For example stray capacitance of a high voltage resistor (OHMITE MOX-4N-131005FE, Through hole resistance, Maxi-Mox, 100 Mohm, 40 kV, Axial conductor, 10 W, ±1%, Maxi-Mox series) has a value in the order of the pico farad[2]. In addition to this problem, i.e. the presence of inherent stray parameters in the circuit itself, also the stray capacitance (between the system and to ground and between the system and the objects that surround it) due to the arrangement of the system has to be taken into account; fortunately this problem can be solved by covering the divider with a metallic shield; the latter make possible to fix the stray capacitance, this means that even if the parasitic parameters are still present they are no longer dependent from the insertion condition of the measurement circuit (e.g. they don't depend on the vicinity of metallic objects or from conductive objects connected to ground). One of the consequences that the parasitic parameters bring with, in addition to the modification of the frequency response of the system, is the possibility that they drain a little current that will no longer flow in the principal circuit..

The study about the compensation of the voltage divider has proceeded both with experiments and with theoretical simulations in parallel. Experiments have been carried out by means of oscilloscope, function generator, impedanceme-

[2]Value found out in the resistor data sheet `http://www.ohmite.com/cat/res_maximox.pdf`

ter and spectrum analyser in order to comprehend the actual influence of the stray parameters on the total transfer function. Theoretical study about the divider has been carried out through some specific software such has MATLAB®, LTspice® and Psim®. The first of the software listed before has been used with the aim to: determine the total theoretical **transfer function** (that is without considering the parasitic effect), comprehend which are the main issues about the circuit and find out which could be the best possible interventions for enlarge the bandwidth.
Issues above refer mainly to the presence of resonances between inductive and capacitive components introduced both by the circuit itself and by the coaxial cable which connects the divider and the probe. Consequently interventions could correspond both to the introduction of new component and, when possible, to the modification of the components just present in order to shift the resonances out from the frequency range to whom we are interested in. From the other point of view MATLAB® code parameters were continuously updated with the data coming from the practical experiments and the simulations in order to fit experimental results.
Instead, simulations through specific simulation software have the objective to verify the results obtained with MATLAB® and, in the case of compatibility between them, to determine the best possible circuital configuration in order to obtain the above results. This approach has to objective to have a good layout for the correlated practical experiments and to have an idea of the component arrangement in the final voltage divider.
In fig.4.3 a principle scheme of the divider is shown: in the left part of the scheme there is the compensated voltage divider itself; from the low voltage side of the divider departs the connection line here represented with a lumped model pi double dipole; then there is the load, i.e. the oscilloscopes necessary for the measurements. In this figure more than one thing is not taken into account, among which: stray parameters, power supply line, connection between the power supply and the circuit which can be schematised in the same way as the downstream connection line, downstream connection line is here reported with only one "*cell*".

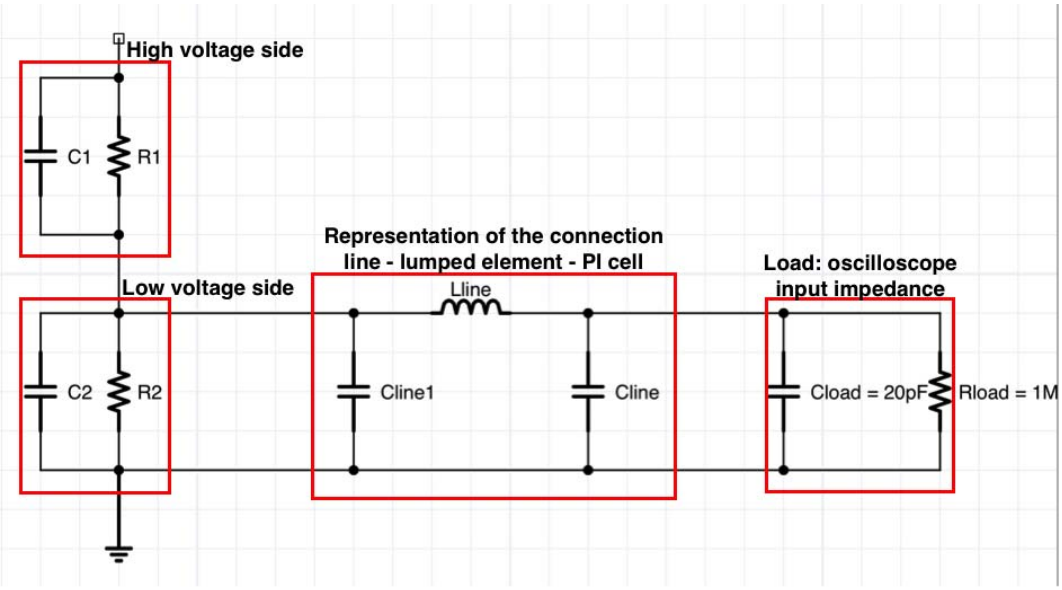

Figure 4.3: Schematic representation of the voltage divider.

4.2 Theoretical consideration

Before the treatment about the project of the voltage divider some theoretical aspects must be taken into account: the reason why the compensation is required and the way to protect it from discharges and faults.

4.2.1 The reason why compensation is required

As said before the aim of a compensated voltage divider is to make its transfer function independent from the frequency in a specific frequency range. Consider now the following simple scheme, fig. 4.4, of a compensated voltage divider in order to make a steady state sinusoidal analysis:

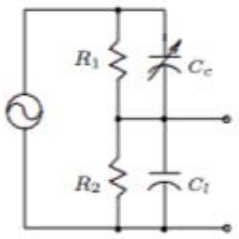

Figure 4.4: Simplest scheme of a compensated voltage divider.

Then the voltage division ratio K (the ratio of output to input signal) is equal to:

$$K = \frac{Z_2}{Z_2 + Z_1}$$

where:

$$Z_1 = \frac{R_1}{1 + j\omega R_1 C_1}$$

$$Z_2 = \frac{R_2}{1 + j\omega R_2 C_2}$$

$$\omega = 2\pi f$$

Substituting Z_1 and Z_2 into K, it is obtained:

$$K = \frac{\frac{R_2}{1+j\omega R_2 C_2}}{\frac{R_2}{1+j\omega R_2 C_2} + \frac{R_1}{1+j\omega R_1 C_1}} = \frac{R_2(1 + j\omega R_1 C_1)}{R_2(1 + j\omega R_1 C_1) + R_1(1 + j\omega R_2 C_2)}$$

If the capacitance were adjusted the divider would be compensated, so that if

$$R_1 C_1 = R_2 C_2$$

then:

$$K = \frac{R_2}{R_2 + R_1}$$

It can be considered compensated since the value of a resistor is constant with the frequency and being K, the transfer function, expressed only in terms of resistances it is independent from frequency.

4.2.2 Guard ring

In high voltage (HV) dividers, and in general in HV applications, it is possible that some point of the voltage divider is subjected to sufficiently high voltage to trigger a discharge. The solutions for the discharge to be avoided could be two: changing the dielectric material that surrounds the circuit, replacing the present one with another having better electrical properties; utilizing some precaution to avoid the concentration of electric field in some restricted points. The second solution is the one that will be analysed here.
In the particular application of interest for this thesis it is considered a voltage divider composed of several series resistances. On the HV side the linking point between the resistances can be subjected to a very high electric potential and because of this the electric field could be sufficiently high to trigger a discharge

on the dielectric that surrounds the point itself.
The first, and most important effect that should be avoided is the presence of "*effluvi di corrente*". *Effluvio* is an electric discharge in gas that happens when the electric field is strongly not uniform and particularly intense in the proximity of a single point. If that point is sharp, the electric field is sufficiently intense to provoke the acceleration of the electrons, naturally present in the gas, and produce an impact ionization.
The effects that the *effluvio* can bring to the system are:

- Non linearity: it could be possible that the effluvio occurs at a specific voltage and do not at a lower one; furthermore it is possible that the effect is nonlinear with the changing of the electric potential of the point. Because of this, if the effect is nonlinear, the draw off of current will be different at different voltage values, and since resistance, current and voltage are related through Omh law the diveder ratio would change with the value of voltage applied to the circuit. In particular, assuming that the effluvio occurs only over 50 kV (example) until 50 kV the divider ratio would be exactly that of the project, but over this voltage, due to the effluvio, the current on the resistor will be less than before and so that the voltage drop on a single resistance will be minor than before and finally the divider ratio results less than that of the project.

- Another problem could be that of the temperature on the point.

To avoid these effects a conductive ring, not necessarily high performant, should be electrically connected to the point of interest. The only restriction, on the shape of the ring, is to avoid sharp edges.
The reason of the introduction of the ring are essentially two:

- Avoid the presence of radial electric field surrounding the circuit: the radial electric field is quite likely leading to *affluvi*;

- The presence of more than one ring results in a uniformation of electric field along the series resistances.

A brief discussion on the radial electric field in present of a guard ring is reported in the following. A single charged point emit a radial electric field as the figure below shows:

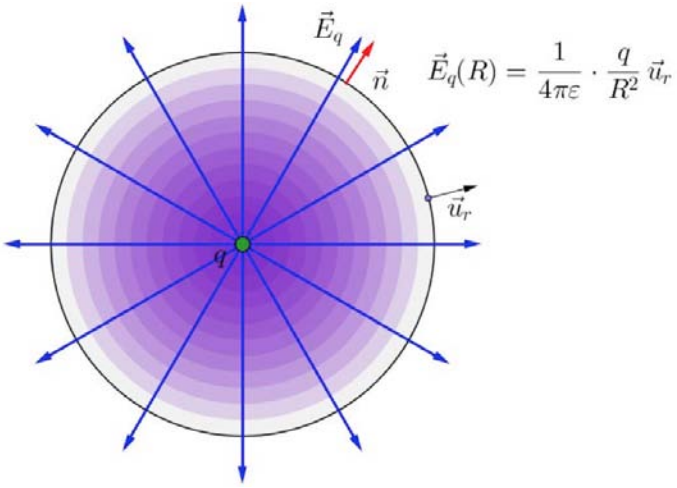

Figure 4.5: Radial electric field produced by a single charged point and its analytical form. Taken from `https://goo.gl/images/wf7QRH`

In the case in which a conductive ring is electrically connected to the point the situations change drastically since the resulting electric field will be completely axial, as can be seen in the figure below:

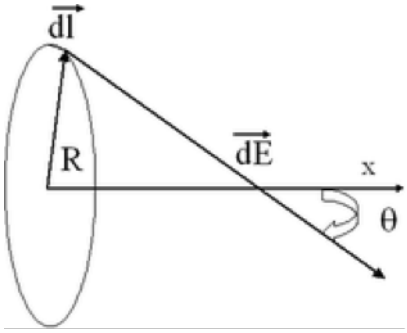

Figure 4.6: Axial electric field produced by a charged conductive ring.

Since for every infinitesimal elements dq of the ring there is another dq' diametrically opposed which generates an electric field orthogonal to the x-axis opposite to that produced by dq, the total electric field in the point P is completely axial.
The field produced by a single charged element of the ring dq is:

$$dE_x = dE\cos(\theta) = \frac{1}{4\pi\varepsilon_0}\frac{dq}{(x^2+R^2)}\frac{|x|}{(x^2+R^2)^{\frac{1}{2}}}$$

From which the total electric field is the integral over the entire ring of the result above:

$$E_x = \frac{1}{4\pi\varepsilon_0}\frac{|x|}{(x^2+R^2)^{\frac{3}{2}}}\int_q dq = \frac{Q}{4\pi\varepsilon_0}\frac{|x|}{(x^2+R^2)^{\frac{3}{2}}}$$

This field has the form:

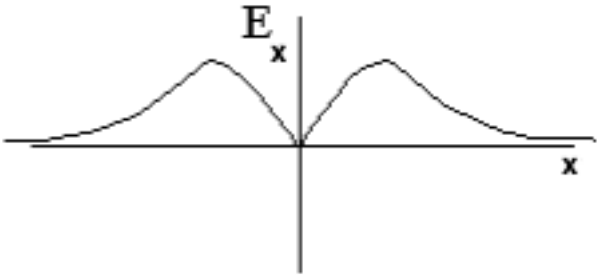

Figure 4.7: Axial electric field produced by a charged conductive ring.

Furthermore the presence of more than one ring one near the other, as in the case of a high voltage divider, contribute to the smoothness of the electrical field which would have a quasi-axial distribution at all.

4.2.3 Passband Bandwidth

In electronics it refers to **passband bandwidth**, or more precisely to 3dB passband, in order to indicate the range of frequency that a specific instrumentation is able to treat. As a convention the *cut frequency*, which defines the passband bandwidth, is defined as the frequency at which, given a value for the input signal, the power of the output signal is reduced of 3dB with respect to the maximum obtained with that input signal.

4.2.4 Rise time and passband

Often, during the following chapter of this thesis, the correlation between the rise time and the passband will be mentioned. First of all it has to be pointed out what the rise time is: it is the time in which a generic signal goes from the 10% to the 90% of its regime value; the more rapid the increase, the smaller the rise time.

Theoretically speaking there is a more or less (it depends on the type of the system under analysis) precise correlation between the passband and the rise time. This relation can be found out by taking into account a first order system described by the following generic transfer function:

$$W(s) = \frac{K}{s+p}$$

where s is the term relative to the Laplace transform and equal to $j\omega$ in the frequency domain, p is a generic pole and K is a constant; K and p belong to $\mathbb{R}_+$. In order to find the relation between the rise time and the passband it has to be considered the response of this simple system to the unit step:

$$U(s) = \frac{1}{s}$$

The response to this input in terms of forced evolution is:

$$W_{-1}(s) = \frac{W(s)}{s} = \frac{K}{p}\left[\frac{1}{s} - \frac{1}{s+p}\right] = W(0)\left[\frac{1}{s} - \frac{1}{s-p}\right]$$

In the time domain it can be written:

$$w_{-1}(t) = W(0)[1 - e^{-pt}]\delta_{-1}(t)$$

where δ_{-1} is the unit step.
The rise time (at 10%) can be found out through the following relation:

$$w_{-1}(t_r) = 0.9w_{-1}(+\infty) = 0.9W(0) \quad \Rightarrow \quad 1 - e^{-pt_r} = 0.9$$

from which:

$$t_r = \frac{1}{p}\ln\frac{1}{0.1} = \frac{H}{p} \tag{4.1}$$

where, in general, at least for the first order system and for the second order system with only two real pole, $H = 2.31$.
The frequency response of the system is:

$$W(j\omega) = \frac{K}{j\omega + p}$$

which has module equal to:

$$|W(j\omega)|\frac{K}{\sqrt{\omega^2 + p^2}}$$

from which by imposing:

$$|W(jB_p)| = \frac{W(0)}{\sqrt{2}} = \frac{K}{p\sqrt{2}}$$

this relation allows to write down that: $p = B_p$. Then from (4.1):

$$B_p \cdot t_r = H \tag{4.2}$$

From this relation it can be seen that, due to the inverse proportionality, in order that a system's response to the inputs is fast it is better to enlarge the bandwidth. Practically the largest possible bandwidth is not always a good solution so a compromise must be found out [3].
This should justify the fact that is repeatedly established that since the breakdown events occur in a very fast way (with a very steep ascent) the bandwidth of the measurement instruments must be very large.

4.2.5 LC resonances

In the second part of this thesis it is likely to read the term "*resonance*" which is an abbreviation of "*LC resonance*". In particular in electric systems the resonances are correlated to the continuous exchange of energy between capacitance and inductance. Two types of resonances can occur in electrical systems: resonance (also called series resonance) and anti-resonance (also called parallel resonance). When the first occurs the equivalent impedance of the series between a capacitance and an inductance goes to zero and the circuit is equivalent to an ideal short circuit. When the second type of resonance occurs the equivalent impedance of the parallel between a capacitance and an inductance goes to infinite and the circuit is equivalent to an ideal open circuit. Now the analytical analysis is performed trying to find out the resonance frequency.
Consider the series between a capacitance C and an inductance L, the total reactance is:

$$\frac{1}{j\omega C} + j\omega L = \frac{1 - \omega^2 LC}{j\omega L} \quad \rightarrow \quad 0$$

if and only if:

$$\omega^2 LC = 1 \quad \Rightarrow \quad \omega_0 = \sqrt{\frac{1}{LC}}$$

[3] All the mathematical passages have been taken from (20).

Consider now the parallel between a capacitance C and an inductance L, the total reactance is:

$$\frac{1}{\frac{1}{j\omega L} + j\omega C} = \frac{j\omega L}{1 - \omega^2 LC} \quad \rightarrow \quad \infty$$

which again goes to infinity if and only if:

$$\omega^2 LC = 1 \quad \Rightarrow \quad \omega_0 = \sqrt{\frac{1}{LC}}$$

In practice whenever there are two or more reactances and when they can exchange energy with each other and the specific frequency $f = \frac{\omega_0}{2\pi}$ is reached, in relation to the layout of the circuit, one or the other resonance occur.

4.3 Compensated high voltage divider design

Since the voltage divider has to be installed either in correspondence of the extraction grid or of the acceleration grid and the input impedance of the data acquisition system (probe) accepts as maximum input voltage $\pm 20V$, the divider must have a division ratio at least equal to 1:1000. As design guideline it was decided to use the input resistance of the probe as the low voltage resistance of the divider. Since the input resistance is $1M\Omega$ and the division ratio has to be 1:1000, the resistance at the high voltage side of the divider has to be $1G\Omega$. $100M\Omega$ resistors have been chosen and ten of them must be linked in series to obtain the desired total high voltage resistance. The chosen resistances are the following: MOX-3N-131006FE (prod. code), through hole resistor, Maxi-Mox series, 100 $M\Omega$, 30 kV, axial conductors, 4 W, tollerance $\pm 1\%$, non inductive, thick film .

Figure 4.8: Resistor used for the test and for the final divider in the high voltage side of the divider. http://it.farnell.com/ohmite/mox-3n-131006fe/resistor-thick-film-4w-100- mohm/dp/2364040?MER=bn-level5-5NP-EngagementRecSingleItem-3

The actual circuit of the proposed circuit for the PG-ground measurements is reported in figure 4.9. It has to be taken into account that in this figure, fig.4.9, only one pi element is represented but the simulation has been carried out with more than one cell and both with the T synthesis and with the PI synthesis. It can be demonstrated that the two synthesis converge as the number of cells grows; this can be seen with the simulations too. As will be explained later the number of cells, and so their length, serves to overlook the phenomenon of electromagnetic propagation. Here for cell is meant an element composed by inductances and capacitances which can be used in order to outline a transmission line. During the description of the code this concept will be better explained.
The figure 4.9 shows just a principle scheme of the voltage divider as it was firstly thought. The divider actually studied uses only one high voltage side resistor since the final result of this thesis is the design and test of a 10kV voltage divider.

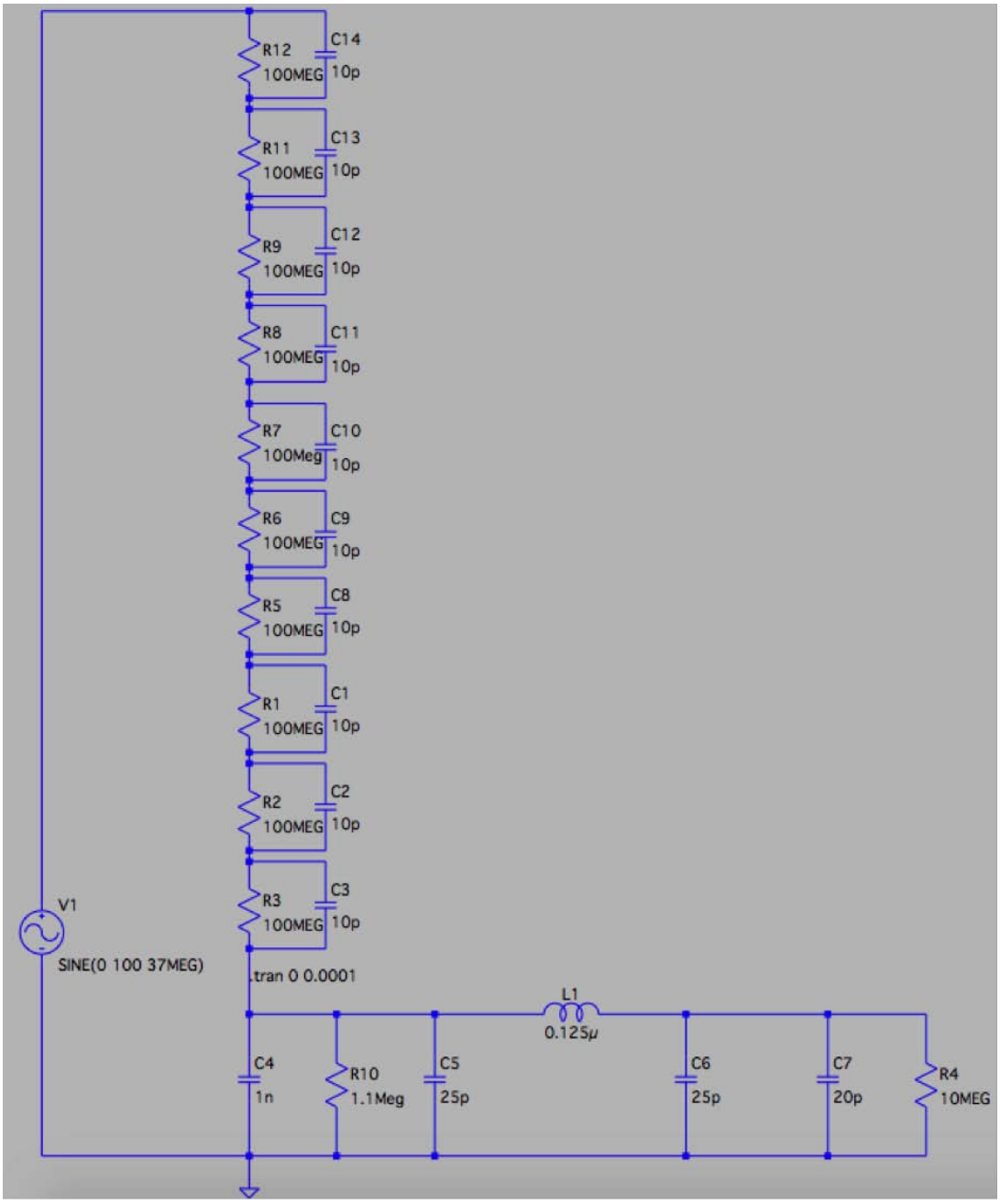

Figure 4.9: Actual scheme of the voltage divider.

Before to start the description of the codes and the design of the voltage divider it must be understood why a wide bandwidth is required from the point of view of the experimental data already collected[11]. In (11) the waveform relative to plasma breakdown occurrence has been found. In according to (11) a typical waveform is showed in figure 4.10.

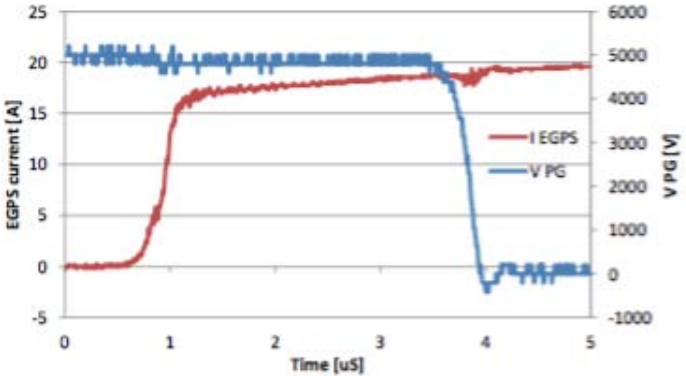

Figure 4.10: Typical behaviour of an evolutive discharge from PG-EG to EG-PA[(11)].

(4.2) This breakdown event is very fast and in line with eq. (4.2) the bandwidth associated to the event is very large. From fig. 4.9 just some fractions of microsecond are needed for the rise; according to the eq. (4.2) the bandwidth should be about 25MHz. A greater value of bandwidth is required in order to guarantee more accurate measurements.

4.3.1 Project data

- Bandwidth: the bandwidth must be greater than 25MHz.
- Division Ratio: 1/1000.
- Probe input impedance: $1000\Omega + j\omega 30 \cdot 10^{-12} F$;

4.3.2 Numerical simulation of the high voltage divider

As said before for the numerical simulation of the high voltage divider the software MATLAB® has been used. This section will present the MATLAB® codes (that can be found in the appendix A.1) which has been used for the simulation and two rearrangements of the latter which serve to perform a parametric study about resistances and capacitances (also these can be found on appendix, respectively A.2 and A.3). The code will be here further used in order to present neatly some design aspects and circuit characteristics. Since the code is a perfect representation of what has been practically done it was considered useful to exploit it for a greater clarity of exposure.

Finally the results of the simulation will be presented, examined and discussed when needed.

4.3.2.1 The main MATLAB® code

The code in appendix A.1 refers to the circuit in figure 4.11:

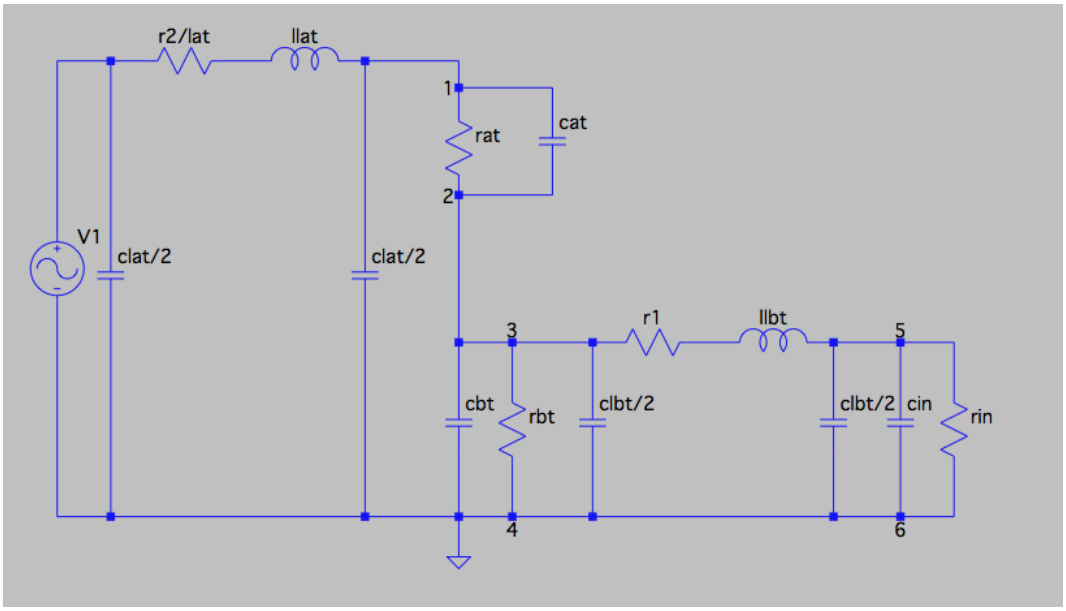

Figure 4.11: Reference circuit for the MATLAB® code.

From line 1 to 9 besides the definition of the needed physical constants, i.e. electrical permittivity and magnetic permeability a logarithmic vector is created. This vector allows to do a frequency sweep from 0 Hz to 100 MHz, with 100.000 points in this range of frequency, in order to simulate a spectrum analyser in the frequency range of interest. In fact the code simulates the circuit by means of impedance and admittance and then throughout the frequency sweep finds out the frequency response of the entire system.
From line 10 to line 14 the length of the line which connects the low voltage side of the divider (clamps 3-4) and the probe (clamps 5-6) is firstly inserted; subsequently the number of cells used by the synthesis of the line is chosen and consequently the length of each single element. It has to be firstly noted that regardless the synthesis done, pi or T, the number of cells is the same. The use of a lumped element model (i.e. the one that uses a pi ot T synthesis of the line) is possible only if the signal's propagation time from the beginning to the

end of the line is negligible with respect to the higher frequency component of the signals themselves. This means that the lumped element model is suitable only for the situation in which the restriction:

$$l \ll \lambda$$

and so as approximation:

$$l < 10\lambda$$

is satisfied. In our case the line can be assumed as electrically small if and only if its length is in the order of some tens of centimetres. This means that if the line get longer the number of elements has to get bigger too so that the length of each element is always in the order of tens centimetres. Actually the lumped element method is an approximate method for the study of conductive line, that's the reason why the things above has been said. Theoretically the line has to be studied through the telegraphist equations (see later in this chapter); nevertheless, as can be seen later, the difference between the two listed methods is not so big for the present purpose.
From line 15 to line 34 a few known parameters of the circuit are indicated and the eventual relative impedance are calculated. In particular at line 29 the ideal division ratio is calculated as the ratio:

$$k = \frac{rbt}{rat + rbt}$$

It is denominated ideal because it would be the division ratio only in the case of DC. The ideal division ratio is the factor 1/1000 which would be achieved in the largest possible range of frequency.
From line 35 to line 41 the inductance of the line (made up with a RG58 cable[30]) is calculated. It is calculated starting from the knowledge of the characteristic impedance and of the capacitance per unit length of the line. Since this three parameters stay in relation in accordance with:

$$Z_0 = \sqrt{\frac{l}{c}}$$

by using the inverse formula it is possible to derive the inductance per unit length of the line.
At line 43 the compensation capacitance of the low voltage side of the divider is calculated. Theoretically this capacitance (c_{bt}) should be k (i.e. the division ratio) times greater than the compensation capacitance at the high voltage

side in order to have, in an ideal divider, equal time constant on both sidess of the divider. Actually, on the low voltage side more capacitances are present due to the line, to the probe and to stray parameters (not included here) in parallel with the compensation one. Since capacitances in parallel sum up, the compensation capacitance at the low voltage side must be decreased by the contribution of the capacitances already present. An approximate form of the reasoning above is the one used in the code:

$$C_{bt} = C_{at} \cdot k - C_{in} - C_{lbt} \cdot l_{bt}$$

where C_{bt} is the compensation capacitance on the low voltage side, C_{at} is the compensation capacitance on the high voltage side, k is the division ratio, C_{in} is the capacitance present at the input of the probe, C_{lbt} is the capacitance per unit length of the line and l_{bt} is the length of the line itself. This can be done by neglecting the inductive reactances at first since this one should be much less that the capacitive reactances.
At lines 45 and 46 an inductance (ind_{bt}) is introduced because of some experimental evidences. This inductance is the one formed in the circuit and due to the fact that the variable compensation capacitance at the low voltage side is supplied with two cables which form a mesh. Since the inductance has to deal with the concatenated magnetic flux with a closed loop an inductance must be added to the model. At first this inductance was not taken into account in the code but during the experiments a resonance was detected in an unexpected frequency region and it was found that it was due to the resonance between the inductance and the capacitance itself. It can be reduced by twisting the connection cable but it can not be avoided completely. At line 47 a null inductance is written in order to make some simulations without the inductance. At line 49 the total compensation reactance taking into account the inductance too, is calculated:

$$z_{cbt} = j\omega(ind_{bt}) + \frac{1}{j\omega c_{bt}}$$

At line 50 the low voltage side resistance is calculated: it is calculated as the ideal resistance, i.e. the ratio between the high voltage side resistance and the division ratio, diminished by the input resistance of the probe. Since it has been decided to utilise the actual input resistance of the probe (r_{in}) as the low voltage side resistance of the divider, the resistance calculated here (r_{bt}) remains infinite (so that, being in parallel to all, it can be neglected since there

is no flow of current through it) as long as the divider is balanced (that is as long as there is no more resistances in parallel to r_{in}). At line 52 the complete impedance of the divider at the low voltage side is calculated ($c_{bt}//r_{bt}$).
From line 53 to line 63 the resistance afferent to the cable is calculated. This is a slightly critic stage in the sense that in the datasheet of the cable the dc resistance of the cable is indicated; for a RG58 cable the datasheet indicates a resistance of $16m\Omega$ per unit length for the external cable and $38m\Omega$ for the internal cable. The problem is that in this case the cable is used in alternating current and so the skin effect must be taken into account. The skin effect is the tendency of an alternating current to distribute in a non uniform way inside a conductor, in particular, as the frequency get higher the current tends to stay in the most external layer of the conductor. Since the resistance depends on the length and the area of the conductor crossed by the current the resistance has to be adjusted in function of the frequency since the area becomes smaller and smaller as the frequency get higher. In practice due to the skin effect a full conductor is as if it were an empty conductor with a thin surface. Knowing the radius (r) and the resistivity of the material of the cable the total ac resistance can be calculated with:

$$r_{coax} = \left[r_{int} \cdot \left(1 + r \cdot \sqrt{\frac{1}{\omega \mu_0 \rho}} \right) + r_{ext} \right] l_{cbt}$$

At first the cable resistance was not considered in the model but it introduces some attenuation effects on the resonances and so in general has a positive influence on the entire system.
From line 66 to line 86 the pi synthesis of the low voltage line and the total transfer function of the line are computed. First of all the longitudinal impedance and the equivalent impedance of the probe plus the first transversal capacitive element of the line are calculated. This serves to be able to find out the total transfer function of the low voltage side, that is the way in which a voltage at the clamps of the low voltage divider side is transmitted at the end of the line on the input of the probe. Consider the following circuit that represents the entire low voltage circuit of the divider:

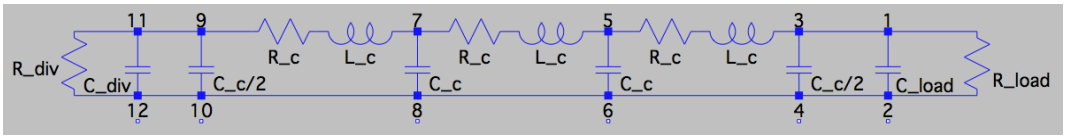

Figure 4.12: Representation of the entire low voltage side of the divider.

The equivalent impedance is calculated through a for loop in which parallels and series of the single impedance element are performed. In practice, in the example above firstly it is done a parallel between Z_{load} and $C_c/2$ then the series with the longitudinal element; and then the parallel with C_c. This process is iterated until clamps 9-10 where the total impedance found out until now is put in parallel with Z_{div}. The equivalent impedance of the low voltage side is calculated in order to find the transfer function with the lumped pi element model, without considering the supply line, of the divider. It is calculated at line 78. Then from line 82 to line 88 the divider transfer function amplitude and phase are both plotted.
From line 91 to line 132 the same things done for the low voltage side are done for the supply line: firstly the known terms are indicated, secondly the longitudinal inductance and the ac resistance are calculated and, in the end, the transfer function of the supply line is determined with more or less the same reasoning done above for the low voltage side circuit. In order to determine the total transfer function (considering always the same example reported in figure 4.12), as it has been done in the code, consider that a voltage at the clamps 1-2 and that at the clamps 3-4 is the same to that present at the clamps of the load. The voltage present at the clamps 5-6 is the voltage at the load minus the voltage drop on the longitudinal impedance component $R_c + j\omega L_c$. Taking into account this, the voltage al the load, given the voltage at the clamps 5-6 can be find out as if there were a voltage divider, in fact:

$$V_{load} = V_{5-6} \cdot \frac{Z_{load}}{Z_{load} + Z_{long}}$$

Then the voltage at the clamps 5-6 can be calculated as if there was a voltage divider between the longitudinal element and the total impedance downstream this one:

$$V_{5-6} = V_{7-8} \cdot \frac{Z_{loadnew}}{Z_{loadnew} + Z_{long}}$$

where $Z_{loadnew}$ is now the total downstream impedance.
Now V_{load} can be expressed in function of V_{7-8} substituting V_{5-6}, obtaining:

$$V_{load} = V_{7-8} \cdot \frac{Z_{loadnew}}{Z_{loadnew} + Z_{long}} \cdot \frac{Z_{load}}{Z_{load} + Z_{long}}$$

In this case:

$$\frac{Z_{loadnew}}{Z_{loadnew} + Z_{long}} \cdot \frac{Z_{load}}{Z_{load} + Z_{long}}$$

is the transfer function between clamps 7-8 and the load. The same reasoning can be iterated until clamps 9-10 (in the example) where the voltage is the same of that at the clamps of the divider resistance. In practice as seen from the calculation above the total transfer function can be determined with the product of the partial transfer function. This process is implemented by the code through a for loop. The same process is done for the low voltage line too in order to determine the transfer function.
Then, from line 126 to line 132, the transfer function (amplitude and phase) of the high voltage line is plotted. Subsequently, from line 135 to line 157 the entire transfer function is calculated through the multiplication of the high voltage line transfer function, the voltage divider transfer function and the low voltage line transfer function and then it is plotted (amplitude and phase). This plot ends the study of the system by using the approximate lumped element method. From now on it will be considered the distributed parameters model through the telegraphist equation.
First of all it must be explained what telegraphist equations and distributed parameters model are and then how this can be fitted to the circuit under study. Regarding the telegraphist equations, it is considered a trunk of a line with a length of Δz:

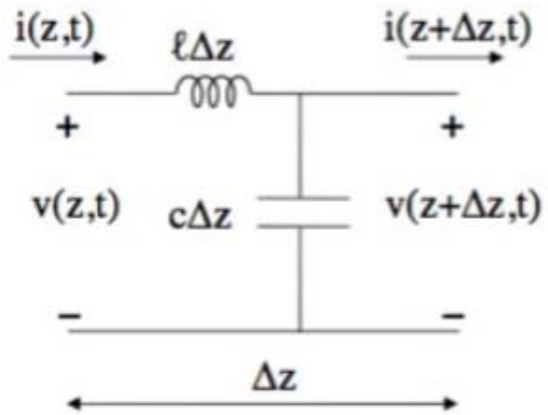

Figure 4.13: A portion of a line taken into account to derive the telegraphist equations.

This line element can be describe analytically by the following set of dif-

ferential equations:

$$\begin{cases} i(z+\Delta z,t) = i(z,t) - c\cdot\Delta z\cdot\frac{\partial}{\partial v}(z+\Delta z,t) \\ v(z+\Delta z,t) = v(z,t) - l\cdot\Delta z\cdot\frac{\partial}{\partial i}(z,t) \end{cases} \tag{4.3}$$

By recasting these equations and remembering the definition of derivative, the following set of equations can be find out:

$$\begin{cases} \lim_{\Delta z\to 0}\frac{i(z+\Delta z,t)-i(z,t)}{\Delta z} = \frac{\partial i(z,t)}{\partial t} = -c\cdot\lim_{\Delta z\to 0}\frac{\partial v(z+\Delta z,t)}{\partial t} = -c\frac{\partial v(z,t)}{\partial t} \\ \lim_{\Delta z\to 0}\frac{v(z+\Delta z,t)-v(z,t)}{\Delta z} = \frac{\partial v(z,t)}{\partial t} = -l\frac{\partial i(z,t)}{\partial t} \end{cases} \tag{4.4}$$

So that, the **telegraphist equations** are derived:

$$\begin{cases} \frac{\partial i(z,t)}{\partial t} = -c\frac{\partial v(z,t)}{\partial t} \\ \frac{\partial v(z,t)}{\partial t} = -l\frac{\partial i(z,t)}{\partial t} \end{cases} \tag{4.5}$$

If the first of the two relations is derived in z a second derivative with respect to z is obtained at the left hand side and a mixed second derivative with respect to t and z is obtained at the right hand side. The same thing can be done with the second of the telegraphist equations but deriving both the member of the equation with respect to t, obtaining a second derivative with respect to time and a mixed second derivative. Thanks to some mathematical passages it is possible to obtain the mono-dimensional equation for the scalar wave:

$$v^2\frac{\partial^2\psi(z,t)}{\partial t^2} = \frac{\partial^2\psi(z,t)}{\partial t^2} \tag{4.6}$$

where $v = \mu\varepsilon = \frac{1}{\sqrt{lc}}$ is the speed of propagation of the wave through the line. Solving this equation two terms are obtained: a forward travelling wave and a backward travelling wave associated both to the voltage and the current. In the case of sinusoidal steady state the solution has the form:

$$\begin{aligned} \overline{V}(z) &= \overline{V}^+(z) + \overline{V}^-(z) = \overline{V}^+e^{-j\beta z} + \overline{V}^-e^{j\beta z} \\ \overline{I}(z) &= \overline{I}^+(z) + \overline{I}^-(z) = \overline{I}^+e^{-j\beta z} + \overline{I}^-e^{j\beta z} \end{aligned} \tag{4.7}$$

where $\beta = \omega\sqrt{\mu\varepsilon}$.

Defining the **characteristic impedance** as the ratio between $\overline{V}$ and $\overline{I}$ at which is associated the positive sign if it is about the forward travelling wave and a negative sign if it is about the backward travelling wave:

$$Z_0 = \sqrt{\frac{l}{c}} \Rightarrow \begin{cases} \overline{V}(z) = \overline{V}^+e^{-j\beta z} + \overline{V}^-e^{j\beta z} \\ \overline{I}(z) = \frac{1}{Z_0}\overline{V}^+e^{-j\beta z} + \frac{1}{Z_0}\overline{V}^-e^{j\beta z} \end{cases} \tag{4.8}$$

Now the **reflection coefficient** and the **trasmission coefficient** can be derived. It is considered a lossless line, in sinusoidal steady state, loaded on an impedance $\dot{Z} = \frac{\overline{V}_L}{\overline{I}_L}$ (where subscript L stands for load); it is known that voltage and current can be written as:

$$\begin{cases} \overline{V}(z_L) = \overline{V}^+ e^{-j\beta z_L} + \overline{V}^- e^{j\beta z_L} \\ \overline{I}(z) = \frac{1}{Z_0}\overline{V}^+ e^{-j\beta z_L} + \frac{1}{Z_0}\overline{V}^- e^{j\beta z_L} \end{cases} \tag{4.9}$$

where z_L is the longitudinal coordinate of the load supposing that the reference system starts from the beginning of the line. The **reflection coefficient** and the **trasmission coefficient** are respectively:

$$\dot{\rho}(z_L) = \frac{\overline{V}^- e^{j\beta z_L}}{\overline{V}^+ e^{-j\beta z_L}} = \frac{\frac{\dot{Z_L}}{\dot{Z_0}} - 1}{\frac{\dot{Z_L}}{\dot{Z_0}} + 1} \tag{4.10}$$

$$\dot{\tau}(z_L) = 1 + \dot{\rho}(z_L) = \frac{\overline{V}_L}{\overline{V}^+ e^{-j\beta z_L}} = \frac{\overline{V}^+ e^{-j\beta z_L} + \overline{V}^- e^{j\beta z_L}}{\overline{V}^+ e^{-j\beta z_L}} \tag{4.11}$$

Lastly the reflection coefficient in a generic section of the line z, $\dot{\rho(z)}$, equal to the ratio between the phasor of the reflected wave on z and the phasor of the incident wave in z, can be expressed in function of the reflection coefficient at the load, in fact:

$$\dot{\rho}(z) = \frac{\overline{V}^- e^{j\beta z}}{\overline{V}^+ e^{-j\beta z}} = \frac{\overline{V}^-}{\overline{V}^+} e^{j2\beta z} \; ; \; \dot{\rho}(z_L) = \frac{\overline{V}^-}{\overline{V}^+} e^{j2\beta z_L} \; \Rightarrow \; \dot{\rho}(z) = \dot{\rho}(z_L) e^{j2\beta(z - z_L)} \tag{4.12}$$

It can be noticed that the module of the reflection coefficient does not vary along the line[29].

From line 159 to line 189 this reasoning has been implemented. Firstly by using the data in the datasheet the relative dielectric constant in a RG58 coaxial cable is calculated and then β as defined before. Subsequently the reflection coefficient al the load is calculated according to eq.(4.10) and also the reflection coefficient at the beginning of the line. As the theory states at line 166 the impedance reported at the upstream of the line is calculated and putted in parallel with the impedance at the low voltage side of the divider. The same thing is then done by the point of view of the supply line: firstly the load impedance is calculated (as the series between the high voltage side impedance and the total low voltage side impedance) and consequently the reflection coefficient too. Then the three different transfer function are calculated (the one relative

to the high voltage line, the one relative to the divider itself and the one relative to the low voltage line) in order to calculate the total transfer function as the product of the single transfer functions. At the end the transfer function is plotted both the module and the phase.
The same thing is done in the case of the presence of the **attenuation** taken into account by the α coefficient. The process is exactly the same just followed with the only difference that the exponential have the real part too instead of the only imaginary part considered before. This correspond to treat the line considering also the longitudinal resistive contribute of the line.
At the end of the code some summary plot are plotted in which there are the modules and the phases of the total transfer function calculated with the three different approaches presented above. The three different plot are overlapped in order to see the difference between them. It can be seen that the difference between the lumped element method and the distribute element method are not so big and that as the number of cells in the lumped element model gets higher the difference between them gets smaller.

4.3.2.1.1 Presentation of the results from the code :

Now the plots that the MATLAB® code returns and the data relative to this graph are presented. All the plot show both the amplitude and the phase of different transfer functions relative to some sub-parts of the voltage divider and to the entire system. The total transfer function representation serves to understand the global behaviour of the voltage divider in terms of frequency response; the graphs relative so some sub-parts of the divider (such as the connection line in low voltage, the connection line in high voltage and so on) have mainly a control function in the sense that if the global transfer function displays some not well understood behaviour these graph could help to comprehend where the error is.
What is of particular interest in all of these graph is the first resonance which is the one that limits the bandwidth. This resonance is the one that must be shifted right or, in the best case possible, completely eliminated, in order to enlarge the bandwidth.
The following set of data is a typical experimental situation:

- Length in meter of the line which connect the low voltage side of the

divider to the probe: 0.5 m;

- Resistance at the high voltage side of the divider: 100 MΩ;
- Compensation capacitance in parallel with the high voltage resistance: 5 pF;
- Input resistance of the probe: 1 MΩ;
- Input capacitance of the probe: 30 pF;
- Capacitance per unit length of the line: 100 pF/m;
- Characteristic impedance of the coaxial line: 50 Ω;
- Inductance which takes into account the supply mesh of the compensation capacitance at the low voltage side: $160 \cdot 10^{-10} H$;
- Inner and outer dc resistance of the rg58 coaxial cable, respectively: 38 mΩ/m, 16 Ω/m;
- Length in meter of the supply line : 0.5 m;

Different combinations of input data (such as different cables with different lengths)) have been considered in order to better understand the behaviour of the circuit and to find out the best possible configuration to get the highest possible bandwidth.

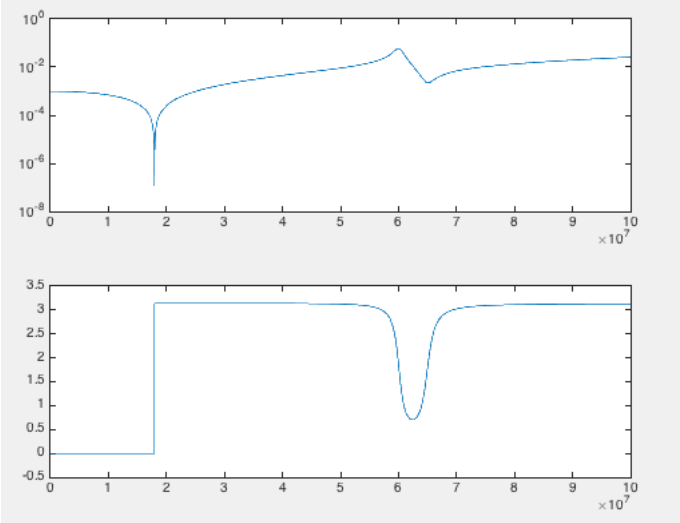

Figure 4.14: Transfer function of the sole divider that is the series of rat//cat and cbt//rbt. The x axis is the frequency, the y axis is respectively the module for the first graph and the phase for the second.

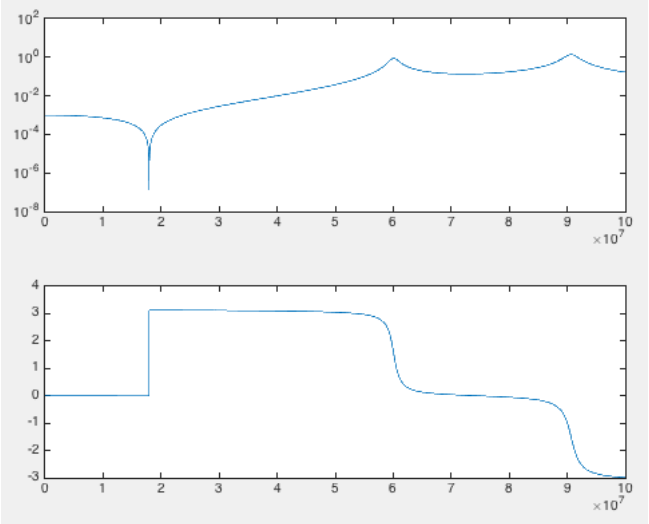

Figure 4.15: Transfer function of the divider considering the connection line between it and the probe too that is the series of rat//cat with all the bt side of the circuit in figure 4.11. The x axis is the frequency, the y axis is respectively the module for the first graph and the phase for the second.

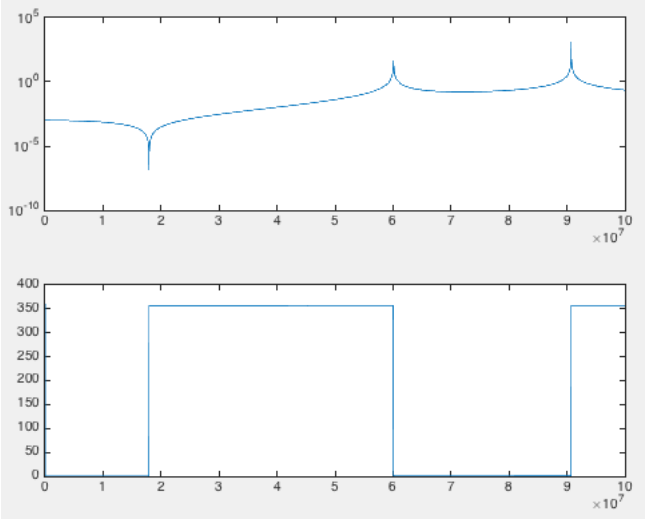

Figure 4.16: Transfer function of the entire system, in figure 4.11, without considering the attenuation with the concentrated model. The x axis is the frequency, the y axis is respectively the module for the first graph and the phase for the second.

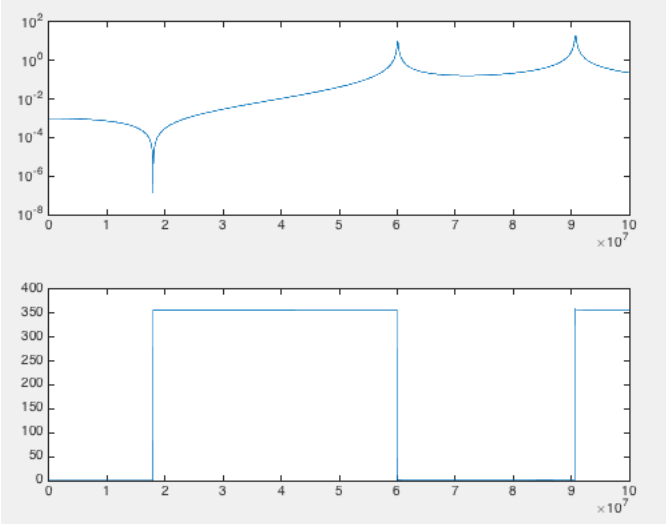

Figure 4.17: Transfer function of the entire system, in figure 4.11, considering also the attenuation with the concentrated model. The x axis is the frequency, the y axis is respectively the module for the first graph and the phase for the second.

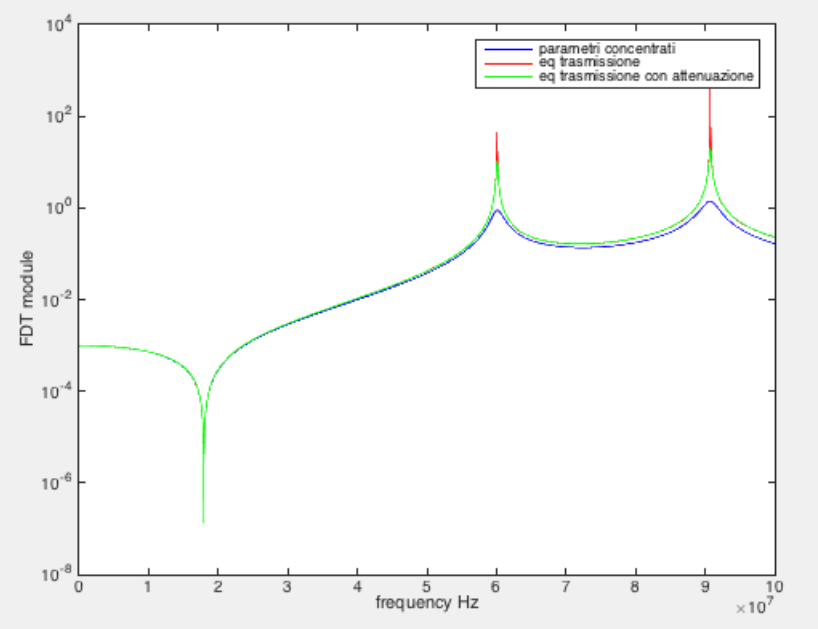

Figure 4.18: Overlapping of the plot of the module of the transfer function of the entire system in figure 4.11.

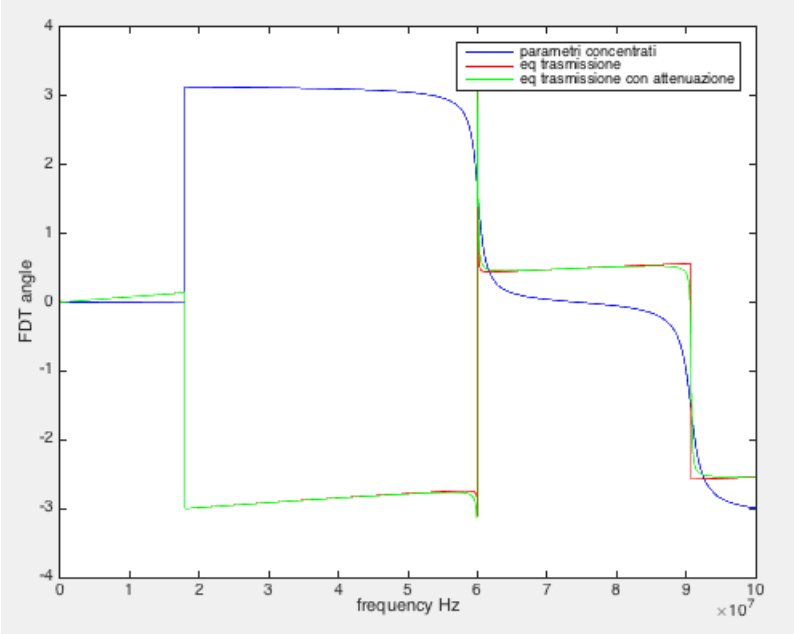

Figure 4.19: Overlapping of the plot of the phase of the transfer function of the entire system in figure 4.11.

4.3.2.2 Resistance parametric study

The study here proposed consist of a parametric study about some resistance inserted in the circuit, the relative code is in the section A.2 of the appendix. It seems that some resistance, inserted in the proper position, could help to attenuate the first resonance. This parametric study has thus two objectives: the first is to find the position (or why not the positions if more than resistance can be useful to the purpose) in which place the resistance (or resistances); the second is to find the best possible value for the resistances in order to attenuate as much as possible the resonance.
In particular the inserted resistances were: in series with the probe's impedance (r_6); in series with the longitudinal impedance element of the low voltage side connection cable (r_5); in series with the high voltage side impedance of the voltage divider (r_4); in series with the longitudinal impedance element of the high voltage side connection cable (r_3). These resistances and their positions can be seen in the figure 4.20.

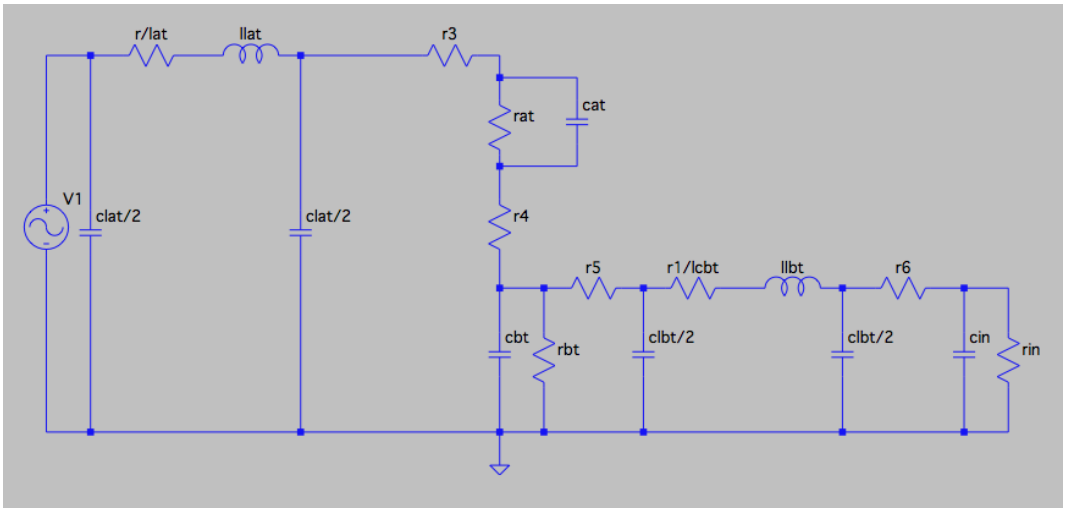

Figure 4.20: Reference circuit for the code about the resistance parametric study.

4.3.2.2.1 Resistances parametric study results

This simulation has been carried out with the same condition listed in the paragraph 3.3.1.1.1. This choice derives from the fact that only with the same simulation conditions the study can be considered complete. In this case from the main MATLAB® derive the results which are modified from the parametric

study; in practice this is a continuation of what has been done in the main code.

The plots resulting from this parametric simulation show how the total transfer function varies, with respect to that presented in the paragraph 3.3.1.1.1 in the figures 4.18 and 4.19, with the insertion of some resistances. Taking into account that: if no resistance is inserted the graph relative to the concentrated parameter model is black; if the resistance r_3 is considered the plot is blue; if the resistance r_4 is considered the plot is magenta; if the resistance r_5 is considered the plot is cyan; if the resistance r_6 is considered the plot is yellow. The resistance chosen for the test is r=50 Ω. The results are:

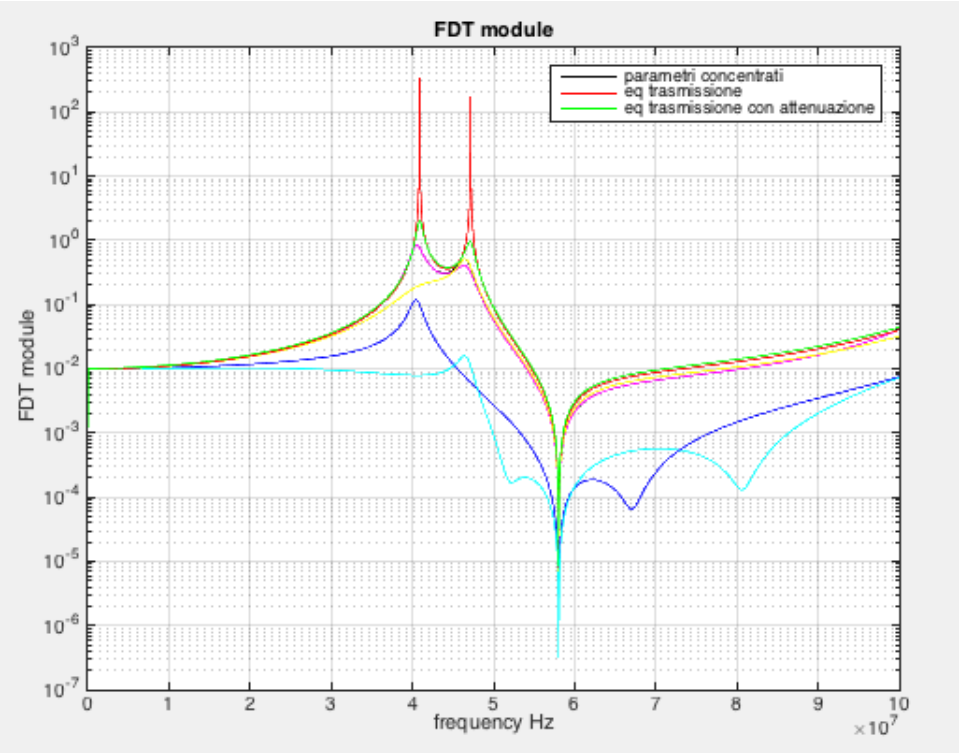

Figure 4.21: Overlapping of the plot of the module of the transfer function of the entire system considering the parametric study about resistance.

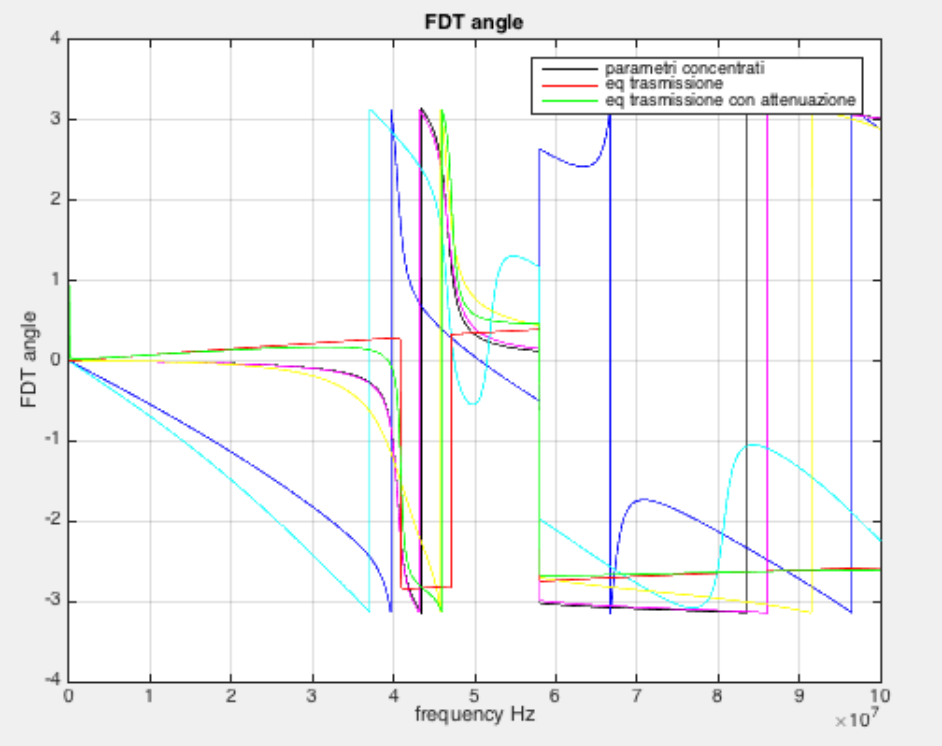

Figure 4.22: Overlapping of the plot of the phase of the transfer function of the entire system considering the parametric study about resistance.

These result show that some resistances help the system to attenuate the resonances, other are useless for the scope. In particular the simulation shows that r_5 is the only effective resistance to increase the bandwidth. r_5 (that cyan in the plots) is the one in series with the low voltage side cable. It can be noticed that even if r_3 resistance helps to reduce the amplitude of the peak of resonances it doesn't help to widen the bandwidth. Further more, 50 ohms is a optimal value since the other value tried don't give such a good result.

4.3.2.3 Capacitance parametric study

The capacitance parametric study serves to vary the compensation capacitance at the low voltage side of the divider (named c_{bt} in the code) and to see how this variation influence the total transfer function 4.18 and 4.19. The capacitance is varied between -10% and +10% (with steps of 1%) with respect to its real value. This variation has been chosen because of in the prototype (see paragraph 3.3.2.4) a capacitive trimmer is installed and allows a capacitance variation of about 10%. The analysis presented in this paragraph shows that this variation of the capacitance is practically useless since the variation of the total transfer function is negligible, as can be seen in the plots reported below.
First of all it can be noticed that the increments of the value of the compensation capacitance are not good for the system since they make the bandwidth diminished; instead the decrements of the value of the compensation capacitance are effective since they make the bandwidth to increase. As can be seen by the simulations done, a greater variation of the compensation capacitance would have a greater influence on the system; in particular: a greater increment would decrease more the bandwidth and a greater decrement would decrease more the bandwidth. Unfortunately greater variation would effect the bandwidth as well as the absolute value of the transfer function which would undergo an increase if the capacitance was smaller and a decrease if the capacitance was greater with respect to that of the project. Since what has been searched is a transfer function with a precise absolute value, or in other words a specific division ratio of the divider, these variation of capacitance are unfortunately not allow.
It has been found that a variation, in less, of a 10% of the compensation capacitance will affect, even if little, the bandwidth with a slightly increase.
As can be seen in the practical experimentations (paragraph 3.3.2.3) the compensation capacitance is put in parallel with a capacitive trimmer with allow us to vary the capacitance of more of less $\pm 10\%$ of its value. For more details please refers to the practical experimentations section.
Below are reported the results of the capacitance parametric study. The correlated code can be found in the appendix at the paragraph A.3.
The code refers to figure 4.23.

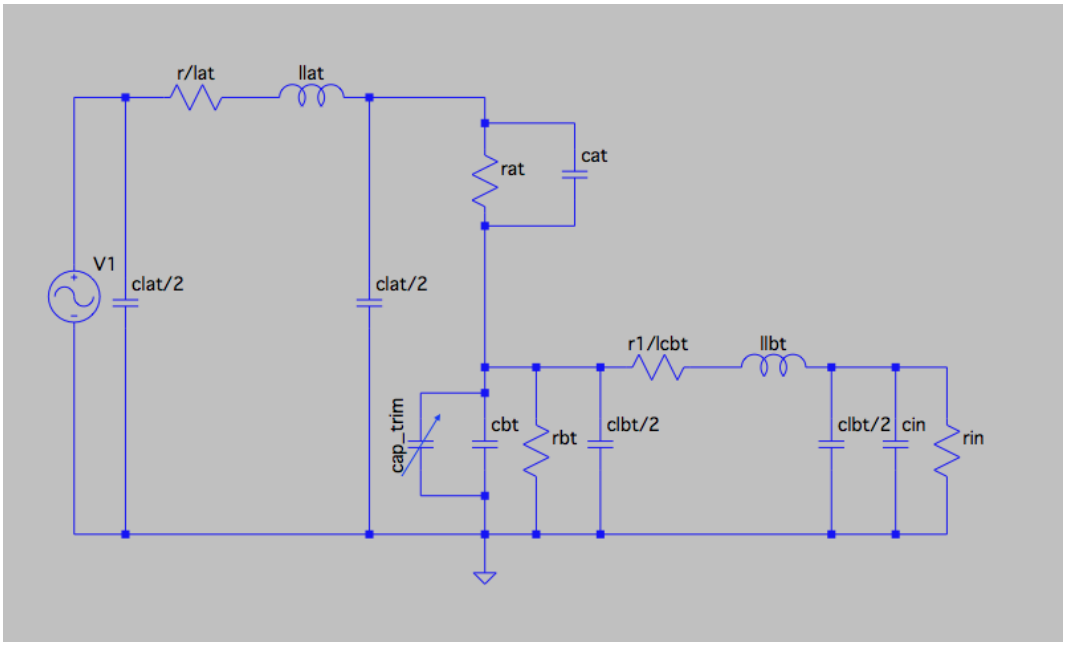

Figure 4.23: Reference circuit for the code about the capacitance parametric study.

4.3.2.3.1 Capacitance parametric study results

Figure 4.24 displays the result of the capacitance parametric study. In this figure are shown 20 transfer functions obtained with different capacitance (c_{bt}) values. It can be seen that even though the variation are not so important by a quantitative point of view a decreasing of c_{bt} (i.e. the compensation capacitance at the low voltage side) results in a shifting toward the right of the first resonance. This means that the bandwidth has been enlarged with a variation, in particular a decrease of the c_{ct}.

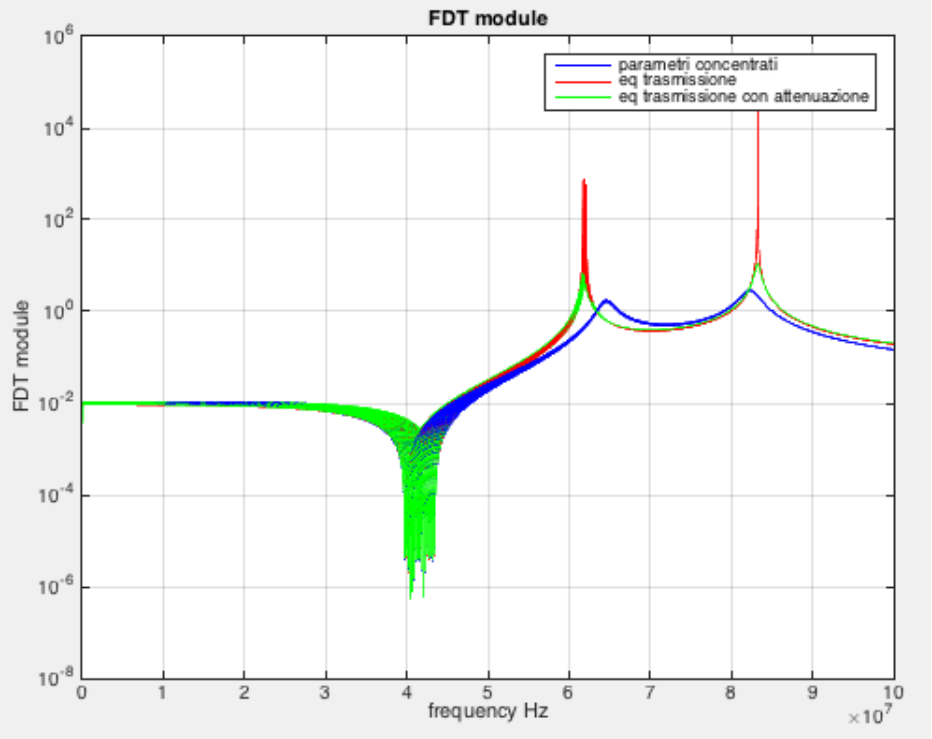

Figure 4.24: Module of the transfer function with different compensation capacitance value. As the capacitance get lower the module of the transfer function would move to the right.

4.3.3 Experimentations on the high voltage divider

In this section the experimental work about the voltage divider is presented. This work has been done step by step seeking to understand the influence of every single component of the circuit on the total transfer function. The same proceedings made with the simulation has been followed in the experimental work too. Firstly it has been find out the transfer function of the single cable in order to understand if they can influence the total transfer function and, in case of an affirmative response, how this influence happens and how to mitigate the effect. Then a simple divider circuit has been built with a resistor and a parallel capacitor (which would "simulate" the high voltage side od the divider) and a variable capacitor in parallel with the input resistance of the instrument (which would simulate the low voltage side of the divider). On this layout more the one experiments have been done in order to find out how to enlarge the bandwidth and diminish the noise. Then a relatively low voltage divider has been built, the one which will be installed on the EGPS (10 kV max) and this

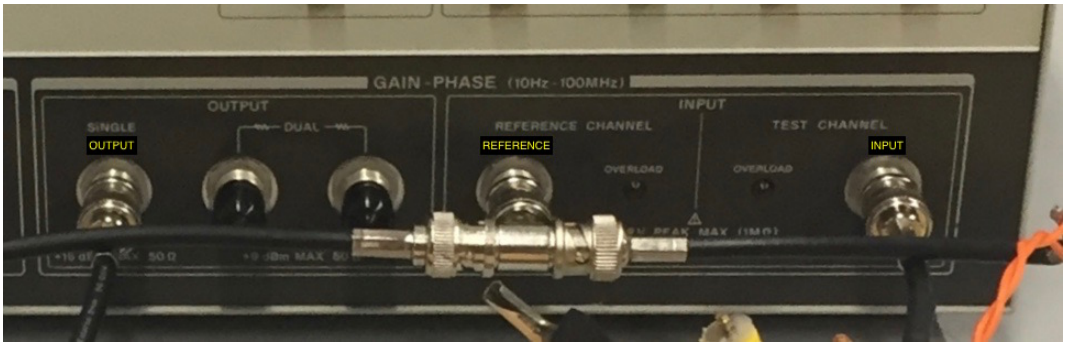

Figure 4.25: Output, input and reference channel of the gain phase analyser.

has been tested with the same scope as before. In between these steps various single components (in particular capacitors, cables, capacitive trimmers and resistances) have been measured through the specific impedance measurement allowed by the instrument in order to comprehend how this component does work and chose the best possible component to install in the circuit.
The experimentations have been mostly outperformed through the spectrum analyser HP 4194A, for this reason in this section the general functioning of such an instrument is firstly described.
However, since the last stage has not been performed during the progress of this thesis, the actual objective of this paragraph is to get a working and performant voltage divider to be installed in the EGPS.
In this section will be presented the design, the measurements set up and the obtained results about the voltage divider which mu be installed in the EGPG.
The impedance analyser can perform two main functions: it can function both as spectrum analyser and as impedance meter. When it operates as spectrum analyser an electric circuit is properly connected to its clamps (which are three as can be seen in figure 4.25: the output, the reference and the input; input and output are opposite for the circuit in the sense that the output of the instrument has to be connected to the input of the circuit and the input of the instrument has to be connected to the output of the circuit) and it makes a frequency sweep, in the supported frequency range. Practically a signal which varies in frequency is in input of the circuit and the instrument acquires the response of the circuit to that signal. Then this frequency response is shown in the instrument's screen in which the frequency is in the horizontal axis and the measure itself is in the vertical axis. Once the measure has been done

Figure 4.26: Input of the impedancemeter.

the spectrum analyser allows the user to make some basic post-processing, such as: evaluate the bandwidth, change some parameters and so on. The frequency sweep is done from 100 Hz to 100 MHz as minimum and maximum respectively, but, inside this interval, any other interval can be chosen by the user.

When the instrument operates as an impedance meter the operation principle is more or less the same but it is applied to only one component, as can be seen in figure 4.26, connected to a specific probe properly connected to the instrument. Once the measure, from 100 Hz to 40 MHz as largest range possible, has been done the instruments can display the impedance in function of frequency in many ways (dB, logarithmic ecc). Also in this case some basic post-processing are allowed, for example: the instrument permits to chose a specific equivalent circuit (5 preset equivalent circuits can be chosen) in relation to the component under measure; then the parameters related to that equivalent circuit are automatically calculated by the instrument. Another useful function, in order to understand if the chosen equivalent circuit was right or not, is the superposition of the original impedance graph and the graph generated by the calculated equivalent circuit: if the two fit each other then the equivalent circuit is right otherwise it has to be chose another equivalent circuit.

One important feature of the instrument is the possibility to compensate the effect of cable connections from impedance analyser and high voltage divider. To better explain this imagine a simple example of measure: it has to be measure the frequency response of a sole simple circuit, which is connected to the instrument through two cables, without considering the influence of the cable which can affects the measure. The cable can be connected to the instrument and measured separately from the circuit. The two calibration measurements needed are: short circuit and open circuit. Once the measures

are properly done the user can set an offset in order to eliminate the influence of the cable in the measure.
During the experimentations both of these two functions have been used: the first in order to study the frequency response of entire circuits and the second in order to study single components and how these could influence the entire circuit.
The following figures show some of the features of the instrument such as the possibility to chose an equivalent circuit in order to better undertand the behaviour of the components measured 4.27.a, the input of the impedance meter with a resistance under measure 4.27.b, the result given by the analysis of the impedance 4.27.c and the connection on a simple circuit to the gain-phase analyser 4.27.d.

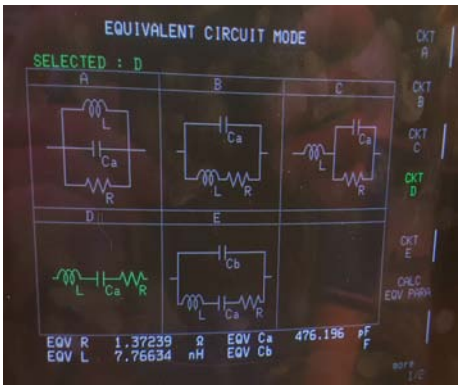

(a) *Equivalent circuit.*

(b) *Impedance meter.*

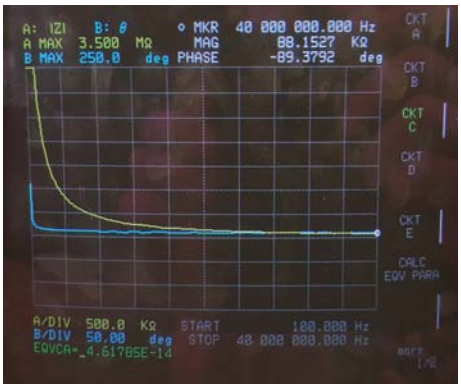

(c) *Result of impedance meter.*

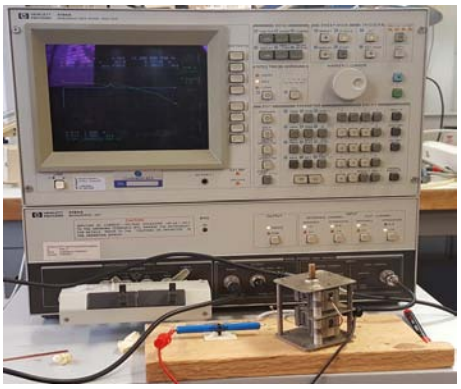

(d) *Freqeucny response of a circuit - gain/phase.*

Figure 4.27: Spectrum analyser utilisation examples.

Figure 4.27.c is the plot of an impedance and in practice it indicates the

value of both the absolute value and the phase of the impedance for each frequency values (the number of measurements can be chosen by the operator) in the range 100Hz-40MHz. In the figure 4.27.d a transfer function is shown. This graph represents the value (both the absolute value and the phase) of the frequency response of a system in the range 100Hz to 100MHz. Also in this case the number of measurements per unit of time can be chosen by the operator.

4.3.3.1 Measurements on cable

First of all various cables have been measured in order to understand theirs frequency behaviour. The problem is that an high frequency must be reached and as the frequency get higher the importance of cable stray parameters becomes greater. Below the most significant results on the measurements on cable are reported.

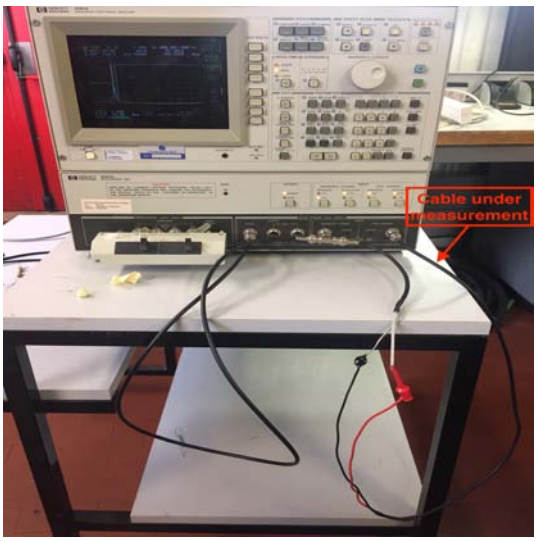

Figure 4.28: In this picture the two cables deriving from the coaxial cable and ending with bananas forms a mesh.

Figure 4.29: Gain/phase relative to the experiment in figure 4.28.

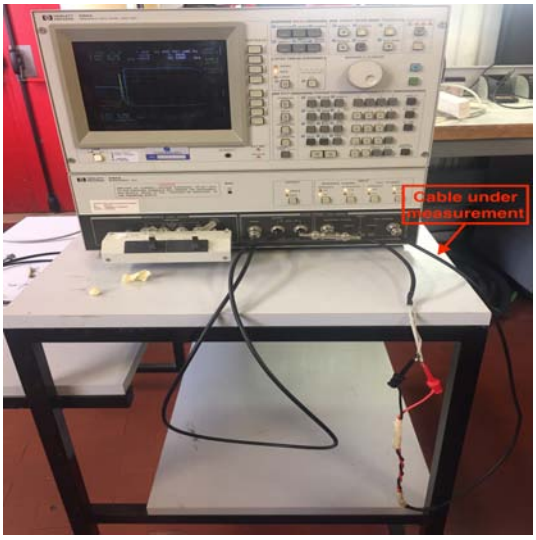

Figure 4.30: In this picture the two cables deriving from the coaxial cable and ending with bananas are twisted in order to form a mesh as smaller as possible to reduce the relative inductance.

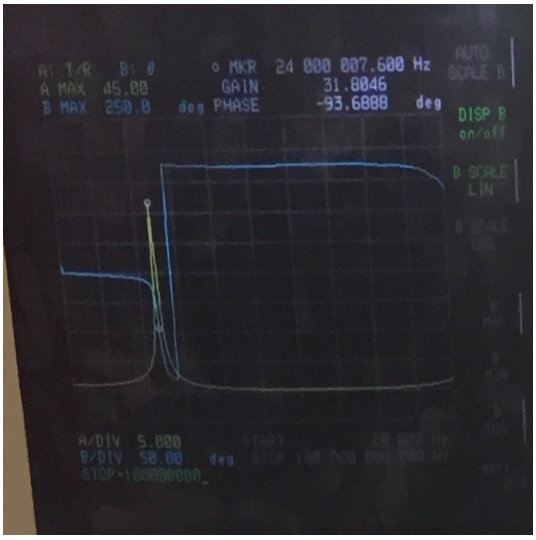

Figure 4.31: Gain/phase relative to the experiment in figure4.30.

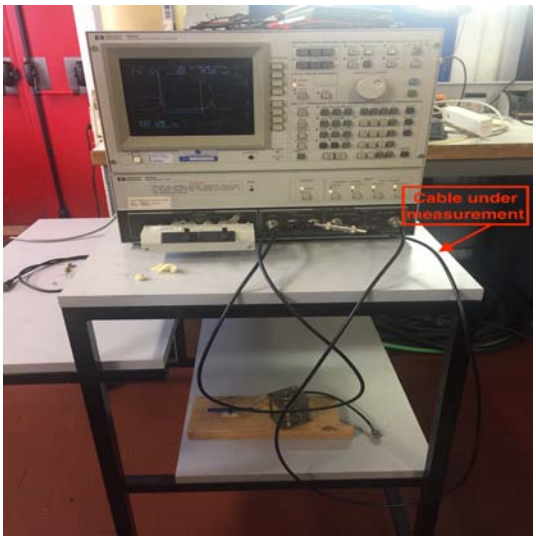

Figure 4.32: Measurement of a single coaxial cable.

Figure 4.33: Gain/phase relative to the experiment in figure 4.32

From this pictures some interesting things can be observed. In the figures 4.32 and 4.33 is shown a measurement which involves only pure coaxial cable; it can be seen that the cable resonates. This resonance could occurs either be-

tween the cable capacitance and the cable inductance (which get higher with the frequency) or between the cable inductance and the input capacitance of the instrument. However, whatever it is the provenance of the resonance, its effects have to be taken into account during the study of the voltage divider. Moreover this resonance is the one which occurs at lower frequency with respect to the other which occur on the entire circuit, so that it is this resonance that limits the bandwidth of the voltage divider. One of the goal is to reduce this effect. One of the possible intervention that could be done in order to limit the effect of the cable in the frequency response of the circuit is to shorten the cable with the aim to reduce drastically the inductance and so to drift on higher frequency the resonance.
From the first two images, figures 4.28 and 4.29, another phenomenon can be seen. Here there the are the cables deriving from the coaxial cable ending with banana clamps. This cable serves to supply the circuit. It can be seen that, from the first image in which the cable forms a loop and the second one in which the cables are twisted and doesn't form a loop, there is a difference in the resonance frequency: in the first case it occurs at about 20 MHz and in the second at about 24 MHz. This means that 4 MHz of bandwidth have been gained by only twisting the supply cable. This is explainable with the following reasoning: a loop introduces series inductance which, at this point, resonates with some capacitance parameter present in the circuit. By twisting the cable the loop's area is considerably reduced and so the stray series inductance does. In this way the resonance is avoided. This is an important design solution that must be taken into account.

4.3.3.2 First voltage divider prototype

In this section the study of a first prototype of a high voltage divider for NIO1 EG-PG gas is reported.
The first prototype, far from being the final solution, is the first attempt to comprehend both the best suitable components to use in the final voltage divider and the best possible layout of the circuit. In this paragraph the project data and the execution of the experimentations are presented.
The first ever divider was composed of: one $100M\Omega$ resistor which would form an ideal 1:100 divider with the input resistance of the spectrum analyser; one compensation capacitance in parallel with the $100M\Omega$ and one variable compensation capacitance in parallel with the input of the instrument and so with the low voltage side resistance. The variable capacitor has a range of some hundreds of picofarads, about between 100pF and 700pF and the variation serves to adjust, as better as possible, the frequency response of the prototype. The study about this first voltage divider helps to understand many things about the voltage divider and the single components and consequently both to adjust the experiments and to modify the code in order to fit better the reality of facts. In particular through this prototype the following aspects have been understood: the fact that in series with the variable capacitance there was an inductance which takes into account the mesh formed by the supply cables; how to properly use the instrument; how the cables affect the total frequency response; if it serves or not to compensate the cable through the offset mode; if the circuit is sensitive to some conductive pieces nearby for the fact the this will introduce some additional stray capacitance; if, consequently, it is essential to shield the divider or if it is only an additional precaution.

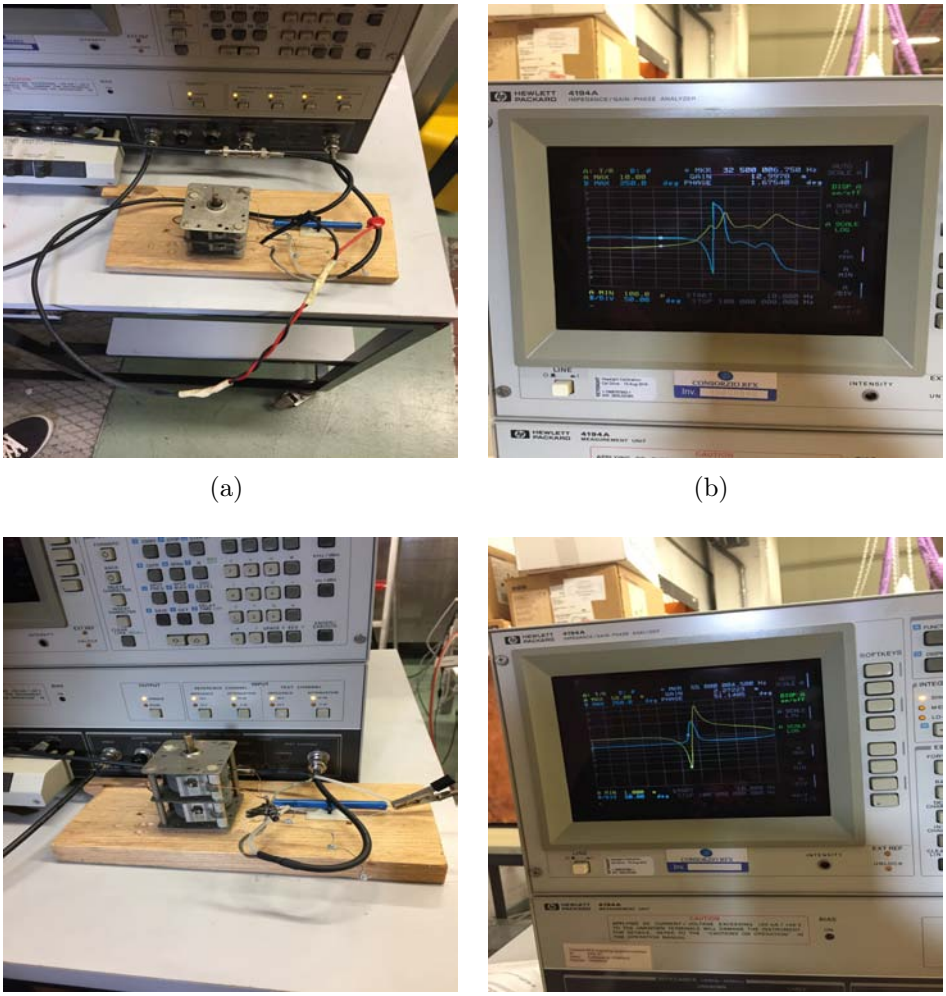

(a) (b)

(c) (d)

Figure 4.34: First voltage divider prototype measurements. Figures (a) and (b) refer to a measure with long connection cable and figures (c) and (d) refer to a measure with shorter cable

Here, in the figures 4.34.a, 4.34.b, 4.34.c and 4.34.d, it is shown that only by changing the length of the connection cable the bandwidth changes considerably. In the pictures can be seen that there are three cables: one which connect the output of the instrument to the reference, one from the reference to the input of the circuit; one from the output of the circuit to the input of the instrument. The reference is the signal that is compared with the input in order to make the frequency study. The cable which connects the output of the instrument with the reference has absolutely no effects on the circuit since it can be compensated. The cables which effects the performance of the circuit

are the one from the reference to the circuit and the one from the circuit to the instrument. The more these two cables are small the greater is the bandwidth of the system.

4.3.3.3 Second voltage divider prototype

Once it has been understood that the variable compensation capacitor had not a good behaviour it has been replaced with another which was expected to have major performance. In particular it has been chosen, for the replacing, a capacitive trimmer specially purchased for the scope. This capacitive trimmer has a nominal range from 0 pF to 65 pF. The capacitive trimmer has been solely tested in order to understand if it is suitable for the required application. It display, fig. 4.36 a perfect capacitive behaviour as expected.

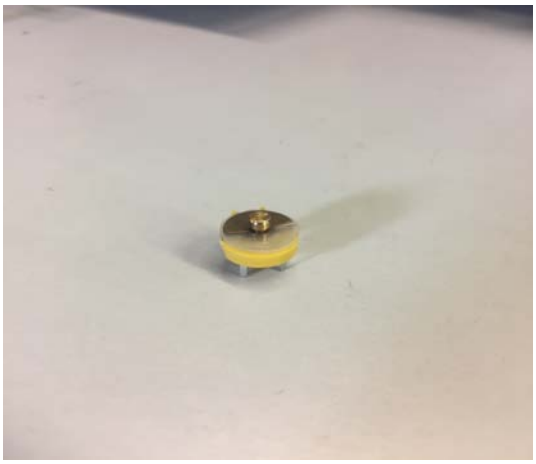

Figure 4.35: Capacitive trimmer

Figure 4.36: Impedance measurement of the capacitive trimmer

The new divider, fig. 4.37 has been tested in different configuration with diverse cables' lengths; here are presented two of the many configuration just to give an example of what has been done. The study with different cable lengths serves to understand how much the cable affects the measure. In the studies shown in figure 4.37 and 4.39 has been performed with very short cables with a length of about 10 cm; the study shown in figure 4.41 with instead a long cable (1 m) used for supply the divider and a short cable (10 cm) for the connection of the divider to the input of the analyser. In the actual installation two scenarios could be considered: in the first possible scenario the divider is

installed directly nearby to the point of measurements and the analyser far from here (some meters) and thus a rather short connection is needed between the EG-PG and a long connection between the divider and the analyser (whatever it is); in the second scenario the divider is installed in the vicinity of the analyser and both of them are far from the measuring point and thus a long connection (some meters depending on the placement of the divider and the analyser) between the EG-PG and the divider is necessary and a rather short connection between the divider and the analyser. Taking this into account, this study experiment has also the objective to understand which of the two presented cases are the best choice in order to get the largest bandwidth possible: short supply cable and long analyser input cable or viceversa long supply cable and short analyser input cable.

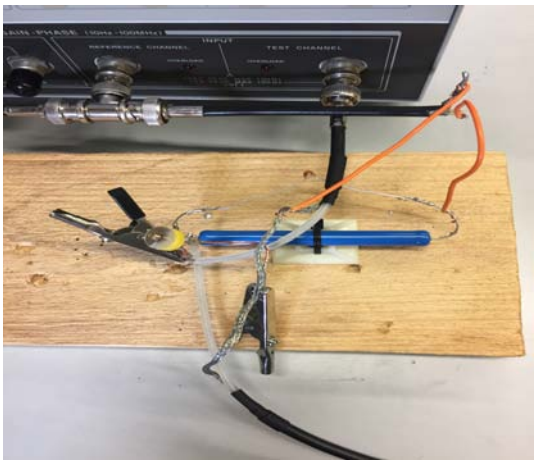

Figure 4.37: Prototype2: cable as short as possible; trimmer completely inserted; maximum capacity.

Figure 4.38: Prototype2: cable as short as possible; trimmer completely inserted; maximum capacity.

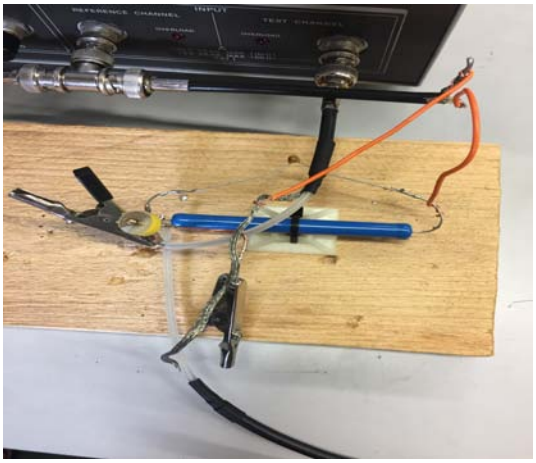

Figure 4.39: Prototype2: cables as short as possible; trimmer partially inserted; about half the full capacity.

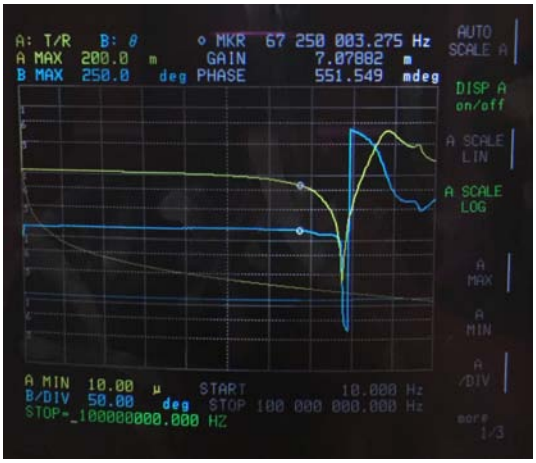

Figure 4.40: Prototype2: cables as short as possible; trimmer partially inserted; about half the full capacity.

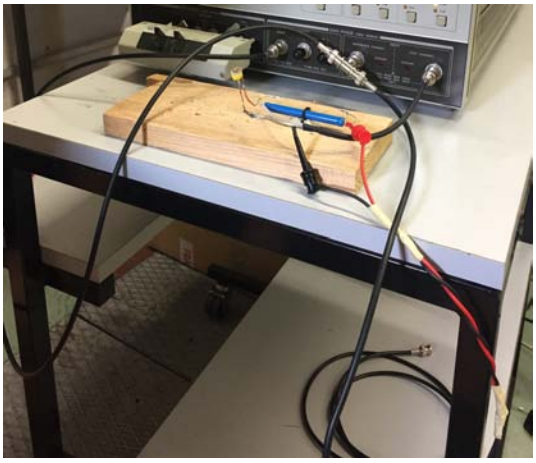

Figure 4.41: Prototype2: long cables; trimmer completely inserted; maximum capacity.

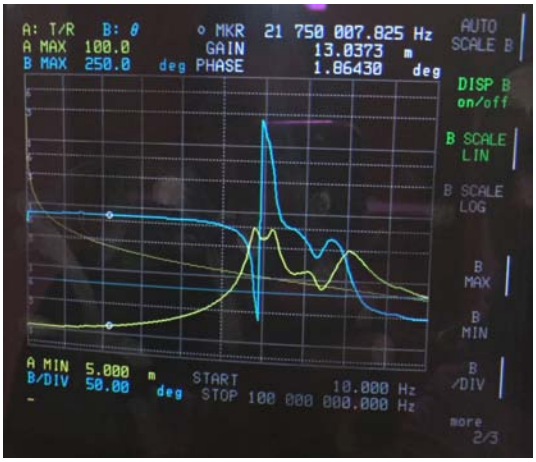

Figure 4.42: Prototype2: long cables; trimmer completely inserted; maximum capacity.

With this divider a 60 MHz bandwidth has been achieved but it must be considered that in the actual installation case in NIO1 experiment this layout cannot be replicated at all. However it is shown that a large bandwidth can be achieved by using performant components such as those used in this case. With long cable (1m), that anyway are not sufficiently long to replicate the actual installation case, an about 20 MHz bandwidth has been achieved. This value is far from that desired (100 MHz) but it can be sufficient to do some important

and precise measurements on NIO1 experiment and in particular about the breakdown occurrence, hoping that the bandwidth could be sufficiently high to pick up the fast events associated with this occurrences. However the challenge is now to enlarge the bandwidth and reach a value as larger as possible.
With this divider prototype has been study also the influence of conductive elements connected to the ground because these can vary the distributions and the value of stray capacitances on the circuit. So a sheath of copper, see fig. 4.43 has been connected to the ground provided by the instrument and through a non-conductive piece of plastic taken in hand has been approached to the circuit with different distances and different to different point. This serves to verify the influence and how this affect the transfer function. It has been found out that practically the object has no effects on the circuit. With more details a little modification of the transfer function occurs but it is not so huge to modify the bandwidth.

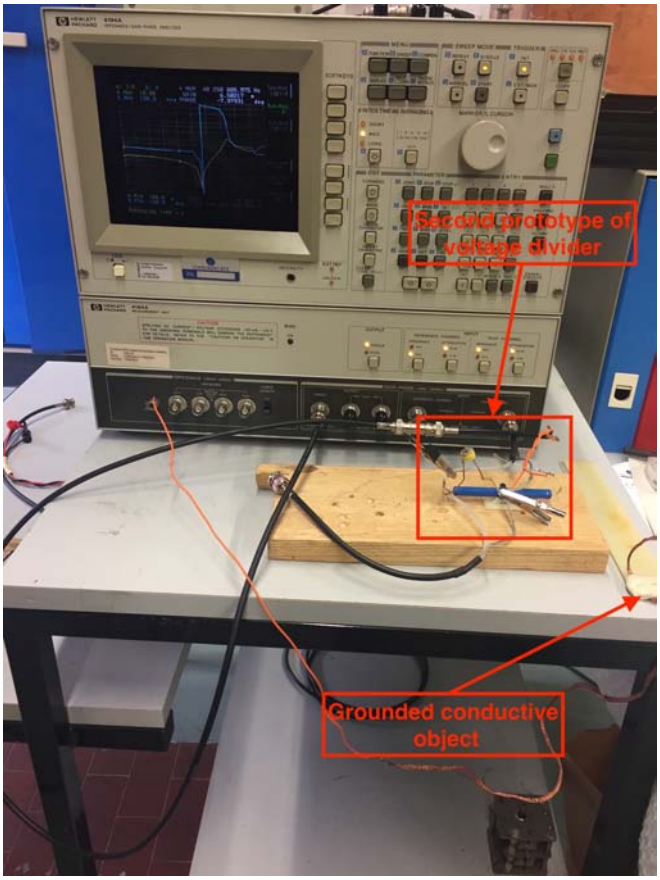

Figure 4.43: Influence of conductive object connected to the ground on the total transfer function.

4.3.3.4 Third voltage divider prototype

This third voltage divider prototype is the first definitive divider sized to withstand 10 kV and in order to be installed on the EG-PG gap. As can be seen in the photos below the divider itself is contained inside a plastic tube which will be clad with a conductive sheath, such as copper or aluminium, in order to have an electrostatic shield. This serves in order to fix the stray capacitance to ground of the high voltage divider and to make sure that the transfer function is not so affected by the place where the divider is installed. This divider has been studied both through impedance meter (fig. 4.45) and through spectrum analyser (fig. 4.46, 4.47, 4.48 and 4.49). With the impedance meter the total impedance between 100Hz and 100MHz is measured and showed. This study has an accessory valance with respect to the study with gain-phase analyser, but it shows that a series resonance occurs at about 15MHz (fig. 4.45). However from this graph it is difficult to analyse the provenance of the resonance; thus, a study through the gain-phase analyser is also necessary.

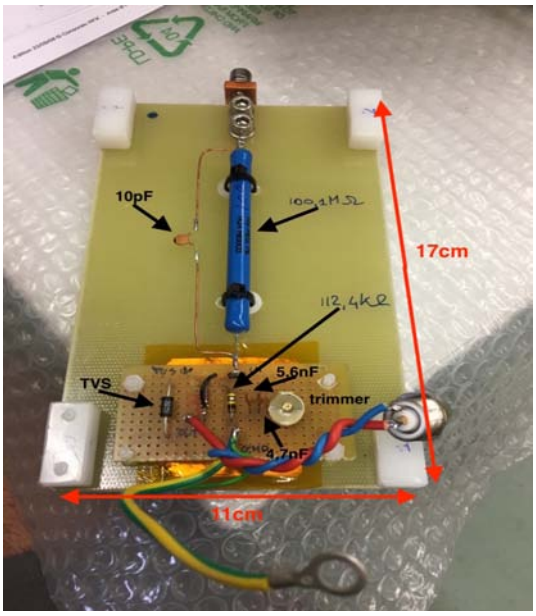

Figure 4.44: Prototype3: the first definitive voltage divider for relatively low voltage applications.

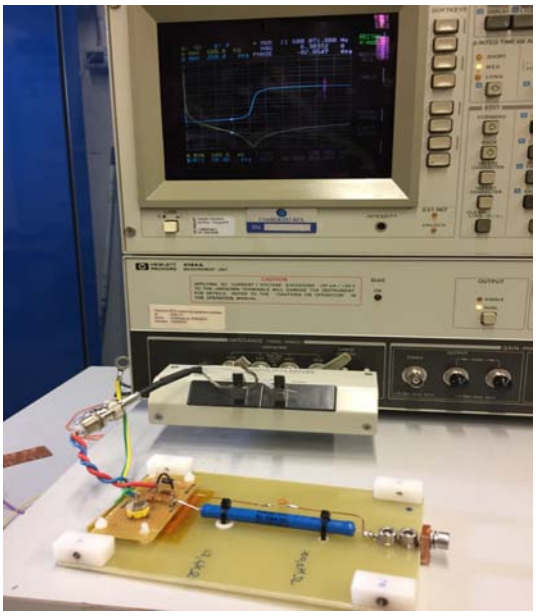

Figure 4.45: Prototype3: study through the impedance meter shows up a resonance occurs at a low frequency at about 10MHz.

Then the divider has been studied by using the spectrum analyser in the gain-phase mode as can be seen in the figures 4.46, 4.47, 4.48 and 4.49.

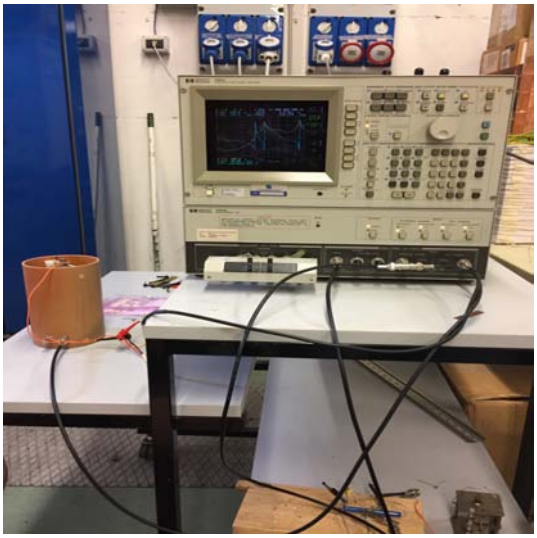

Figure 4.46: Prototype3: longest possible cables with the available lab material.

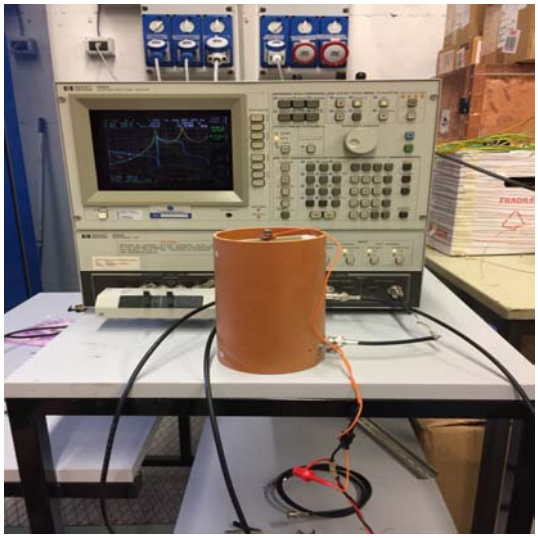

Figure 4.47: Prototype3: shorter cable with respect to the previous test.

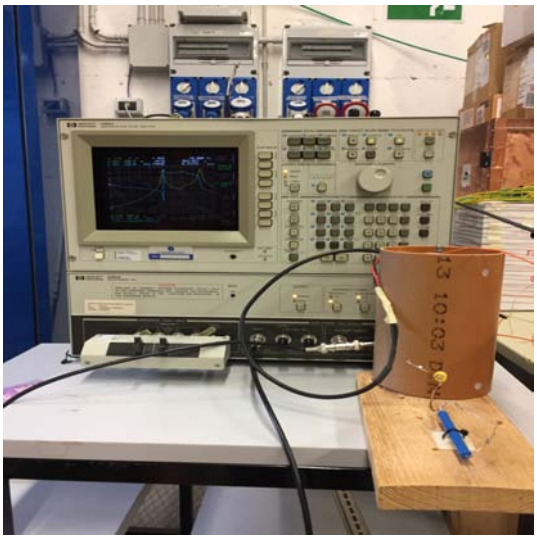

Figure 4.48: Prototype3: shortest possible cables with the available lab material between the divider's output and the analyser; rather long supply cable (50 cm).

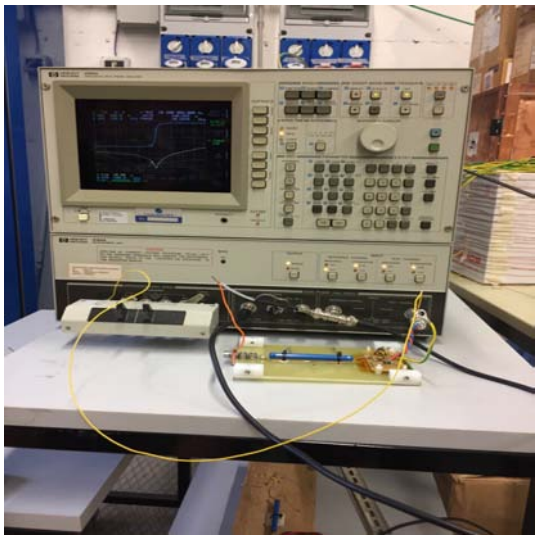

Figure 4.49: Prototype3: changing some parameters such as the capacitance.

The last experimentation, figure 4.49, is the one which better resembles an actual implementation in NIO1 experiment since the probe (i.e. the Red Pitaya) could be installed in the vicinity of the divider and the connection to ground could be rather long in order to reach the more convenient ground point. The fact that both of the cable are the smallest possible should attenuate the parasitic effect introduce by the cables and lead to a betterment of the performance of the divider.

4.3.3.4.1 Comparison between MATLAB and experimental results

The final configuration was reached trying to improve the performance of the third prototype of the voltage divider. The first two configurations, figures 4.46 and 4.47 with both the cables long 1m, display a little bandwidth. The reasons for this come from the facts that there were long cables, a inductance introduced with the non-twisted banana clamps. Furthermore, since the chosen capacitance at the high voltage side has been chosen as little as possible (1pF) according to the parasitic capacitance of the resistance (fraction of the pF), the connection introduces a relatively high capacitance and also the division ratio are not satisfied.
Consequently the test bench has been modified in order to understand if the global performance of the divider could increase with the layout connection and fit the simulation results. In figure 4.48 the modification of the test bench is shown in which a 50cm long cable supplies the circuit and a very short cable (5cm) connects the low voltage side of the divider to the input of the instrument. In the figure 4.52 a comparison between the experimental result and the simulation result is presented; both of two are related to the following set of data:

rat	100.1	$M\Omega$
cat	10	pF
rbt	112.4	$k\Omega$
cbt	10.3	nF
k	1000	[0]
trimmer	0	pF
lbt	5	cm
lat	50	cm

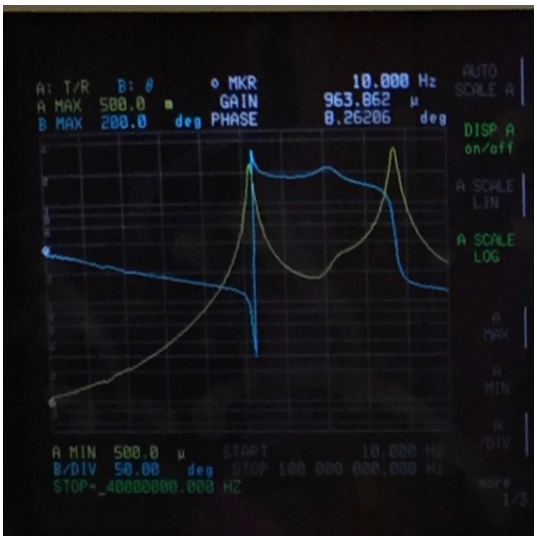

Figure 4.50

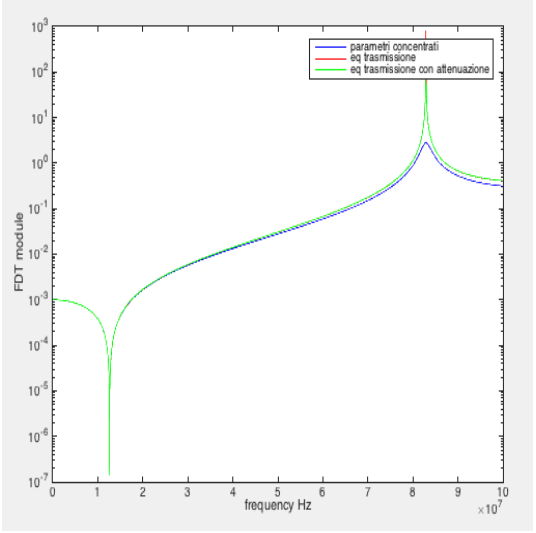

Figure 4.51

Figure 4.52: Comparison between the experimental result and the simulation result.

Event though the frequency response are not the same by the point of view of the form from both of the images, figures 4.50 and 4.51 it can be seen that the bandwidth is about 10MHz.
Since this result are not satisfactory another rearrangement of the test bench has been done according also to the actual layout installation in NIO1 experiment. The result of this rearrangement is shown in figure 4.49.
Now that the voltage divider has been tested with the final version of the layout connection, the obtained results have to be compared with the MATLAB® in order to see if the two are comparable and, if not, understand the reasons why they are different.

The definitive experimental result, relative to the figure 4.49 about the 10kV voltage divider is the one shown in figure 4.53 in which it can be seen that the bandwidth is about 15MHz. This means that only by changing the installation layout and thus the length of the cables 5MHz on band has been obtained.

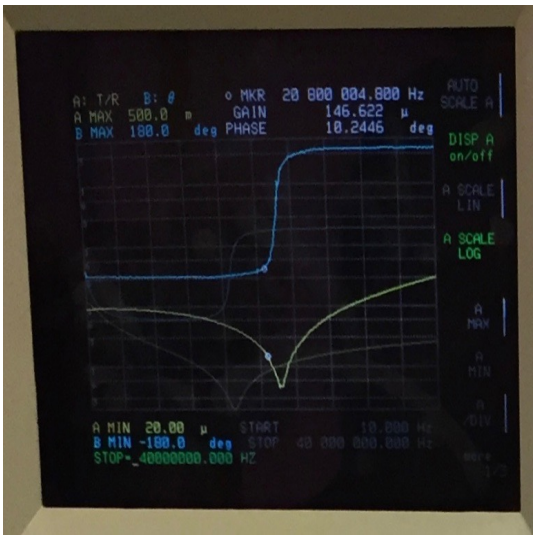

Figure 4.53: Experimental result obtained with the data contained in the table.

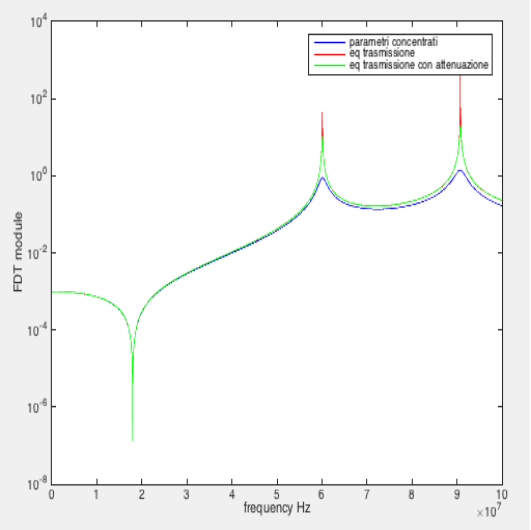

Figure 4.54: Simulation result with the data contained in the table.

This result is obtained with the following values:

rat	100.1	$M\Omega$
cat	10	pF
rbt	112.4	$k\Omega$
cbt	10.3	nF
k	1000	[0]
trimmer	65	pF
lbt	10	cm
lat	20	cm

From the two graphs 4.53 and 4.54 it can be seen that the data coming from experimentations and the simulations fit each other in the sense that the frequency response of the system and thus the bandwidth are more or less the same. The difference depends on some real parameters which can not be taken into account in the MATLAB® code being them unknown and non-constant.

Despite this, it is important that the reality and the simulation fit each other because this means that: the written code is a truthful representation of the reality and it can be used for the design of other wide bandwidth high voltage divider.
With the test done until now it can be noticed that the 10 kV divider has not the expected bandwidth, and in the first layout version it can reach about 10 MHz before to resonate (figure 4.45). Then changing the variable capacitance, and working on the cables length the bandwidth has been enlarged until about 15 MHz. Even if this is far from the desired bandwidth a 15 MHz bandwidth voltage divider could be useful to realise some important measurements on NIO1 experiment about the breakdown events.

Chapter 5

Conclusions

Padua and the Consorzio RFX play a fundamental role in the fusion research since here one of the most important part of a fusion reactor is studied: the injector for plasma heating.
Negative Ion Optimisation step 1 (NIO1) is an experiment built in Padua at the Consorzio RFX in order to characterise the production and the acceleration of negative ions for the neutral beam heating. I work personally on the electrical system of NIO1 in order to improve it and allow NIO1 to reach its rated operation starting from the work already done by other researchers on NIO1.
My predecessor's thesis ends with the following words: "a new passive protection system is under development to fulfil the requirements of NIO1 in terms of extraction and acceleration voltages"; this is exactly the starting point of this master thesis. The main aim of the latter is to design a passive protection system which allows NIO1 experiment to reach, in steady state, the desired and necessary supply voltages in order to obtain a continuous production and acceleration of negatively charged particles up to the rated values. Until now NIO1 has operated at a much less supply voltages with respect to those of regime, because: initially a limited regime of operation is requested, the electrical protection system already present is sized for this limited regime and thus the power supply system was not able to increase the power supplied, plasma breakdowns occur in NIO1 accelerator which do not allow to overcome a given voltage value between the grids.
Thus one of the aims of this thesis is the design of the protection system. Firstly, by considering the characteristics of NIO1 PSs a proper circuit has

been designed in order to generally fulfil the requirements. Then the components for this circuit have been chosen focusing particularly on the over voltage suppressor. The SIDAC (Silicon Diode for Alternating Current) seems the best possible choice for the over voltage suppressor so that a circuit composed by 25 SIDAC has been designed. After that a test bench for the over voltage suppressor has been designed and assembled. Tests on the SIDAC circuit have not been performed yet. Unfortunately I was not able to see the testing of the entire circuit because of the time needed to set up the safety procedures. Since one of the problems which limits the operation of NIO1 is the presence of plasma breakdowns a system to better characterise them is needed. Thus, simultaneously with the work in progress about the passive protection system, another project has been developed: the wide bandwidth high voltage divider to characterise the voltage signal during breakdowns. This is the second main topic of thesis work, directly correlated with the first one (the protection circuit during breakdowns), and complying with important measurements on the power supply system of NIO1 experiment. Indeed the last phrase of the thesis of my predecessor is: "a better understanding of the breakdown phenomena, including the data collected during the present thesis, will be necessary." The wide bandwidth high voltage divider will be necessary for measurements on the high voltage system which supplies the NIO1 experiment in order to get a better characterisation of breakdown events, and other phenomena correlated to this. A constraint for the development of such a diagnostic is necessary is to design a cheap system and in line with this assumption a data acquiring board has been found: the Red Pitaya. The input voltage of Red Pitaya is not compatible with the voltages present on NIO1 so a voltage divider is necessary in order to use the Red Pitaya probe. This voltage divider has been designed, simulated through MATLAB codes and tested with a spectrum analyser. The aim of the simulations and tests was to have a voltage divider with a precise division ratio (1:1000) over a large bandwidth (25MHz) defined according to the measurements done before by other researchers. A final prototype of the voltage divider has been obtained and it satisfies the requirements: division ratio of 1:1000 with a bandwidth of 15MHz. The bandwidth is not the value required yet but it is a temporarily acceptable step towards it considering that it can be improved by suitable layout choices in the final realisation.
This thesis has a natural continuation in both the aspects treated: the voltage

suppressor must be properly tested and if it responds to the requirements the entire protection system has to be built, tested and installed in NIO1; the 10kV voltage divider has not the required bandwidth yet and thus some study in order to enlarge it are necessary. Based on this experience for NIO1 also a 60kV compensated voltage divider will be realised in order to complete the set of measurements about the breakdown events.
From the few lines above it sounds clear that the two projects, subjects of this thesis, are strictly correlated and both of them of paramount importance for the NIO1 experiment to reach its maximum potential.
I'll take this opportunity to thank with all the team I work with for the help, the availability, the patience, for sharing with me some of their experience and finally for allowing me to participate in this work and for my master thesis: Bruno Laterza, Tommaso Patton, Mauro Recchia, Gianluigi Serianni, Piergiorgio Sonato.

Sebastiano Mancin

Appendix A

MATLAB® codes

A.1 Main MATLAB® code

```
clear all
close all
clc
% frequency, angular velocity and physical constants
f=logspace(0,8,1E5);
w=2*pi*f;
s=i*w;
mu0=4*pi*10^(-7);
eps0=8.854*10^(-12);
% bt line length [m]
lbt=0.5;
% number of elements and length of each element [m]
ncbt=10;
lcbt=lbt/ncbt;
% known circuital parameters definition
% high voltage side resistance [ohm]
rat=1e8;
% high voltage side compensation capacitance [F]
cat=10e-12;
zcat=1./(s.*cat);
% equivalent impedance rat//zcat
z1=rat.*zcat./(rat+zcat);
```

```
% probe's input resistance [ohm]
rin=1.e5;
% probe's input capacitance [F]
cin=30.e-12;
zcin=1./(s.*cin);
% ideal division ratio
k=rat/rin;
% probe's equivalent input impedance
zin=rin.*zcin./(rin+zcin);
% line's capacitance per unit length [F/m]
clbt=100.e-12;
zclbt=1./(s.*clbt);
% line's characteristic impedance [ohm]
z0=50;
% line's inductance per unit length [H/m]
llbt=(z0^2)*clbt;
zllbt=s.*llbt;
zclbt=1./(s.*(clbt*lcbt));
zllbt=s.*(llbt*lcbt);
% low voltage side compensation capacitance [F]
cbt=((cat)*k)-cin-clbt*lbt;
% inductance for take into account the supply mesh of
    the capacitor
% a 0 inductance can be chosen too
indbt=160e-10;
%indbt=0;
% actual probe's input reactance
zcbt=(s.*indbt)+1./(s.*cbt);
rbt=((rat/k)^(-1)-(1/rin))^-1;
% adding a resistance in order to fit better the
    collected data
zcbt1=(rbt.^-1+(zcbt).^-1).^-1
% cable resistance calculation
% outer conductor's resistance [Ohm/m]
rext=16*10^(-3);
```

```
% inner conductor's resistance [Ohm/m]
rint=38*10^(-3);
% inner conductor's diameter and section
% cable length is lbt
r=0.5*0.91*10^(-3);
S=pi*r^2;
ro=1.68e-8;
r1=(rint*(1+r*sqrt(w*mu0*ro^-1))+rext)*lcbt;
%-------------------------------------------------------------
%-------------------------------------------------------------
% PI LUMPED ELEMENT MODEL OF THE LINE
% longitudinal impedance of a single cell of the bt line
zcl=r1+zllbt;
% probe's equivalent impedance//right side line element's capacitor
% PI + first longitudinal element
zpi=zin.*(zclbt*2)./(zin+(zclbt*2))+zcl;
% i = number of cells - 1
for i=1:(ncbt-1)
zpi=((zpi.*(zclbt))./(zpi+zclbt))+zcl;
end
% adding up the last left side capacitance of the line
zlcpi=((zpi).*(zclbt*2))./((zpi)+(zclbt*2));
% low voltage side equivalent impedance
z2pi=zlcpi.*zcbt./(zlcpi+zcbt);
% total transfer function with luped PI element method
fdtp=z2pi./(z1+z2pi);
figure('Name','Voltage divider transfer function');
grid on
title('Voltage divider transfer function')
subplot(2,1,1)
semilogy(f,abs(fdtp))
subplot(2,1,2)
plot(f,angle(fdtp))
%-------------------------------------------------------------
```

```
90  %-------------------------------------------------------------------
91  % supply line inclusion in the model
92  % supply line length [m]
93  lat=0.5;
94  % number of elements and length of each element [m]
95  ncat=10;
96  lcat=lat/ncat;
97  % hv cable impedance definition
98  % line's capacitance per unit length [F/m]
99  clat=100.e-12;
100 zclat=1./(s.*clat);
101 % line's characteristic impedance [ohm]
102 z0=50;
103 % line's inductance per unit length [H/m]
104 llat=(z0^2)*clat;
105 zllat=s.*llat;
106 zclat=1./(s.*(clat*lcat));
107 zllat=s.*(llat*lcat);
108 % cable resistance calculation
109 r2=(rint*(1+r*sqrt(w*mu0*ro^-1))+rext)*lcat;
110 % longitudinal impedance for a single cell
111 zrl=r2+zllat;
112 % PI lumped elemtn model equivalent impedance of the hv
      line
113 % parallel between z1+z2 e zclat
114 zpiat=((z1+z2pi).*(zclat*2))./((z1+z2pi)+(zclat*2));
115 vz=zeros(ncat,length(w));
116 % i = number of cells - 1
117 for i=1:(ncat)
118 fdt=zpiat./(zpiat+zrl);
119 zpiat=(zpiat+zrl).*zclat./(zpiat+zrl+zclat);
120 vz(i,:)=fdt;
121 end
122 % supply line transfer function
123 % the votlage across the divider clamps is Vp=Vin*fdt
```

```
124 fdtal=prod(vz,1);
125 % power supply line transfer function's plot
126 figure('Name','Power supply line's transfer function');
127 grid on
128 title('Power supply line's transfer function')
129 subplot(2,1,1)
130 semilogy(f,abs(fdtal))
131 subplot(2,1,2)
132 plot(f,angle(fdtal))
133 %-------------------------------------------------------------
134 %-------------------------------------------------------------
135 % low voltage side effects inclusion
136 % equivalent impedance of the line with pi lumped
      element model
137 % parallel between the series of z1+z2 and zclat
138 zpibt=zin.*(zclbt*2)./(zin+(zclbt*2));
139 vzbt=zeros(ncbt,length(w));
140 % i = numberof cells - 1
141 for i=1:(ncbt)
142 fdtbt=zpibt./(zpibt+zcl);
143 zpibt=(zpibt+zcl).*zclbt./(zpibt+zcl+zclbt);
144 vzbt(i,:)=fdtbt;
145 end
146 % line's transfer function
147 % the votlage across the divider clamps is Vp=Vin*fdt
148 fdtcoll=prod(vzbt,1);
149 % total transfer function with pi element lumped model
150 fdtpi=fdtal.*fdtp.*fdtcoll;
151 figure('Name','Total transfer function');
152 grid on
153 title('Total transfer function')
154 subplot(2,1,1)
155 semilogy(f,abs(fdtpi))
156 subplot(2,1,2)
157 semilogx(f,angle(fdtpi))
```

```
158 %-------------------------------------------------------------------
159 %-------------------------------------------------------------------
160 % STUDY OF THE LINE WITH DISTRIBUTED PARAMETERS --> ELECTROMAGNETIC PROPAGATION + without attenuation + without distorsion
161 % 2.25 = RG58 relative electric permittivity (calculater through data sheet datum about the progation velocity)
162 epsr=2.25;
163 beta=w*sqrt(mu0*epsr*eps0);
164 roCARICO=((zin/z0)-1)./((zin/z0)+1);
165 ro=roCARICO.*exp(1i*(-2*beta*lbt));
166 % load impedance reported upstream the low votlage line
167 ZBTtras=z0*(1+ro)./(1-ro);
168 ZBTtotTRAS=(ZBTtras.^-1+zcbt.^-1).^-1;
169 % total low voltage impedance + zat
170 Zloadout1=ZBTtotTRAS+z1;
171 roCARICO=((Zloadout1/z0)-1)./((Zloadout1/z0)+1);T
172 FDTalimDIST=(exp(-1i*beta*lat).*(1+roCARICO))./(1+roCARICO.*exp(-2*1i*beta*lat));
173 FDTtras=ZBTtotTRAS./(ZBTtotTRAS+z1);
174 FDTlinea=((exp(-1i*beta*lbt)).*(1+roCARICO))./(1+ro);
175 FDTtotDISTR=FDTtras.*FDTalimDIST.*FDTlinea;
176 figure('Name','sign verify');
177 grid on
178 title('sign verify')
179 % --> since the phase is plotted rightly the used signs are right
180 subplot(2,1,1)
181 loglog(f,abs(ZBTtras))
182 subplot(2,1,2)
183 semilogx(f,angle(ZBTtras))
184 figure('Name','Transfer function without attenuation');
185 grid on
186 title('Transfer function without attenuation')
```

```
187 subplot(2,1,1)
188 semilogy(f,abs(FDTtotDISTR))
189 subplot(2,1,2)
190 semilogx(f,wrapTo360(angle(FDTtotDISTR)))
191 %-------------------------------------------------------------------
192 %-------------------------------------------------------------------
193 % STUDY OF THE LINE WITH DISTRIBUTED PARAMETERS --> ELECTROMAGNETIC PROPAGATION + with attenuation + without distorsion
194 % 2.25 = RG58 relative electric permittivity (calculater thtough data sheet datum about the progation velocity)
195 alfabt=(r1.*sqrt(clbt/llbt));
196 alfaat=(r2.*sqrt(clat/llat));
197 kbt=alfabt+1i.*beta;
198 kat=alfabt+1i.*beta;
199 roCARICO=((zin/z0)-1)./((zin/z0)+1);
200 roatt=roCARICO.*exp(-2*kbt*lbt);
201 % load impedance reported upstream the low votlage line
202 ZBTtrasatt=z0*(1+roatt)./(1-roatt);
203 ZBTtotTRASatt=(ZBTtrasatt.^-1+zcbt.^-1).^-1;
204 % total low voltage impedance + zat
205 Zloadout1att=ZBTtotTRASatt+z1;
206 roCARICOatt=((Zloadout1att/z0)-1)./((Zloadout1att/z0)+1);
207 FDTalimDISTatt=(exp((alfaat-(1i*beta))*lat).*(1+roCARICOatt))./(1+roCARICOatt.*exp(-2*kat*lat));
208 FDTtrasatt=ZBTtotTRASatt./(ZBTtotTRASatt+z1);
209 FDTlineaatt=((exp((alfaat-1i*beta)*lat)).*(1+roCARICOatt))./(1+roatt);
210 FDTtotDISTRatt=FDTtrasatt.*FDTalimDISTatt.*FDTlineaatt;
211 figure('Name','Transfer function with attenuation');
212 grid on
213 title('Transfer function with attenuation')
214 subplot(2,1,1)
```

```
semilogy(f,abs(FDTtotDISTRatt))
subplot(2,1,2)
semilogx(f,wrapTo360(angle(FDTtotDISTRatt)))
%------------------------------------------------------------------
%------------------------------------------------------------------
% superposed transfer function plots
figure('Name','FDT');
grid on
title('FDT module');
semilogy(f,abs(fdtpi),'b');
hold on
semilogy(f,abs(FDTtotDISTR),'r');
semilogy(f,abs(FDTtotDISTRatt),'g');
xlabel('frequency Hz');
ylabel('FDT module');
legend('lumped parameters','transmission','transmission+
    attenuation');
figure('Name','FDT');
grid on
title('FDT angle');
plot(f,(angle(fdtpi)),'b');
hold on
plot(f,(angle(FDTtotDISTR)),'r');
plot(f,(angle(FDTtotDISTRatt)),'g');
xlabel('frequency Hz');
ylabel('FDT angle');
legend('lumped parameters','transmission','transmission+
    attenuation');
```

A.2 Resistance parametric study

```
clear all
close all
clc
% frequency, angular velocity and physical constants
```

```
f=logspace(0,8,1E5);
w=2*pi*f;
s=i*w;
mu0=4*pi*10^(-7);
eps0=8.854*10^(-12);
r=100;
r3=[0 r 0 0 0];
r4=[0 0 r 0 0];
r5=[0 0 0 r 0];
r6=[0 0 0 0 r];
% bt line length [m]
lbt=0.5;
% number of elements and length of each element [m]
ncbt=10;
lcbt=lbt/ncbt;
% known circuital parameters definition
% high voltage side resistance [ohm]
rat=1e8;
% high voltage side compensation capacitance [F]
cat=10e-12;
zcat=1./(s.*cat);
% equivalent impedance rat//zcat
z1=rat.*zcat./(rat+zcat);
% probe's input resistance [ohm]
rin=1.e5;
% probe's input capacitance [F]
cin=30.e-12;
zcin=1./(s.*cin);
% ideal division ratio
k=rat/rin;
% probe's equivalent input impedance
zin=rin.*zcin./(rin+zcin);
% line's capacitance per unit length [F/m]
clbt=100.e-12;
zclbt=1./(s.*clbt);
```

```
% line's characteristic impedance [ohm]
z0=50;
% line's inductance per unit length [H/m]
llbt=(z0^2)*clbt;
zllbt=s.*llbt;
zclbt=1./(s.*(clbt*lcbt));
zllbt=s.*(llbt*lcbt);
% low voltage side compensation capacitance [F]
cbt=((cat)*k)-cin-clbt*lbt;
for j=1:5
% inductance for take into account the supply mesh of
    the capacitor
% a 0 inductance can be chosen too
indbt=160e-10;
%indbt=0;
% actual probe's input reactance
zcbt=(s.*indbt)+1./(s.*cbt);
rbt=((rat/k)^(-1)-(1/rin))^-1;
% adding a resistance in order to fit better the
    collected data
zcbt1=(rbt.^-1+(zcbt).^-1).^-1
% cable resistance calculation
% outer conductor's resistance [Ohm/m]
rext=16*10^(-3);
% inner conductor's resistance [Ohm/m]
rint=38*10^(-3);
% inner conductor's diameter and section
% cable length is lbt
r=0.5*0.91*10^(-3);
S=pi*r^2;
ro=1.68e-8;
r1=(rint*(1+r*sqrt(w*mu0*ro^-1))+rext)*lcbt;
%-------------------------------------------------------%
%-------------------------------------------------------%
% PI LUMPED ELEMENT MODEL OF THE LINE
```

```
% longitudinal impedance of a single cell of the bt line
zcl=r1+zllbt;
% probe's equivalent impedance//right side line element's capacitor
% PI + first longitudinal element
zpi=zin.*(zclbt*2)./(zin+(zclbt*2))+zcl;
% i = number of cells - 1
for i=1:(ncbt-1)
zpi=((zpi.*(zclbt))./(zpi+zclbt))+zcl;
end
% adding up the last left side capacitance of the line
zlcpi=((zpi).*(zclbt*2))./((zpi)+(zclbt*2));
% low voltage side equivalent impedance
z2pi=zlcpi.*zcbt./(zlcpi+zcbt);
% total transfer function with luped PI element method
fdtp=z2pi./(z1+z2pi);
%-------------------------------------------------------------------------%
%-------------------------------------------------------------------------%
% supply line inclusion in the model
% supply line length [m]
lat=0.5;
% number of elements and length of each element [m]
ncat=10;
lcat=lat/ncat;
% hv cable impedance definition
% line's capacitance per unit length [F/m]
clat=100.e-12;
zclat=1./(s.*clat);
% line's characteristic impedance [ohm]
z0=50;
% line's inductance per unit length [H/m]
llat=(z0^2)*clat;
zllat=s.*llat;
zclat=1./(s.*(clat*lcat));
zllat=s.*(llat*lcat);
```

```
107 % cable resistance calculation
108 r2=(rint*(1+r*sqrt(w*mu0*ro^-1))+rext)*lcat;
109 % longitudinal impedance for a single cell
110 zrl=r2+zllat;
111 % PI lumped elemtn model equivalent impedance of the hv
    line
112 zr=z1+z2pi+r4(j);
113 zpiat=((zr).*(zclat*2))./((zr)+(zclat*2));
114 vz=zeros(ncat,length(w));
115 % i = number of cells - 1
116 for i=1:(ncat)
117 fdt=zpiat./(zpiat+zrl+r3(j));
118 zpiat=(zpiat+zrl).*zclat./(zpiat+zrl+zclat);
119 vz(i,:)=fdt;
120 end
121 % supply line transfer function
122 % the votlage across the divider clamps is Vp=Vin*fdt
123 fdtal=prod(vz,1);
124 %-------------------------------------------------------%
125 %-------------------------------------------------------%
126 % low voltage side effects inclusion
127 % equivalent impedance of the line with pi lumped
    element model
128 z6=zin+r6(j);
129 % parallel between the series of z1+z2 and zclat
130 zpibt=z6.*(zclbt*2)./(z6+(zclbt*2));
131 vzbt=zeros(ncbt,length(w));
132 % i = numberof cells - 1
133 for i=1:(ncbt)
134 fdtbt=zpibt./(zpibt+zcl+r5(j));
135 zpibt=(zpibt+zcl).*zclbt./(zpibt+zcl+zclbt);
136 vzbt(i,:)=fdtbt;
137 end
138 % line's transfer function
139 % the votlage across the divider clamps is Vp=Vin*fdt
```

```
140 fdtcoll=prod(vzbt,1);
141 % total transfer function with pi element lumped model
142 fdtpi=fdtal.*fdtp.*fdtcoll;
143 %-------------------------------------------------------------------%
144 %-------------------------------------------------------------------%
145 % STUDY OF THE LINE WITH DISTRIBUTED PARAMETERS --> ELECTROMAGNETIC PROPAGATION + without attenuation + without distorsion
146 % 2.25 = RG58 relative electric permittivity (calculater through data sheet datum about the progation velocity)
147 epsr=2.25;
148 beta=w*sqrt(mu0*epsr*eps0);
149 roCARICO=((zin/z0)-1)./((zin/z0)+1);
150 ro=roCARICO.*exp(1i*(-2*beta*lbt));
151 % load impedance reported upstream the low votlage line
152 ZBTtras=z0*(1+ro)./(1-ro);
153 ZBTtotTRAS=(ZBTtras.^-1+zcbt.^-1).^-1;
154 % total low voltage impedance + zat
155 Zloadout1=ZBTtotTRAS+z1;
156 roCARICO=((Zloadout1/z0)-1)./((Zloadout1/z0)+1);T
157 FDTalimDIST=(exp(-1i*beta*lat).*(1+roCARICO))./(1+roCARICO.*exp(-2*1i*beta*lat));
158 FDTtras=ZBTtotTRAS./(ZBTtotTRAS+z1);
159 FDTlinea=((exp(-1i*beta*lbt)).*(1+roCARICO))./(1+ro);
160 FDTtotDISTR=FDTtras.*FDTalimDIST.*FDTlinea;
161 %-------------------------------------------------------------------%
162 %-------------------------------------------------------------------%
163 % STUDY OF THE LINE WITH DISTRIBUTED PARAMETERS --> ELECTROMAGNETIC PROPAGATION + with attenuation + without distorsion
164 % 2.25 = RG58 relative electric permittivity (calculater thtough data sheet datum about the progation velocity)
165 alfabt=(r1.*sqrt(clbt/llbt));
```

```
166 alfaat=(r2.*sqrt(clat/llat));
167 kbt=alfabt+1i.*beta;
168 kat=alfabt+1i.*beta;
169 roCARICO=((zin/z0)-1)./((zin/z0)+1);
170 roatt=roCARICO.*exp(-2*kbt*lbt);
171 % load impedance reported upstream the low votlage line
172 ZBTtrasatt=z0*(1+roatt)./(1-roatt);
173 ZBTtotTRASatt=(ZBTtrasatt.^-1+zcbt.^-1).^-1;
174 % total low voltage impedance + zat
175 Zloadout1att=ZBTtotTRASatt+z1;
176 roCARICOatt=((Zloadout1att/z0)-1)./((Zloadout1att/z0)+1)
      ;
177 FDTalimDISTatt=(exp((alfaat-(1i*beta))*lat).*(1+
      roCARICOatt))./(1+roCARICOatt.*exp(-2*kat*lat));
178 FDTtrasatt=ZBTtotTRASatt./(ZBTtotTRASatt+z1);
179 FDTlineaatt=((exp((alfaat-1i*beta)*lat)).*(1+roCARICOatt
      ))./(1+roatt);
180 FDTtotDISTRatt=FDTtrasatt.*FDTalimDISTatt.*FDTlineaatt;
181 %-------------------------------------------------------------------%
182 %-------------------------------------------------------------------%
183 % superposed transfer function plots
184 figure(1);
185 colorstring = 'kbmcy';
186 grid on
187 title('FDT module');
188 semilogy(f,abs(fdtpi),'Color',colorstring(j));
189 hold on
190 semilogy(f,abs(FDTtotDISTR),'r');
191 semilogy(f,abs(FDTtotDISTRatt),'g');
192 xlabel('frequency Hz');
193 ylabel('FDT module');
194 legend('lumped parameters','transmission eqs','
      transmission eqs with attenuation');
195 figure(2);
196 grid on
```

```
197 title('FDT angle');
198 plot(f,(angle(fdtpi)),'Color',colorstring(j));
199 hold on
200 plot(f,(angle(FDTtotDISTR)),'r');
201 plot(f,(angle(FDTtotDISTRatt)),'g');
202 xlabel('frequency Hz');
203 ylabel('FDT angle');
204 legend('lumped parameters','transmission eqs','
    transmission eqs with attenuation');
205 end
```

A.3 Capacitance parametric study

```
1  clear all
2  close all
3  clc
4  c=linspace(-9,9,19);
5  c1=c/100;
6  % frequency, angular velocity and physical constants
7  f=logspace(0,8,1E5);
8  w=2*pi*f;
9  s=i*w;
10 mu0=4*pi*10^(-7);
11 eps0=8.854*10^(-12);
12 r=100;
13 r3=[0 r 0 0 0];
14 r4=[0 0 r 0 0];
15 r5=[0 0 0 r 0];
16 r6=[0 0 0 0 r];
17 % bt line length [m]
18 lbt=0.5;
19 % number of elements and length of each element [m]
20 ncbt=10;
21 lcbt=lbt/ncbt;
22 % known circuital parameters definition
```

```
% high voltage side resistance [ohm]
rat=1e8;
% high voltage side compensation capacitance [F]
cat=10e-12;
zcat=1./(s.*cat);
% equivalent impedance rat//zcat
z1=rat.*zcat./(rat+zcat);
% probe's input resistance [ohm]
rin=1.e5;
% probe's input capacitance [F]
cin=30.e-12;
zcin=1./(s.*cin);
% ideal division ratio
k=rat/rin;
% probe's equivalent input impedance
zin=rin.*zcin./(rin+zcin);
% line's capacitance per unit length [F/m]
clbt=100.e-12;
zclbt=1./(s.*clbt);
% line's characteristic impedance [ohm]
z0=50;
% line's inductance per unit length [H/m]
llbt=(z0^2)*clbt;
zllbt=s.*llbt;
zclbt=1./(s.*(clbt*lcbt));
zllbt=s.*(llbt*lcbt);
% low voltage side compensation capacitance [F]
cbt1=((cat)*k)-cin-clbt*lbt;
% the following operation makes cbt to vary between its
   -9% and ita +9%
cbt=cbt1+(cbt1*c1);
for j=1:length(c)
% inductance for take into account the supply mesh of
   the capacitor
% a 0 inductance can be chosen too
```

```
indbt=160e-10;
%indbt=0;
% actual probe's input reactance
zcbt=(s.*indbt)+1./(s.*cbt);
rbt=((rat/k)^(-1)-(1/rin))^-1;
% adding a resistance in order to fit better the
    collected data
zcbt1=(rbt.^-1+(zcbt).^-1).^-1
% cable resistance calculation
% outer conductor's resistance [Ohm/m]
rext=16*10^(-3);
% inner conductor's resistance [Ohm/m]
rint=38*10^(-3);
% inner conductor's diameter and section
% cable length is lbt
r=0.5*0.91*10^(-3);
S=pi*r^2;
ro=1.68e-8;
r1=(rint*(1+r*sqrt(w*mu0*ro^-1))+rext)*lcbt;
%-------------------------------------------------------%
%-------------------------------------------------------%
% PI LUMPED ELEMENT MODEL OF THE LINE
% longitudinal impedance of a single cell of the bt line
zcl=r1+zllbt;
% probe's equivalent impedance//right side line element'
    s capacitor
% PI + first longitudinal element
zpi=zin.*(zclbt*2)./(zin+(zclbt*2))+zcl;
% i = number of cells - 1
for i=1:(ncbt-1)
zpi=((zpi.*(zclbt))./(zpi+zclbt))+zcl;
end
% adding up the last left side capacitance of the line
zlcpi=((zpi).*(zclbt*2))./((zpi)+(zclbt*2));
% low voltage side equivalent impedance
```

```
89  z2pi=zlcpi.*zcbt./(zlcpi+zcbt);
90  % total transfer function with luped PI element method
91  fdtp=z2pi./(z1+z2pi);
92  %-------------------------------------------------------------%
93  %-------------------------------------------------------------%
94  % supply line inclusion in the model
95  % supply line length [m]
96  lat=0.5;
97  % number of elements and length of each element [m]
98  ncat=10;
99  lcat=lat/ncat;
100 % hv cable impedance definition
101 % line's capacitance per unit length [F/m]
102 clat=100.e-12;
103 zclat=1./(s.*clat);
104 % line's characteristic impedance [ohm]
105 z0=50;
106 % line's inductance per unit length [H/m]
107 llat=(z0^2)*clat;
108 zllat=s.*llat;
109 zclat=1./(s.*(clat*lcat));
110 zllat=s.*(llat*lcat);
111 % cable resistance calculation
112 r2=(rint*(1+r*sqrt(w*mu0*ro^-1))+rext)*lcat;
113 % longitudinal impedance for a single cell
114 zrl=r2+zllat;
115 % PI lumped elemtn model equivalent impedance of the hv
      line
116 zr=z1+z2pi+r4(j);
117 zpiat=((zr).*(zclat*2))./((zr)+(zclat*2));
118 vz=zeros(ncat,length(w));
119 % i = number of cells - 1
120 for i=1:(ncat)
121 fdt=zpiat./(zpiat+zrl);
122 zpiat=(zpiat+zrl).*zclat./(zpiat+zrl+zclat);
```

```
123 vz(i,:)=fdt;
124 end
125 % supply line transfer function
126 % the votlage across the divider clamps is Vp=Vin*fdt
127 fdtal=prod(vz,1);
128 %-------------------------------------------------------------%
129 %-------------------------------------------------------------%
130 % low voltage side effects inclusion
131 % equivalent impedance of the line with pi lumped
      element model
132 z6=zin;
133 % parallel between the series of z1+z2 and zclat
134 zpibt=z6.*(zclbt*2)./(z6+(zclbt*2));
135 vzbt=zeros(ncbt,length(w));
136 % i = numberof cells - 1
137 for i=1:(ncbt)
138 fdtbt=zpibt./(zpibt+zcl);
139 zpibt=(zpibt+zcl).*zclbt./(zpibt+zcl+zclbt);
140 vzbt(i,:)=fdtbt;
141 end
142 % line's transfer function
143 % the votlage across the divider clamps is Vp=Vin*fdt
144 fdtcoll=prod(vzbt,1);
145 % total transfer function with pi element lumped model
146 fdtpi=fdtal.*fdtp.*fdtcoll;
147 %-------------------------------------------------------------%
148 %-------------------------------------------------------------%
149 % STUDY OF THE LINE WITH DISTRIBUTED PARAMETERS -->
      ELECTROMAGNETIC PROPAGATION + without attenuation +
      without distorsion
150 % 2.25 = RG58 relative electric permittivity (calculater
      through data sheet datum about the progation
      velocity)
151 epsr=2.25;
152 beta=w*sqrt(mu0*epsr*eps0);
```

```
153 roCARICO=((zin/z0)-1)./((zin/z0)+1);
154 ro=roCARICO.*exp(1i*(-2*beta*lbt));
155 % load impedance reported upstream the low votlage line
156 ZBTtras=z0*(1+ro)./(1-ro);
157 ZBTtotTRAS=(ZBTtras.^-1+zcbt.^-1).^-1;
158 % total low voltage impedance + zat
159 Zloadout1=ZBTtotTRAS+z1;
160 roCARICO=((Zloadout1/z0)-1)./((Zloadout1/z0)+1);T
161 FDTalimDIST=(exp(-1i*beta*lat).*(1+roCARICO))./(1+
        roCARICO.*exp(-2*1i*beta*lat));
162 FDTtras=ZBTtotTRAS./(ZBTtotTRAS+z1);
163 FDTlinea=((exp(-1i*beta*lbt)).*(1+roCARICO))./(1+ro);
164 FDTtotDISTR=FDTtras.*FDTalimDIST.*FDTlinea;
165 %-------------------------------------------------------------%
166 %-------------------------------------------------------------%
167 % STUDY OF THE LINE WITH DISTRIBUTED PARAMETERS --->
        ELECTROMAGNETIC PROPAGATION + with attenuation +
        without distorsion
168 % 2.25 = RG58 relative electric permittivity (calculater
        thtough data sheet datum about the progation
        velocity)
169 alfabt=(r1.*sqrt(clbt/llbt));
170 alfaat=(r2.*sqrt(clat/llat));
171 kbt=alfabt+1i.*beta;
172 kat=alfabt+1i.*beta;
173 roCARICO=((zin/z0)-1)./((zin/z0)+1);
174 roatt=roCARICO.*exp(-2*kbt*lbt);
175 % load impedance reported upstream the low votlage line
176 ZBTtrasatt=z0*(1+roatt)./(1-roatt);
177 ZBTtotTRASatt=(ZBTtrasatt.^-1+zcbt.^-1).^-1;
178 % total low voltage impedance + zat
179 Zloadout1att=ZBTtotTRASatt+z1;
180 roCARICOatt=((Zloadout1att/z0)-1)./((Zloadout1att/z0)+1)
        ;
```

```
FDTalimDISTatt=(exp((alfaat-(1i*beta))*lat).*(1+roCARICOatt))./(1+roCARICOatt.*exp(-2*kat*lat));
FDTtrasatt=ZBTtotTRASatt./(ZBTtotTRASatt+z1);
FDTlineaatt=((exp((alfaat-1i*beta)*lat)).*(1+roCARICOatt))./(1+roatt);
FDTtotDISTRatt=FDTtrasatt.*FDTalimDISTatt.*FDTlineaatt;
%-------------------------------------------------------------------------%
%-------------------------------------------------------------------------%
% superposed transfer function plots
figure(1);
grid on
title('FDT module');
semilogy(f,abs(fdtpi),'b');
hold on
semilogy(f,abs(FDTtotDISTR),'r');
semilogy(f,abs(FDTtotDISTRatt),'g');
xlabel('frequency Hz');
ylabel('FDT module');
legend('lumped parameters','transmission eqs','transmission eqs with attenuation');
figure(2);
grid on
title('FDT angle');
plot(f,(angle(fdtpi)),'b');
hold on
plot(f,(angle(FDTtotDISTR)),'r');
plot(f,(angle(FDTtotDISTRatt)),'g');
xlabel('frequency Hz');
ylabel('FDT angle');
legend('lumped parameters','transmission eqs','transmission eqs with attenuation');
levelmax=length(c);
Mcolors=jet(levelmax);
a=Mcolors(j,:);
figure(3);
```

```
212 hold on
213 grid on
214 title('FDT module');
215 semilogy(f,abs(fdtpi),'Color',a);
216 xlabel('frequency Hz');
217 ylabel('FDT module');
218 figure(4);
219 hold on
220 grid on
221 title('FDT module');
222 semilogy(f,abs(FDTtotDISTR),'Color',a);
223 xlabel('frequency Hz');
224 ylabel('FDT module');
225 figure(5);
226 hold on
227 grid on
228 title('FDT module');
229 semilogy(f,abs(FDTtotDISTRatt),'Color',a);
230 xlabel('frequency Hz');
231 ylabel('FDT module');
232 end
```

Bibliography

[1] T. Patton, B. Laterza, M. Recchia, *Electrical Tests on Overvoltage Protection Circuit for NIO1 Facility*, Technical Note, Consorzio RFX, Padova, 2016.

[2] M. Recchia, M. Bigi, M. Cavenago, *Conceptual Design and Circuit Analyses fo the Power Supplies of the NIO1 Experiment*, Fusion Engineering and Design, Elsevier, `http://www.elsevier.com/locate/fusengdes`, 2011.

[3] T. Patton, B. Laterza, M. Recchia, *NIO1 HV Protection System*, Technical Note, Consorzio RFX, Padova, 2015.

[4] M. Recchia, B. Laterza, L. Baseggio, T. Patton, D. Ravarotto, *Test of the NIO1 High Voltage Power Supply Protection System*, Technical Note, Consorzio RFX, Padova, 2015.

[5] M. Recchia, B. Laterza, L. Baseggio, T. Patton, D. Ravarotto, *Tests with Included Breakdown on NIO1 Electrical Circuit Components*, Technical Note, Consorzio RFX, Padova, 2015.

[6] M. Cavenago, G. Serianni, M. De Muri, P. Veltri, V. Antoni. Baltador, M. Barbisan, M. Brombin, A. Galata, N. Ippolito, T. Kulevoy, R. Pasqualotto, S. Petrenko, A. Pimazzoni, M. Recchia, E. Sartori, F. Taccogna, V. Variale, B. Zaniol, P. Barbato, L. Baseggio, V. Cervaro, D. Fasolo, L. Franchin, R. Ghiraldelli, B. Laterza, M. Maniero, D. Martini, L. Migliorato, A. Minarello, F. Molon, G. Moro, T. Patton, D. Ravarotto, R. Rizzieri, A. Rizzolo, M. Sattin, F. Stivanello, S. Zucchetti, *Improvements of the Versatile Multiaperture Negative Ion Source NIO1*, Consorzio RFX, Padova.

[7] Jeffrey Freidberg, *Plasma Physics and Fusion Energy*, Cambridge University Press, 2007.

[8] Wesson, J. (2004). Tokamaks, third edition. Oxford: Clarendon Press

[9] ZONG Wen-zhi , LI Yue ,CHENG Yang-chun ,ZHANG Chun-yu , XUE Yang ,LI Guan-gmao, *The Design of a Wide-Band High-Voltage Divider*, International Conference on Power System Technology, 2010.

[10] Robert Tarzwell, Ken Bahl, *High Voltage Printed Circuit Design and Manufacturing Notebook*, Sierra Proto Express, 2004.

[11] Tommaso Patton, *NIO1 Experiment, a Source of Negative Hydrogen and Deuterium Ions Accelerated Up To 60kV: Commissioning and Analysis of Firsts Experimental Results of Ion Beam Extraction*, master thesis, Consorzio RFX, Padova, 2016.

[12] Peter D. Hiscocks, James Gaston, *Oscilloscope Probes:Theory and Practice*, Syscomp Electronic Design Limited, 2007.

[13] Suat Ilhan, Aydogan Ozdemir, *Effects of Corona Ring Design on Electric Field Intensiy and Potential Distribution Along an Insulator String*, Electrical Engineering Department, Faculty of Electrical and Electronics, Istanbul Technical. University, 34469, Maslak, Istanbul, Turkey.

[14] HP 4194A Impedance/Gain-Phase Analiser Operation Manual.

[15] IPC-2221A, A standard developed by IPC, Generic Standard in Printed Board Design, `http://www.sphere.bc.ca/class/downloads/ipc_2221a-pcb%20standards.pdf`.

[16] A.V. Saushkin, N.A. Ratakhin, V.F. Feduschak, N.V. Zharova, *High Voltage Pulse Capacitors for High Current Pulse Generators*, Institute of High Current Electronics SB RAS, Tomsk, Russia.

[17] C. Mazzetti di Pietralata, Emanuele Freddi, *Appunti di Tecnica delle Alte Tensioni*, `http://laeman.altervista.org/Blog/lecture-notes/`.

[18] Antonio Paolucci, *Lezione di Trasmissione nell'Energia Elettrica*, Cleup, Padova, 1998.

[19] Giuseppe Biondo, Enrico Sacchi, *Manuale di Elettrotecnica e Telecomunicazioni*, Quinta edizione, Hoepli, 2005.

[20] M. Biasiacco, M.E. Valcher, *Controlli Automatici*, II edizione, Edizioni Libreria Progetto Padova, Padova, 2015.

[21] Mauro Dalla Palma, *Additional heating and current drive system*, lecture of the Thermonuclear Fusion course, A.Y. 2016-2017, 29-04-2017, Padova.

[22] Emanuele Sartori, *Neutral beam injectors for fusion*, lecture of the Thermonuclear Fusion course, A.Y. 2016-2017, 4-05-2017, Padova.

[23] `http://blog.optimumdesign.com/clearance-and-creepage-rules-for\ -pcb-assembly`

[24] `https://it.wikipedia.org/wiki/Linea_di_trasmissione`.

[25] `https://it.wikipedia.org/wiki/Impedenza_caratteristica`.

[26] `http://www.electronicdesign.com/embedded/ engineer-s-guide-high-quality-pcb-design`.

[27] `https://www.allaboutcircuits.com/technical-articles/ practical-pcb-layout-tips/`.

[28] `http://blog.optimumdesign.com/clearance-and-creepage-rules-for\ -pcb-assembly`

[29] Daniele Desideri, *Trasmission lines*, lecture of the Electrical and Electromagnetic micro and nano devices, slides 26 and 27, second cycle degree in Electrical Energy Engineering, A.Y. 2016/2017, Padova.

[30] Flexible RG58 Coax Cable Single Shielded with Black PVC (NC) Jacket Datasheet, `https://www.pasternack.com/images/ProductPDF/ RG58C-U.pdf`.

[31] Sidac SMP100MC-400 datasheet, `http://www.st.com/content/ ccc/resource/technical/document/datasheet/53/2f/58/02/7d/ 28/43/60/CD00003449.pdf/files/CD00003449.pdf/jcr:content/ translations/en.CD00003449.pdf`

[32] https://it.wikipedia.org/wiki/DIAC

[33] https://www.electronics-notes.com/articles/electronic-components/scr/what-is-a-diac.php

[34] http://www.sargom.it/catalogo/doc/Vetronite.pdf

[35] http://www.ptr.eu/en/know-how/terminal-blocks/approvals-regulations/clearance-and-creepage-distances/

[36] https://it.wikipedia.org/wiki/Comparative-Tracking-Index

[37] https://en.wikipedia.org/wiki/Spark-gap